

HYDROGENOLYSIS OF HYDROCARBONS ON IRON CATALYSTS

By

JACQUES MONNIER, B.Sc. (Ch.E.)

A Thesis

Submitted to the School of Graduate Studies

in Partial Fulfilment of the Requirements

for the Degree

Doctor of Philosophy

McMaster University

© September 1983

HYDROGENOLYSIS OF HYDROCARBONS ON IRON CATALYSTS

By

JACQUES MONNIER, B.Sc. (Ch.E.)

A Thesis

Submitted to the School of Graduate Studies

in Partial Fulfilment of the Requirements

for the Degree

Doctor of Philosophy

McMaster University

© September 1983

HYDROGENOLYSIS OF HYDROCARBONS ON IRON CATALYSTS

To my parents

DOCTOR OF PHILOSOPHY (1983)  
(Chemical Engineering)

McMASTER UNIVERSITY  
Hamilton, Ontario

TITLE: Hydrogenolysis of Hydrocarbons on Iron Catalysts

AUTHOR: Jacques Monnier, B.Sc. (Ch.E.) (Laval University)

SUPERVISOR: Professor R.B. Anderson

NUMBER OF PAGES: xvi, 186

## ABSTRACT

In the hydrogenolysis of hydrocarbons, iron is unique among the transition metals since it breaks molecules extensively and produces large quantities of methane even at low conversion. Hydrogenolysis of propane, isopentane and n-hexadecane were studied at 325 and 355°C over reduced Fe and carbided Fe catalysts prepared from a commercial NH<sub>3</sub> synthesis catalyst. Reaction network analysis applied to the selectivity data yielded a quantitative estimate of the relative importance, for an adsorbed species, of desorbing or undergoing C-C bond splitting; this method indicated that product desorption is the slow step in the reaction mechanism. Power rate expressions were obtained for hydrogenolysis of propane and isopentane at 325°C. Used catalysts, characterized by Mössbauer spectroscopy, contained α-Fe at high feed ratios of H<sub>2</sub> to hydrocarbon, and Fe<sub>3</sub>C, at low ratios. The formation of bulk iron carbides led to changes in selectivity, yielding less methane and more intermediate hydrocarbons. In hydrogenolysis of n-hexadecane, the analysis of the C<sub>7</sub>-C<sub>15</sub> products by gas chromatography-mass spectrometry showed the presence of alkylbenzenes, alkenes and branched alkanes, which account altogether for as much as 20 mole % of the heavier hydrocarbons. The data also suggest that the breaking of paraffins on iron possibly occurs by rapid demethylation. Hydrogenolysis of hydrocarbons is completely inhibited when carbon monoxide is added to the feed, even at concentration as low as 4 mole %; CO is

presumably more strongly adsorbed on the catalyst than hydrocarbons. The products obtained were similar to those found in the Fischer-Tropsch synthesis. Traces of water in the feed reduce the rate of hydrogenolysis. An increase in the  $K_2O$  content of Fe catalyst decreases its activity but does not affect its selectivity. A new method of deriving selectivity equations from reaction networks is presented. Network analysis is shown to apply to irreversible reactions for hydrogenolysis and isomerization.

## ACKNOWLEDGEMENTS

The author would like to thank many who have contributed to this research.

I am deeply indebted to Professor Robert B. Anderson, my supervisor, for his patience and for his guidance.

I also wish to extend my appreciation to Dr. Georges Dénès for the catalyst characterization by Mössbauer spectroscopy, and to Dr. Michael A. Quilliam, for the hydrocarbon analysis by combined gas chromatography-mass spectrometry, and Mr. Faj Ramelan for operating the GC-MS equipment.

I would like to acknowledge the contributions of Dr. P.T. Dawson and Dr. A.E. Hamielec, members of my Ph.D. committee. I also thank Dr. Dawson for characterizing some samples by Auger electron spectroscopy.

I gratefully acknowledge Dr. T. Birchall for providing access to the Mössbauer spectroscopy equipment.

I would also like to thank the ladies of the Faculty of Engineering Word Processing Centre for carefully typing this thesis, and Mrs. Peggy Johnstone, for some figure legends.

Special thanks to my parents for their encouragement and their support.

The author is grateful to the Department of Chemical Engineering, the Natural Sciences and Engineering Research Council, and Prof. R.B. Anderson for providing scholarships, and financial assistance.



## TABLE OF CONTENTS

	<u>Page</u>
Chapter 1 <u>Introduction</u>	1
1.1 Hydrogenolysis of Ethane	1
1.1.1 Experimental Work	1
1.1.2 Theoretical Explanations for Difference in Catalytic Activity	3
1.1.3 Reaction Mechanisms	4
1.1.4 Intermediate Species	8
1.2 Hydrogenolysis of Higher Molecular Weight Hydrocarbons	8
1.2.1 Experimental Work	8
1.2.2 Intermediate Species	11
1.2.3 Reaction Mechanisms	11
1.3 Changes in Catalyst Composition	13
1.4 Catalyst Poisoning	14
1.5 Aims of the Present Research	14
Chapter 2 <u>Thermodynamics Considerations</u>	16
2.1 Hydrogenolysis Reactions	16
2.2 Formation of Iron Carbides	18
2.3 Magnetic Properties	21
Chapter 3 <u>Experimental</u>	23
3.1 Experimental Set-up	23
3.1.1 Differential Reactor	23
3.1.2 Recycle System	25
3.1.3 Feed System	28
3.1.4 Analytical System	30
3.2 Catalysts	34
3.3 Operating Procedures	36

Table of Contents (continued)

Chapter 4	<u>Reaction Networks and Selectivity Equations</u>	40
4.1	Description of a Reaction Network	40
4.2	A New Derivation of Selectivity Equations	43
4.3	An Example of Hydrogenolysis with Isomerization	51
4.4	Selectivity Equations for Hydrogenolysis of Hexadecane	55
Chapter 5	<u>Hydrogenolysis of Isopentane</u>	58
5.1	Rate Determining Step in Hydrogenolysis over Iron	58
5.2	Effect of Carbon on Iron in Hydrogenolysis	62
5.2.1	Selectivity, Rate and Feed Ratio of H <sub>2</sub> to Isopentane	62
5.2.2	Selectivity and Formation of Bulk Carbides	65
5.2.2.1	Hydrogenolysis at a Feed Ratio of 2.8 H <sub>2</sub> : 1 i-C <sub>5</sub> H <sub>12</sub>	70
5.2.2.2	Hydrogenolysis at a Feed Ratio of 0.8 H <sub>2</sub> : 1 i-C <sub>5</sub> H <sub>12</sub>	71
5.3	Discussion	72
Chapter 6	<u>Hydrogenolysis of Propane and Hexadecane</u>	74
6.1	Hydrogenolysis of Propane: Rate and Selectivity	74
6.2	Hydrogenolysis of Hexadecane	76
6.2.1	Hydrogenolysis of Hexadecane at 355°C	77
6.2.2	Hydrogenolysis of Hexadecane at 325°C	91
6.3	Discussion	97
Chapter 7	<u>Effect of Water, Potassium Promoter and Carbon Monoxide in Hydrogenolysis</u>	108
7.1	Hydrogenolysis of Propane in Presence of Water	108

Table of Contents (continued)

7.2	Hydrogenolysis of Propane over Potassium-enriched Catalyst	111
7.3	Effect of Carbon Monoxide on Hydrogenolysis over Iron	113
7.3.1	Effect of Carbon Monoxide on Hydrogenolysis of Hexadecane	114
7.3.2	Effect of Carbon Monoxide on Hydrogenolysis of Propane	117
Chapter 8	<u>Conclusions</u>	122
	References	125
Appendix A	Characterization of Fe Catalysts by Mössbauer Spectroscopy	132
Appendix B	Surface Characterization by Auger Electron Spectroscopy	141
Appendix C	Combined Gas Chromatography-Mass Spectrometry	143
Appendix D	Calculation Procedures and Experimental Data	172

## List of Figures

<u>Figure</u>		<u>Page</u>
3.1	Diagram of the experimental set-up	26
3.2	Reversible saturator	29
4.1	Reaction network for hydrogenolysis of isopentane	41
4.2	Algorithm for the calculation of $Q_N$ factor	45
4.3	Pathways for the derivation of Q factors for the hydrogenolysis of isopentane	46
4.4	Selectivity equations for the hydrogenolysis of isopentane	47
4.5	Reaction network for hydrogenolysis and isomerization of isobutane over Pt catalyst	49
4.6	Pathways and selectivity equations for the reactions of isobutane over Pt catalyst	50
4.7	Product selectivity curves for the hydrogenolysis and isomerization of isobutane over Pt on alumina at 426°C	52
4.8	Calculated versus experimental selectivities in the hydrogenolysis-isomerization of isobutane over Pt on alumina	53
4.9	Pathways for hydrogenolysis of normal hexadecane, exclusively by demethylation	56
5.1	Selectivity curves for hydrogenolysis of $i-C_5H_{12}$ over Fe at 355°C and 7.0 FR (test 5.3)	59
5.2	Experimental and calculated rates of hydrogenolysis of isopentane at 325°C	63
5.3	Product selectivities as a function of mole % $H_2$ in the feed during hydrogenolysis at 325°C	64
5.4	Selectivity curves for hydrogenolysis of $i-C_5H_{12}$ over Fe at 355°C and 0.8 FR (test 5.4)	68
5.5	Selectivity curves for hydrogenolysis of $i-C_5H_{12}$ over Fe at 355°C and 0.8 FR (test 5.4)	69

List of Figures (continued)

6.1	Product selectivities as a function of mole % $H_2$ in the feed during hydrogenolysis of $C_3H_8$ at $325^\circ C$	75
6.2	Gas chromatogram of $C_7^+$ products in hydrogenolysis of hexadecane at $355^\circ C$ and 9.1 FR (test 6.1)	78
6.3	Gas chromatogram of $C_7^+$ products in hydrogenolysis at $355^\circ C$ after 10-fold magnification of Figure 6.2 and expansion of time axis	79
6.4	Homologous series for $C_7^+$ products in hydrogenolysis of hexadecane at $355^\circ C$ and 9.1 FR (test 6.1)	83
6.5	Gas chromatogram of $C_7^+$ products in hydrogenolysis of hexadecane at $325^\circ C$ and 0.7% conversion (test 6.2)	92
6.6	Gas chromatogram of $C_7^+$ products in hydrogenolysis of hexadecane at $325^\circ C$ and 7.7% conversion (test 6.3)	93
6.7	Gas chromatogram of $C_7^+$ products in hydrogenolysis of hexadecane at $325^\circ C$ and 15.9% conversion (test 6.4)	94
6.8	Gas chromatogram of $C_7^+$ products in hydrogenolysis of hexadecane at $325^\circ C$ and 15.9% conversion (test 6.4) after 10-fold magnification of Figure 6.7 and expansion of time axis	95
6.9	Carbon number distribution curves for $C_8-C_{15}$ hydrocarbons in hydrogenolysis of hexadecane at $325^\circ C$ (tests 6.2, 6.3 and 6.4)	100
7.1	Selectivity for ethane in hydrogenolysis of propane at $330^\circ C$ with or without $H_2O$ , as a function of conversion of propane	110
7.2	Gas chromatogram of $C_8^+$ products in hydrogenolysis of hexadecane at $325^\circ C$ without (I) or with (II) 5.7 mole % CO in the feed	115
A1	Mössbauer spectrum of used catalyst in test 5.1: only $\alpha-Fe$ is found	135
A2	Mössbauer spectrum of fresh pre-carbided catalyst: $Fe_5C_2$	136

List of Figures (continued)

A3	Mössbauer spectrum of used Fe catalyst after $i\text{-C}_5\text{H}_{12}$ hydrogenolysis at $355^\circ\text{C}$ and 0.8 FR (test 5.4): $\text{Fe}_3\text{C}$	137
A4	Mössbauer spectrum of used carbided catalyst after hydrogenolysis at $325^\circ\text{C}$ and 2.8 FR (test 5.2): 66 weight % $\alpha\text{-Fe}$ and 33% $\text{Fe}_3\text{C}$	138
A5	Mössbauer spectrum of used iron catalyst after hydrogenolysis of hexadecane at $325^\circ\text{C}$ and 9.1 FR: 93 weight % $\text{Fe}_3\text{C}$ and 7% $\alpha\text{-Fe}$	139
A6	Mass spectrum of n-nonane (peak 15)	145
A7	Mass spectrum of n-undecane (peak 42)	146
A8	Mass spectrum of n-tridecane (peak 65)	147
A9	Mass spectrum of n-tetradecane (peak 75)	148
A10	Mass spectrum of n-hexadecane (peak 86)	149
A11	Mass spectrum of branched decane (peak 22)	150
A12	Mass spectrum of branched decane (peak 23)	151
A13	Mass spectrum of nonene (peak 16)	152
A14	Mass spectrum of nonene (peak 17)	153
A15	Mass spectrum of decene (peak 27)	154
A16	Mass spectrum of decene (peak 28)	155
A17	Mass spectrum of m,p-xylene (peak 10)	156
A18	Mass spectrum of o-xylene (peak 13)	157
A19	Mass spectrum of n-propylbenzene (peak 19)	158
A20	Mass spectrum of $\text{C}_3$ -alkylbenzene (peak 20)	159
A21	Mass spectrum of $\text{C}_3$ -alkylbenzene (peak 26)	160
A22	Mass spectrum of $\text{C}_4$ -alkylbenzene (peak 33)	161
A23	Mass spectrum of n-butylbenzene (peak 34)	162

List of Figures (continued)

A24	Mass spectrum of C <sub>5</sub> -alkylbenzene (peak 45)	163
A25	Mass spectrum of C <sub>5</sub> -alkylbenzene (peak 46)	164
A26	Mass spectrum of C <sub>6</sub> -alkylbenzene (peak 57)	165
A27	Mass spectrum of n-hexylbenzene (peak 58)	166
A28	Mass spectrum of C <sub>7</sub> -alkylbenzene (peak 68)	167
A29	Mass spectrum of C <sub>7</sub> -alkylbenzene (peak 69)	168
A30	Mass spectrum of C <sub>8</sub> -alkylbenzene (peak 78)	169
A31	Mass spectrum of C <sub>8</sub> -alkylbenzene (peak 79)	170
A32	Mass spectrum of naphthalene and branched dodecane	171

List of Tables

<u>TABLE</u>		<u>Page</u>
2.1	Free Energies of Formation, $\Delta G_f^\circ$ , in kcal/mole	17
2.2	Minimum Mole Fraction of Hydrogen to Avoid Formation of Carbides and Graphite during Hydrogenolysis at 128 kPa	20
2.3	Magnetic Properties	22
3.1	Materials	24
3.2	Settings of Gas Chromatographs	31
3.3	Physical Properties of Hydrocarbons	33
4.1	Parameters for the Hydrogenolysis-Isomerization of Isobutane over Pt on Alumina at 426°C	54
5.1	Parameters for the Hydrogenolysis of Isopentane over Fe at 355°C and 7.0 FR	61
5.2	Product Selectivities and Reaction Rates for Hydrogenolysis of Isopentane over Fe Catalysts at 325°C and 2.8 FR	66
5.3	Product Selectivities and Reaction Rates for Hydrogenolysis of Isopentane over Reduced Fe Catalyst at 355°C	67
6.1	Summary of Compounds Identified by Capillary Column GC-MS Analysis, in Hydrogenolysis of n-C <sub>16</sub> H <sub>34</sub>	84
6.2	Product Distribution for Hydrogenolysis of Hexadecane (C <sub>9</sub> -C <sub>14</sub> range) in Mole % of Carbon Number Fraction	90
6.3	Product Selectivities in Hydrogenolysis of Hexadecane at 9.1 FR	98
6.4	Carbon Number Distribution for Hydrogenolysis of Hexadecane at 325°C	99
7.1	Product Selectivities and Reaction Rates for Hydrogenolysis of C <sub>3</sub> H <sub>8</sub> over Reduced Fe with or without Addition of H <sub>2</sub> O, at 330°C and 4.7 FR	109



List of Tables (continued)

7.2	Product Selectivities and Reaction Rates in Hydrogenolysis of $C_3H_8$ with a 4.8 FR	112
7.3	Hydrogenolysis of Propane at $335^\circ C$ and 4.3 FR with Different Concentrations of CO in the Feed	118
7.4	Molar Ratios of Products from CO Pulse Experiments during Hydrogenolysis of Propane at $340^\circ C$ and 4.9 FR	120
A1	$^{57}Fe$ Mössbauer Data of the Catalysts at Room Temperature	140
A2	Hydrogenolysis of Isopentane at $325^\circ C$ and Various $H_2$ Concentration in the Feed	174
A3	Data for Power Rate Expression in Hydrogenolysis of Isopentane at $325^\circ C$	176
A4	Hydrogenolysis of Isopentane over Reduced Iron at $325^\circ C$ and 2.8 Feed Ratio (test 5.1)	177
A5	Hydrogenolysis of Isopentane over $Fe_5C_2$ at $325^\circ C$ and 2.8 Feed Ratio (test 5.2)	178
A6	Hydrogenolysis of Isopentane over Reduced Fe at $355^\circ C$ and 7.0 Feed Ratio (test 5.3)	179
A7	Hydrogenolysis of Isopentane over Reduced Fe at $355^\circ C$ and 0.8 Feed Ratio, $1\% < \text{Conversion} < 10\%$ (test 5.4)	180
A8	Hydrogenolysis of Isopentane over Reduced Iron at $355^\circ C$ and 0.8 Feed Ratio with a Conversion less than $1\%$ (test 5.4)	181
A9	Data for Power Rate Expression in Hydrogenolysis of Propane at $325^\circ C$	182
A10	Experimental Data from Hydrogenolysis of Propane at $325^\circ C$ and Various $H_2$ Concentration in the Feed	183
A11	Hydrogenolysis of Propane over Reduced Iron at $330^\circ C$ and 4.7 FR, with or without Water in the Feed	184
A12	Hydrogenolysis of Propane over Reduced Iron Catalyst at $325^\circ C$ and 4.8 FR	185
A13	Hydrogenolysis of Isobutane over Platinum or Catalyst at $425^\circ C$ and 3.0 FR (Fig. 4.7)	186

### Nomenclature

$A_x$	=	Adsorbed hydrocarbon with x carbon atoms
$C_x$	=	Gaseous hydrocarbon with x carbon atoms
$C_x^+$	=	Hydrocarbon with x carbon atoms or more
$F, f, f'$	=	Splitting factors
$FR$	=	Ratio of hydrogen to hydrocarbon in the feed
$J$	=	Intermediate
$J'_x$	=	$k'_x / (k'_x + k_x^*)$
$k_x$	=	Rate constant for adsorption
$k'_x$	=	Rate constant for desorption
$k_x^*$	=	Rate constant for splitting of C-C bonds
$k_I$	=	Rate constant for isomerization
$k_x^n$	=	Overall 1st order rate constant
$K_e$	=	Equilibrium constant
$P$	=	Product
$P_E, P_H$	=	Partial pressures
$P_T$	=	Total pressure
$P_M^*$	=	Virtual pressure of methane
$Q_p$	=	Factor for selectivity equations
$R$	=	Reactant
$R_I$	=	Fraction of converted reactant undergoing isomerization
$R_{i^*}$	=	$1 - R_I$
$R_p, R_R, R_x$	=	Differential reaction rates
$S_p$	=	Selectivity of product p

SS = Summation of selectivities

X = Conversion of hydrocarbon reactant

CHAPTER 1  
INTRODUCTION

The present thesis investigates the hydrogenolysis of hydrocarbons over iron catalysts. These exothermic reactions involve the splitting of C-C bonds and the hydrogenation of the newly formed hydrocarbon fragments. This chapter is divided into 5 sections, of which the first 2 present a literature review on hydrogenolysis of ethane and of larger paraffinic hydrocarbons. In these 2 sections, iron is shown to be unique among transition metal catalysts. The third section describes the different Fe carbides that can be formed during reaction involving hydrocarbons and the fourth considers catalyst poisoning and its influence on selectivity. The last section describes the aims of the present research.

1.1 Hydrogenolysis of Ethane

1.1.1 Experimental Work

Hydrogenolysis reactions over metal catalysts were first studied with ethane by Morikawa, Benedict and Taylor (85,86,115) using cobalt, nickel, copper and iron catalysts. Interest in hydrogenolysis reactions arose because according to Taylor, they might provide a measure of the tendency of different metal catalysts to break C-C bonds relative to their ability to grow hydrocarbons during the hydrogenation of carbon monoxide.

Taylor et al. (115) found that Co was less active for hydrogenolysis than Ni but more active than Cu. Furthermore, the reaction rate was inversely proportional to the partial pressure of  $H_2$  on Co and Ni.

Morikawa et al. (85,86) explained this dependence of the rate by the dissociative adsorption of  $C_2H_6$  to form  $C_1$  adsorbed species, which react faster than ethane to form  $CH_4$  with hydrogen and which are in larger amount on the catalyst surface at lower  $H_2$  partial pressure. The authors also suggested that the number of pairs of adjacent sites necessary for  $C_2H_6$  chemisorption may be inversely proportional to the  $H_2$  partial pressure.

A few years later, experimental results of Kemball and Taylor (55) confirmed that in hydrogenolysis over nickel, the power rate equation had a negative exponent,  $-1.2$ , for the  $H_2$  partial pressure and a positive one,  $+0.7$ , for  $C_2H_6$ . Activation energy was about  $+52$  kcal/mole.

Of experimental power rate expressions given in the literature, Fe is the only group VIII metal which has a positive  $H_2$  order (94,95, 100,101,103,104,123). For the other metals, the reaction rate is more or less enhanced by a decrease in  $H_2$  partial pressure, depending on the size of the exponent. However, the  $H_2$  order varies with temperature, becoming less and less negative with increasing temperature (13,45,46, 61,67,102). The rate of hydrogenolysis is close to 1st order in  $C_2H_6$  partial pressure for all metals.

A list of metal activities prepared by Sinfelt (104) indicates

that Fe has one of the lowest hydrogenolysis activities of transition metals:



Finally, Somorjai (108,109) observed, using surface characterization techniques, that changes in the metallic crystal faces such as the number of kinks and steps, influence the rate of splitting of C-C bonds.

#### 1.1.2 Theoretical Explanations for Difference in Catalytic Activity

Some workers tried to relate the difference in hydrogenolysis activity of the different metal catalysts to their electronic structure. Sinfelt correlated the catalytic activity of the group VIII metals with their % d-character (103,104). The % d-character is a concept defined in the "Resonating-valence-bond" theory of metals developed by Linus Pauling (89) and it represents the extent of participation of d-orbital electrons in the bonding of atoms in a metal lattice. It is calculated from the atomic radius and the saturation magnetic moment. The bond strength between metal atoms usually increases with the % d-character.

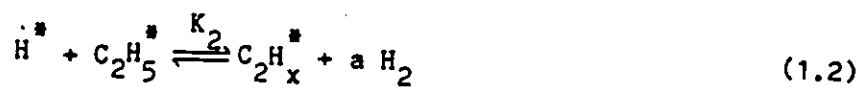
By plotting the relative specific activity of copper and group VIII transition metals as a function of their % d-character, Sinfelt could draw a straight line through the points corresponding to the metals of the second and third periods (Ru-Rh-Pd and Os-Ir-Pt). However, only a curve could be passed through the points for Fe, Co, Ni and Cu. Consequently, Sinfelt suggested for the determination of the catalytic activity, an additional criterion, the lattice spacing, which

is smaller for non-noble metals than for noble ones. Other theories were put forward to explain the behavior of transition metals but were not very successful (64).

### 1.1.3 Reaction Mechanisms

Reaction mechanisms were proposed for  $C_2H_6$  hydrogenolysis over transition metal catalysts. The basic catalytic mechanism consists of 3 steps: adsorption of the reactants on the catalyst sites, reaction between the adsorbed species and desorption of the products. The mechanisms for hydrogenolysis reactions follow this general principle.

The most recent mechanism for hydrogenolysis of ethane on transition metals was proposed by Sinfelt (106), based on earlier mechanisms developed by Cimino et al. (26) and Sinfelt (102). The rate determining step was assumed to be the splitting of the C-C bonds of the adsorbed hydrocarbon based on experiments showing that, over most metals, hydrogen-deuterium exchange occurs at lower temperature than hydrogenolysis reactions (26). In this model, hydrogen and ethane do not compete for active sites. The following equations summarize the mechanism proposed by Sinfelt:





where 
$$a = \left(\frac{6-x}{2}\right) \quad (1.5)$$

To account for the decrease in order of  $\text{H}_2$  partial pressure with increasing temperature, the first 2 steps involve rapid chemisorption of  $\text{C}_2\text{H}_6$  to form  $\text{C}_2\text{H}_5^*$  and further dehydrogenation to  $\text{C}_2\text{H}_x^*$ . These steps proceed rapidly and may be regarded as being at equilibrium. The rate of formation of  $\text{C}_2\text{H}_5^*$  is therefore equal to the disappearance of  $\text{C}_2\text{H}_x^*$ . Splitting of the C-C bonds and hydrogenation of the  $\text{C}_1$  species occur rapidly. Rate equations were derived from this mechanism, the subscripts 1,2,3 referring to steps in the mechanism and letters E and H, to  $\text{C}_2\text{H}_6$  and  $\text{H}_2$ :

$$\text{Rate} = \frac{k_1 P_E}{(1 + bP_H^a)} \quad (1.6)$$

$$\text{where } b = \frac{k_1'}{k_3 K_2} \quad (1.7)$$

or

$$\text{Rate} = k P_E^n P_H^{-na} \quad (1.8)$$

$$\text{where } k = k_3 \left[ \frac{k_1}{k_1'} K_2 \right]^n \quad (1.9)$$

Equation 1.8 is a Freundlich approximation of equation 1.6.

At low temperature,  $(bP_H^a)$  is much larger than unity and equation 1.6 can be written



$$\text{Rate} = \frac{k_1 P_E}{b P_H^a} = k_3 \frac{k_1}{k_1} K_2 \frac{P_E}{P_H^a} \quad (1.10)$$

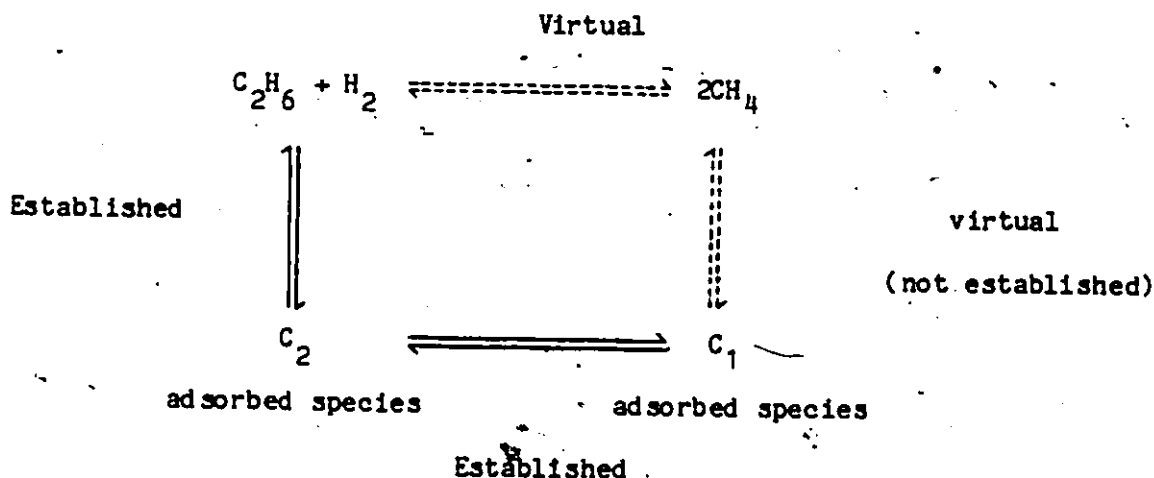
At high temperature or at low hydrogen partial pressure, more extensive dehydrogenation of  $C_2H_6$  occurs and the reaction rate becomes independent of  $H_2$  pressure, ( $b P_H^a$ ) being very small compared to unity.

Values of integer  $a$  were obtained by fitting eq. 1.8 to the experimental data. The parameter  $x$ , the number of H atoms in the  $C_2$  adsorbed species, was calculated with eq. 1.5. According to Sinfelt (106), Pt, Pd and Rh have a hydrogen deficient adsorbed species ( $x=0$ ), Ru, Ni, Os and Ir, an acetylene-type adsorbed species ( $x=2$ ) and Co, an ethylene-type ( $x=4$ ).

If the experimental data for hydrogenolysis over Fe are fitted to the power rate equation, the order of  $H_2$  partial pressure is positive, implying a negative value of  $x$ , which is physically impossible. Application of Sinfelt's rate equations to iron catalysts, is therefore not possible since one of the assumptions, the splitting of C-C bonds as rate determining step wouldn't be valid for hydrogenolysis over Fe. Instead Sinfelt, suggested desorption of the adsorbed  $C_1$  species as rate limiting step since hydrogen-deuterium exchange of ethane does not occur on Fe at low temperature, even though hydrogenolysis does (104).

Dowie et al. (34) also confirmed the validity of this rate limiting step with their hydrogenolysis experiments in presence of deuterium where methane is completely exchanged to form  $CD_4$ . The authors proposed a simple reaction mechanism where desorption is rate determining. They used in this mechanism, the concept of "virtual

pressure" developed by Temkin and Pyzhev (116) for the decomposition of  $\text{NH}_3$  over promoted iron catalyst. The virtual pressure which is a fictitious pressure, can be considered as the "fugacity of the adsorbed species" on the catalyst surface, as suggested by Bokhoven et al. (14). The following diagram describes the proposed mechanism:



The adsorbed  $\text{C}_2$  species are cracked into  $\text{C}_1$  which accumulate on the surface due to slow desorption until equilibrium is reached with a hypothetical pressure of  $\text{CH}_4$ , called its virtual pressure, also in equilibrium with  $\text{C}_2\text{H}_6$  and  $\text{H}_2$ , in the gas phase. Therefore, the value of the virtual pressure can be expressed as a function of the actual pressures of the reactants. In hydrogenolysis of ethane, the virtual pressure of methane is:

$$P_M^* = (K_e P_E P_H)^{1/2} \quad (1.11)$$

At  $325^\circ\text{C}$ , the equilibrium constant,  $K_e$ , is about  $1.5 \times 10^6$  atm and in the presence of 1 atm  $\text{C}_2\text{H}_6$  and 1 atm  $\text{H}_2$ , the  $\text{CH}_4$  virtual pressure

is about 1,200 atm which is larger than the actual pressure of  $\text{CH}_4$ . Consequently, more  $\text{C}_1$  species are present on the surface than  $\text{C}_2$ . According to Kemball (56), the high value of  $\text{CH}_4$  virtual pressure during  $\text{C}_2\text{H}_6$  hydrogenolysis would lead to higher surface coverage by  $\text{C}_1$  species than during  $\text{D}_2$  exchange reactions and this would explain why exchange is slower than hydrogenolysis over Fe catalysts.

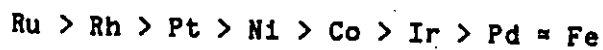
#### 1.1.4 Intermediate Species

The intermediate species usually found in hydrogenolysis of  $\text{C}_2\text{H}_6$  are  $\alpha, \beta$ -diadsorbed species which are more or less strongly bonded to the catalyst sites depending on the metal involved (105). At high reaction temperature,  $\alpha, \alpha$ -diadsorbed species have also been found as hydrogenolysis intermediates (47).

### 1.2 Hydrogenolysis of Higher Molecular Weight Hydrocarbons

#### 1.2.1 Experimental Work

Hydrogenolysis of hydrocarbons containing more than 2 C atoms (straight and branched alkanes, cyclic molecules, olefins, aromatics) have been studied over various metals. Hydrocracking is more extensive on Fe than on any other group VIII metal. Isomerization and cyclization are very often side reactions during hydrogenolysis of hydrocarbons over Pt metals (78). The catalytic activity of these transition metals was measured by Kikuchi et al. (62) in reactions with normal pentane and the following sequence in order of decreasing activity was obtained:



Iron is also less active than other group VIII metals during hydrogenolysis of hexanes (73).

Paraffinic hydrocarbons react faster on a given metal as the number of C atoms increases (3), since the activation energy for splitting a C-C bond reported per C atom, is inversely proportional to the length of the paraffin (9,106,111). Branched alkanes are more reactive than straight chain hydrocarbons on Ni and Co (63,73) but less reactive on Ru (60). The activation energy for adsorption of cycloalkanes being smaller than for alkanes, the hydrogenolysis of cycloalkanes is faster.

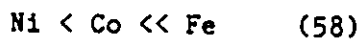
Power rate expressions were used by different workers (72,97, 117) to fit the experimental data. With  $C_3H_8$ , the exponent of the  $H_2$  partial pressure is usually negative, except for Fe catalysts, varying between -2.5 and -2.0 for Ni catalysts and -1.9 and -0.61 for Co. Machiels and Anderson (72) observed that with Fe supported on silica and promoted with magnesia, an increase of reaction temperature changed the sign of the exponent: -0.53 at  $314^\circ C$  and 0.78 at  $353^\circ C$ . This increase in the order of  $H_2$  partial pressure has also been noticed by other workers (13,78,106).

During hydrogenolysis reactions, the selectivity of a catalyst for different hydrocarbons varies from one metal to another. The selectivity for product P is defined as the ratio of the rate of formation of P over the rate of reaction of R.

$$S_P = -R_P/R_R \quad (1.12)$$

Comparisons can be made between the selectivity of different

metals. The proportion of methane in the products increases in the following order:



In their experiments with  $\text{C}_6$  isomers, Machiels and Anderson (73) observed that the selectivity for ethane decreased depending on the metal being used:



In fact, over Fe, methane was the main product and only traces of  $\text{C}_2\text{H}_6$  and  $\text{C}_3\text{H}_8$  could be found.

Higher reaction temperatures led also to more extensive C-C bond splitting.

Furthermore, Dowie et al. (32) did some low conversion hydrogenolysis experiments using deuterium over evaporated Fe at  $188^\circ\text{C}$  and found that more than 80% of the products were completely exchanged and transformed into perdeuterio-compounds:  $\text{CD}_4$ ,  $\text{C}_2\text{D}_4$ ,  $\text{C}_3\text{D}_6$ . With neo- $\text{C}_5\text{H}_{12}$ , there was also extensive hydrocracking, more than 99% of the total products being methane.

These differences in selectivity between metals are very often due to variations in their pattern of splitting the C-C bonds of a given hydrocarbon. Nickel performs a demethylation of the adsorbed hydrocarbons, breaking C-C bonds adjacent to terminal C atoms (3,62,63, 73,77). On the contrary, over ruthenium catalyst, all the C-C bonds of a straight chain hydrocarbon have an equal chance of being broken. Furthermore, tertiary C atoms are more easily attacked by nickel and cobalt than by ruthenium, which explains why during hydrogenolysis of

isopentane, more  $n\text{-C}_4\text{H}_{10}$  than  $i\text{-C}_4\text{H}_{10}$  is formed over nickel and cobalt (74). However, Ru (60) breaks the bonds at the straight end of this branched alkane, making more  $i\text{-C}_4\text{H}_{10}$  than  $n\text{-C}_4\text{H}_{10}$ . Furthermore, methyl groups are not easily removed from quaternary atoms as found in experiments with 2,2-dimethylbutane and neopentane (73).

### 1.2.2 Intermediate Species

Intermediate species for hydrogenolysis are usually linked by 2 C atoms to the metal active sites. Based on deuterolysis experiments over evaporated Fe films, Dowie et al. (33,34) suggested that  $\alpha,\gamma$ -adsorption (1st and 3rd C atoms) is irreversible and leads to complete breaking of the hydrocarbons to methane since no  $\alpha,\gamma$ -exchanged products are found from  $\text{D}_2$  exchange of  $\text{neo-C}_5\text{H}_{12}$ . Furthermore, deuterium exchange reactions would involve different intermediates:  $\alpha$ -,  $\alpha,\alpha$ - and  $\alpha,\beta$ -adsorbed species.

The lower rate of hydrogenolysis of ethane over group VIII metals, compared to higher molecular weight hydrocarbons, could be explained by the impossibility for  $\text{C}_2\text{H}_6$  of forming  $\alpha,\gamma$ -adsorbed species (5,34). Double bonds could also be formed between a metal site and one of the C atoms:  $\alpha,\alpha,\beta$ -adsorbed species from  $\text{C}_2\text{H}_6$  and  $\alpha,\alpha,\gamma$ -species from heavier hydrocarbons (20,75).

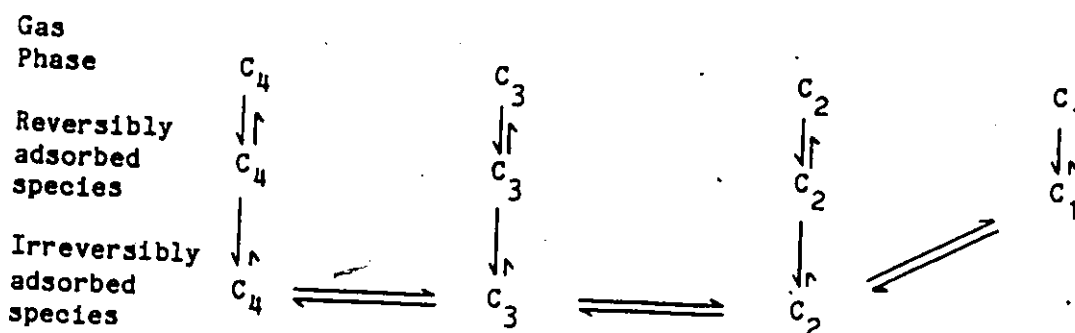
Hydrogenolysis of cyclic compounds usually involves  $\pi$ -adsorbed species as intermediates (5,63,75).

### 1.2.3 Reaction Mechanism

Since most products were completely exchanged with  $\text{D}_2$  during

deuterolysis experiments over Fe catalysts, desorption of hydrocarbon species was assumed by Dowie et al. (34) to be the rate limiting step. On nickel or ruthenium catalysts, Kempling and Machiels found that C-C bond splitting was the slowest step, based on estimation of parameters in selectivity equations derived from reaction networks (60,72,73). For cobalt, the C-C bond splitting was slightly faster than product desorption.

Dowie et al. (34) suggested a reaction mechanism for Fe catalysts, that takes account of 2 types of adsorbed species: reversibly chemisorbed, which could undergo deuterium exchange and irreversibly chemisorbed in the  $\alpha,\alpha,\gamma$ -position, which could be hydrocracked to smaller species. The following diagram describes the reaction mechanism applied to normal butane.



The rate of a given reaction is related to the length of the corresponding arrow. According to this mechanism, a species which undergoes C-C bond splitting is therefore broken completely into methane while an adsorbed species that is not irreversibly adsorbed, remains on the surface of the catalyst long enough for complete deuterium exchange (32). These workers suggested also  $CH_4$  desorption as the rate limiting

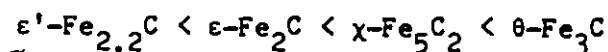
step in hydrogenolysis reactions over iron catalysts.

### 1.3 Changes in Catalyst Composition

Review of the literature on iron-catalyzed reactions shows that reduced catalysts may change composition, oxidize, nitride or carbide during reaction; carbiding is discussed in this section.

Iron catalysts prepared from reduction of fused magnetite are usually converted during hydrogenation of carbon monoxide, into Hägg carbide,  $\text{Fe}_5\text{C}_2$  and iron oxide,  $\text{Fe}_3\text{O}_4$  (7,9,36). Similar results were obtained by Matsumoto and Bennett (79) during transient experiments. The temperature of the reaction determines the iron carbide produced.

Niemantsverdriet et al. (87) gave the following list of carbides in order of increasing temperature of formation:



Cementite,  $\theta-\text{Fe}_3\text{C}$ , cannot be formed at temperature less than  $350^\circ\text{C}$  during Fischer-Tropsch synthesis. The authors also suggested that the relative stability of these carbides is directly related to their formation temperature, which is lower for the less stable ones.

The nature of the carbides formed in supported iron catalysts can be different at a given temperature from those in bulk catalysts. Amelse et al. (2) identified  $\epsilon'-\text{Fe}_{2.2}\text{C}$  in a silica-supported Fe catalyst after reaction in a  $3 \text{H}_2 : 1 \text{CO}$  gas mixture at  $255^\circ\text{C}$ . Raupp and Delgass (90) suggested that the carbide composition depended on the average particle size and that smaller particles favor less stable carbides,  $\epsilon-\text{Fe}_2\text{C}$  and  $\epsilon'-\text{Fe}_{2.2}\text{C}$ . In their experiments at  $250^\circ\text{C}$ , the Fe catalyst



with less than 6.1 nm diameter crystallites, contained only  $\epsilon'$ -Fe<sub>2.2</sub>C while the catalyst with 10 nm particles became  $\chi$ -Fe<sub>5</sub>C<sub>2</sub>.

Finally, Le Caër et al. (66) reviewed in a recent paper the different Fe carbides formed during FT synthesis, using Mössbauer spectroscopy data.

The presence of iron carbides in the catalyst during CO hydrogenation led Fischer and Tropsch (40) as well as Craxford and Rideal (28) to propose them as intermediates in the formation of long chain hydrocarbons.

#### 1.4 Catalyst Poisoning

Craxford (29) observed that 60% of the wax deposited on the surface of a cobalt catalyst during 3 weeks of CO hydrogenation, could be removed in less than 3 hours when the feed composition is changed from a 2 H<sub>2</sub>: 1 CO mixture to pure H<sub>2</sub>. Furthermore, workers at the Bureau of Mines (54) found that hydrogenation of carbon monoxide over ruthenium produces CH<sub>4</sub> and higher hydrocarbons, up to wax, while only CH<sub>4</sub> is obtained from CO<sub>2</sub> hydrogenation over the same metal, which is a good hydrogenolysis catalyst (114). These results suggest that carbon monoxide inhibits the hydrogenolysis of hydrocarbons.

#### 1.5 Aims of the Present Research

The present thesis investigates the hydrogenolysis of alkanes over iron catalysts and more precisely the reasons behind the very high production of methane with Fe, compared to other group VIII transition

metals. Experimental conditions like the conversion of the reactant, the hydrocarbon to hydrogen feed ratio and the molecular weight of the initial alkane, were varied to study how selectivities for  $\text{CH}_4$  and for other hydrocarbon products are modified by them. The experimental data were fitted to power rate expressions and to selectivity equations derived from reaction networks where no rate determining step was assumed. Characterization of the used catalysts was done for detection of changes in composition during reaction. Hydrogenolysis reactions were also studied over carbided Fe catalysts. The influence of poisons like CO and  $\text{H}_2\text{O}$  was examined in relation to the selectivity and the rate of the reaction. All the data collected during these experiments were used to elucidate the mechanism of hydrogenolysis of hydrocarbons over Fe catalysts.

## CHAPTER 2

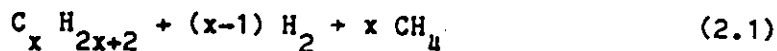
### THERMODYNAMIC CONSIDERATIONS

Thermodynamic calculations can predict all of the possible products from a set of reactants. These studies are useful to discriminate between products which are possible and those which are not.

Table 2.1 gives values for hydrocarbons of the Gibbs free energy of formation,  $\Delta G_f^\circ$ , at temperatures varying between 400 and 800 K. In this table,  $\Delta G_f^\circ$ 's for hydrogen and graphite,  $C_g$ , are assumed to be equal to 0.0. Equilibrium constants,  $K_e$ , and changes in Gibbs free energy,  $\Delta G^\circ$ , which are calculated for a given reaction, indicate the operating conditions at which this reaction is possible.

#### 2.1 Hydrogenolysis Reactions

For hydrogenolysis of alkanes, the breaking of all C-C bonds to form only  $CH_4$  is the most thermodynamically favourable reaction since its  $\Delta G^\circ$  is the smallest:



Furthermore, if splitting of C-C bonds occurs sequentially, one bond at a time, the demethylation reaction is strongly favoured,  $CH_4$  having the lowest  $\Delta G_f^\circ$  among all hydrocarbons. Similarly,  $CH_4$  would be the only hydrocarbon product from CO hydrogenation if equilibrium occurred between all species, as shown by thermodynamics calculations of Lee et al. (68).

TABLE 2.1  
Free Energies of Formation,  $\Delta G_f^\circ$ , in kcal/mole (112).

Compound	400 K	500 K	600 K	700 K	800 K
CH <sub>4</sub>	-10.07	-7.85	-5.51	-3.06	-0.56
C <sub>2</sub> H <sub>6</sub>	-3.45	1.16	5.96	10.90	15.91
C <sub>2</sub> H <sub>4</sub>	17.69	19.25	20.92	22.68	24.49
C <sub>3</sub> H <sub>8</sub>	1.19	8.23	15.50	22.93	30.45
n-C <sub>4</sub> H <sub>10</sub>	5.10	14.55	24.27	34.19	44.21
1-C <sub>4</sub> H <sub>10</sub>	4.58	14.39	24.48	34.75	45.13
1-C <sub>5</sub> H <sub>12</sub>	8.21	20.25	32.61	45.18	57.87
n-C <sub>16</sub> H <sub>34</sub>	58.23	97.08	136.74	176.96	217.46
H <sub>2</sub> O	-53.52	-52.36	-51.16	-49.92	-48.65
CO	-35.01	-37.19	-39.36	-41.53	-43.68
CO <sub>2</sub>	-94.33	-94.39	-94.45	-94.50	-94.54
Ni <sub>3</sub> C <sup>a</sup>	7.91	7.127	4.653	—	—
Fe <sub>5</sub> C <sub>2</sub> <sup>a</sup>	3.866 <sup>b</sup>	3.821	3.458	3.140 <sup>c</sup>	—
Fe <sub>3</sub> C <sup>a</sup>	4.043	3.461	2.82	2.16	—

Note:  $\Delta G_f^\circ$  for C (graphite) and H<sub>2</sub>, is taken as 0.0.

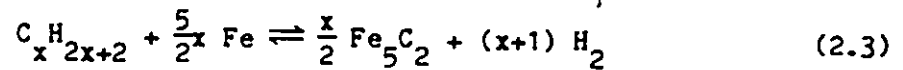
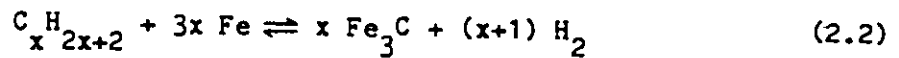
a) from reference (8).

b) at 450 K.

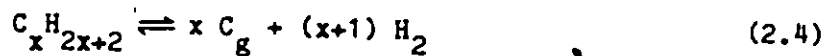
c) at 650 K.

## 2.2 Formation of Iron Carbides

Hägg carbide,  $\text{Fe}_5\text{C}_2$ , and cementite,  $\text{Fe}_3\text{C}$ , are included in the thermodynamics calculations because they can be formed during hydrogenolysis reactions, as shown in the following equations (where  $x$  is an integer equal to 1, 2, 3 or more):



Calculations were also done for the possible formation of elemental carbon according to



Once  $\Delta G^\circ$  is calculated, the equilibrium constant,  $K_e$ , is obtained from

$$K_e = e^{-\frac{\Delta G^\circ}{RT}} \quad (2.5)$$

$K_e$  is also equal to the ratio of partial pressures of  $\text{H}_2$  and hydrocarbon, which for equations 2.2, 2.3 and 2.4, is

$$K_e = \frac{[\text{H}_2]^{x+1}}{[\text{C}_x\text{H}_{2x+2}]} \quad (2.6)$$

or

$$K_e = \frac{(P_T y_H)^{x+1}}{(P_T y_C)} = \frac{P_T^x y_H^{x+1}}{y_C} \quad (2.7)$$

At a given temperature, this becomes

$$\frac{y_H^{x+1}}{1 - y_H} = \frac{1}{P_T^x} e^{-\frac{\Delta G^\circ}{RT}} = A \quad (2.8)$$

which can be written

$$y_H^{x+1} + A y_H - A = 0 \quad (2.9)$$

The variable  $y_H$  in equation 2.8 represents the minimum  $H_2$  mole fraction in the feed mixture above which formation of Fe carbides or of elemental C is not possible. As shown in equation 2.8,  $y_H$  is dependent on temperature and total pressure.

Table 2.2 gives values of  $y_H$  for a system involving  $H_2$  and  $C_3H_8$  at a total pressure of 128 kPa. If the hydrocarbon reactants are  $i-C_5H_{12}$  or  $n-C_{16}H_{34}$ , the minimum  $H_2$  partial pressure will be even larger. The hydrogen to hydrocarbon feed ratios used in our experiments, which varied between 0.8 and 10.0, were therefore too low to prevent carburization of the catalyst, according to Table 2.2.

However, the equilibrium conditions are quite different if  $CH_4$  is the hydrocarbon reactant in equations 2.2, 2.3 and 2.4. The minimum  $H_2$  mole fraction,  $y_H$ , for reaction at  $325^\circ C$ , is about 0.0266 to prevent formation of cementite, 0.042 for Hägg carbide, and 0.0842 for elemental carbon. These values increase with reaction temperature. They also indicate that the mole fraction of  $CH_4$  has to be very large to carburize the catalyst, as observed by Browning et al. (16). Therefore, hydrogenation of the carbidic phases is expected from the thermodynamics calculations involving  $CH_4$  while the opposite is favoured by the presence of higher hydrocarbons.

TABLE 2.2

Minimum Mole Fraction of Hydrogen to Avoid Formation of Carbides and Graphite during Hydrogenolysis at 128 kPa.

I Hydrogenolysis of $C_3H_8$		
	<u>327°C</u>	<u>355°C</u>
$Fe_3C$	.994777 (190.4) <sup>a</sup>	.999351 (1539)
$Fe_5C_2$	.999655 (2895)	.999937 (1.59 x 10 <sup>4</sup> )
$C_g$	.999995 (2.22 x 10 <sup>5</sup> )	.999999 (8.03 x 10 <sup>5</sup> )
II Hydrogenolysis of $i-C_5H_{12}$		
	<u>327°C</u>	
$Fe_3C$	.999 999 44 (1.80 x 10 <sup>6</sup> ) <sup>b</sup>	
$C_g$	.999 999 999 999 6 (2.385 x 10 <sup>11</sup> )	

a) Feed ratio of  $H_2$  to propane.

b) Feed ratio of  $H_2$  to isopentane.

Thermodynamics calculations also show that decomposition of Hägg carbide and cementite to  $\alpha$ -Fe and elemental carbon is possible, at the reaction temperature.

### 2.3 Magnetic Properties

Transition metals, like Fe, Co and Ni, are considered ferromagnetic because they are formed of small domains which are spontaneously magnetic. This magnetism arises from the interatomic exchange interactions which act to align parallel to each other and in the same direction, all the atomic magnetic moments which originate from the spinning of unpaired electrons of their d-shell orbitals and from the rotation of these electrons around the atomic nuclei. When a block of ferromagnetic metal is placed in a magnetic field of sufficient magnitude, all the spins are aligned in the same direction and magnetization is maximum for a given temperature (25,96). Table 2.3 gives magnetic properties for some group VIII metals as well as for iron carbides. Variations in the magnetic moment at a given temperature may indicate changes in the number of unpaired electrons.



TABLE 2.3  
Magnetic Properties

	Curie Temperature (°C)	Magnetic moment <sup>a</sup> (Bohr Magnetron) Metal Atom	Specific magnetization <sup>a</sup> (emu/mole)
$\alpha$ -Fe (b.c.c.)	770 <sup>c,f</sup>	2.2 $\mu_B$ <sup>d,e</sup>	12,180 <sup>e,f</sup>
$\alpha$ -Co <sup>b</sup> (h.c.p.)	797-877 <sup>e</sup> 857	1.7 $\mu_B$ <sup>d,e</sup>	9,430 <sup>e,f</sup>
$\beta$ -Co <sup>b</sup> (f.c.c.)	1100 <sup>c</sup> 1115 <sup>f</sup>		
Ni (f.c.c.)	353-360 <sup>c</sup>	0.6 $\mu_B$ <sup>d,e</sup>	3,210 <sup>e,f</sup>
$\theta$ -Fe <sub>3</sub> C (orthorhombic)	208 <sup>d</sup> 210 <sup>f</sup>	1.5 $\mu_B$	24,960 <sup>f</sup>
$\epsilon$ -Fe <sub>2</sub> C (h.c.p.)	380 <sup>f</sup>	1.6 $\mu_B$	17,320 <sup>f</sup>
$\epsilon'$ -Fe <sub>2.2</sub> C	450 <sup>f</sup>		
FeC	250 <sup>f</sup>		
$\chi$ -Fe <sub>5</sub> C <sub>2</sub> (Hägg) (monoclinic)	252 <sup>g</sup>	1.5 $\mu_B$	42,460 <sup>f</sup>

a) measured at room temperature.

b)  $\alpha$ -Co is stable at  $T < 440^\circ\text{C}$ , and  $\beta$ -Co at  $T > 440^\circ\text{C}$ .

c) from (39).

d) from (12).

e) from (21).

f) from (52).

g) from (90).

## CHAPTER 3

### EXPERIMENTAL

This chapter is divided into 3 sections which present the experimental set-up, the catalyst preparation and the operating procedures. A list of materials, including reactants and calibration gases, is given in Table 3.1.

#### 3.1 Experimental Set-Up

This section describes the main elements of the experimental set-up: the differential reactor, the recycle system, the feed system and the analytical system, which are shown in Figure 3.1.

##### 3.1.1 Differential Reactor

The differential reactor, 1 in Figure 3.1, was made of a cylindrical aluminium block (20 cm long, 15 cm O.D.) which has been drilled at its centre for a 39 cm long stainless steel tube (0.75 cm I.D.). A smaller tube was inserted in this tube to hold a 200-mesh stainless steel gauze covered with glass wool supporting 1 to 3 grams of catalyst. Glass beads (3 mm O.D.) were placed above the catalyst bed to form a preheating-mixing zone in the reactor. Six holes were drilled half-way between the centre and the edge of the block, at equal intervals, and six 15-cm long 250 W cartridge heaters were installed in these holes for a total output of 1500 W. The reactor temperature

TABLE 3.1

## Materials

	<u>Grade and Purity</u>	<u>Suppliers<sup>a</sup></u>
A) Reactants		
Hydrogen	UHP, 99.999%	1,2
Propane	Instrument, 99.5%	1,2
Isobutane	Instrument, 99.5%	1,2
Isopentane	99+%	4
Hexadecane	99%	4
Carbon monoxide	CP, 99.5%	1
B) Inert Gases		
Argon	Prepurified, 99.998%	2,3
Helium	UHP, 99.999%	1
C) Calibration		
Methane	UHP, 99.97%	1,2
Ethane	CP, 99.0%	1
n-butane	CP, 99.0%	1
Ethylene	CP, 99.5%	1
D) Carrier gases		
Argon	Prepurified, 99.998%	2,3
Hydrogen	Prepurified, 99.95%	2,3

- a) Suppliers: 1) Matheson  
 2) Canadian Liquid Air  
 3) Linde  
 4) Aldrich Chemical Co., Milwaukee, Wisconsin.

measured by a chromel-alumel thermocouple at the centre of the catalyst bed, was regulated with an electronic proportional controller, 3, Model NER 910 JT K2C, manufactured by United Electric Controls Company, Watertown, Massachusetts. This controller kept the temperature constant to within  $0.1^{\circ}\text{C}$ . A Variac, 4, reduced the power output of the cartridge heaters, if necessary. A back-pressure regulator Fairchild-Hiller, 5, maintained the reactor pressure at about 128 kPa.

In experiments where surface characterization by Auger electron spectroscopy was necessary, a  $14.3 \times 4.8 \times 0.127$  mm Fe foil was placed in the reactor, near the catalyst bed and was held with a stainless steel wire spotwelded on the thermocouple. Iron foils, 99.99% pure, were obtained from Alfa, Danvers, Massachusetts.

### 3.1.2 Recycle System

To keep rate and selectivity differential in tests at high conversions, the reactor was coupled to a recycle system with a metal bellows pump, 2, Model MB-41, supplied by Metal Bellows Corporation, Sharon, Massachusetts. This pump which has stainless steel bellows and check valves, is leaktight and maintenance free. Furthermore, no pulsations were noticed in the flow rate since the volume of the pump was small (less than  $4 \text{ cm}^3$ ) and its operating speed, very high, 3000 pulses per minute. The flow rate varied between 3 to 4.5 l/min depending on the pressure in the system and the opening of the recycle by-pass.

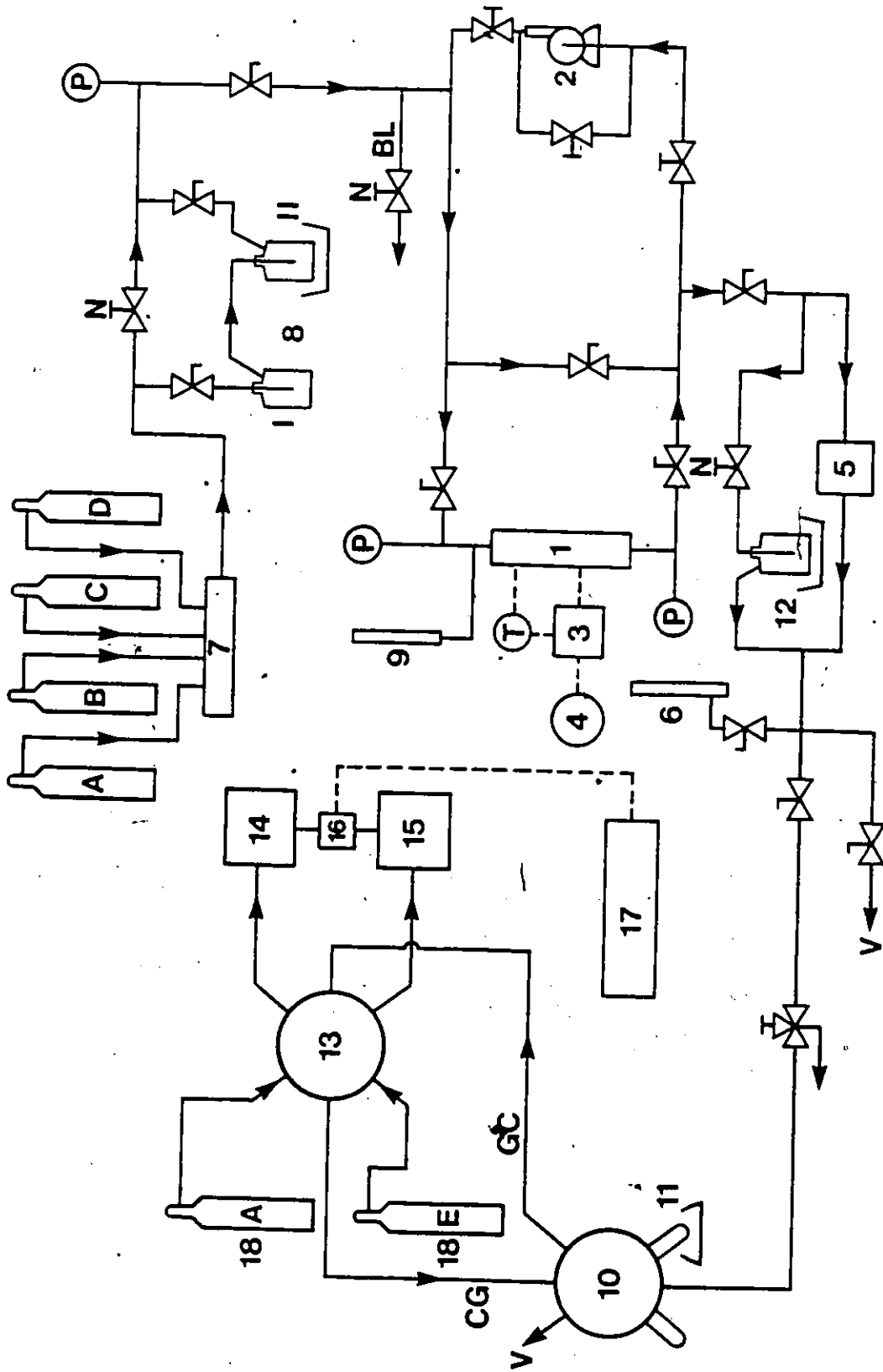


Figure 3.1: Diagram of the experimental set-up. Legend on the next page.

LEGEND OF FIGURE 3.1

1. Differential reactor
2. Metal bellows pump
3. Temperature controller
4. Variac
5. Back-pressure regulator
6. Bubble flow meter
7. Electronic mass flow controller
8. Saturator, combining an evaporator (I) and a trap at 0°C (II)
9. Multispeed transmission pump for syringe
10. Sampling valve (8-port)
11. Trap in liquid nitrogen bath (if necessary)
12. Trap in dry ice-acetone bath (if necessary)
13. Switching valve (6-port)
14. Gas chromatograph for H<sub>2</sub> analysis
15. Gas chromatograph for hydrocarbon analysis
16. Switch box for output signal from GC's
17. Integrator-recorder
18. Carrier gas

BL: Bleeding line

CG: Carrier gas for gas chromatograph

GC: Line going to gas chromatograph

A: Hydrogen

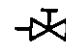
B: Propane or isobutane


C: Carbon monoxide

D: Helium or argon

E: Argon

V: Vent

 Valve

 Needle valve

 Toggle valve

 Pressure gauge or Hg manometer

 Thermocouple

### 3.1.3 Feed System

The flows of the feed gases, like  $H_2$ ,  $C_3H_8$  and CO, were set with an electronic mass flow controller, 7, Model 8249, supplied by Matheson Gas Product, East Rutherford, New Jersey. Gases could be delivered accurately in the 0-500  $cm^3$  (STP)/minute range, at outlet pressures up to 1000 kPa. CO was passed through a heated tube to decompose the Fe carbonyls that may be present.

The other hydrocarbon reactants, isopentane,  $i-C_5H_{12}$ , and hexadecane,  $n-C_{16}H_{34}$ , are liquid at room temperature. Since the boiling point of  $i-C_5H_{12}$  is quite low ( $28^\circ C$ ), a device, 8, was built to saturate  $H_2$  with  $i-C_5H_{12}$ . The saturator, as shown in Figure 3.2, is divided into 2 sections: an evaporator (I), where  $i-C_5H_{12}$  saturated  $H_2$  at room temperature, and a cold trap (II) in an ice-water bath, where excess  $i-C_5H_{12}$  condensed. To increase contact between gaseous and liquid phases, small glass tubes were placed inside the saturator. Pressure drops were negligible. Furthermore, the reactants were not contaminated by any foreign matter, like grease, in this all glass and metal apparatus. The saturator was reversible, the trap becoming the evaporator and vice-versa: this permitted using it for long periods of time before adding isopentane. Since the vapour pressure of  $i-C_5H_{12}$  at  $0^\circ C$  is 257 mm Hg, as calculated with Antoine equation, the feed ratio, FR, was set to about 2.8  $H_2$ : 1  $i-C_5H_{12}$ . To increase FR,  $H_2$  was partly diverted from the saturator with a by-pass. During experiments on water poisoning of hydrogenolysis of  $C_3H_8$ , the saturator was filled with water and a mixture of  $C_3H_8$  and  $H_2$  bubbled through it.

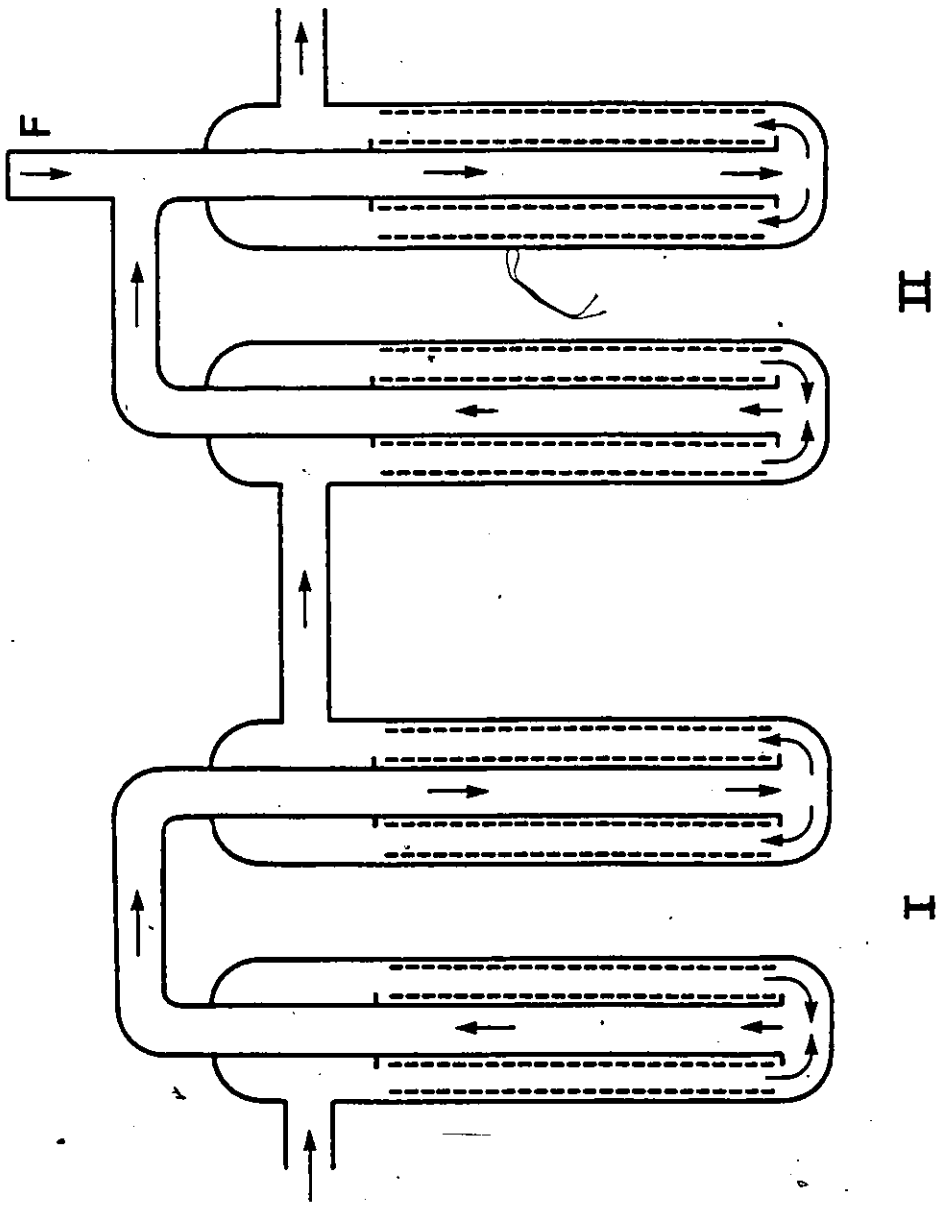


Figure 3.2: Reversible saturator (I = evaporator, II = cold trap, F = feed inlet).

6



Hexadecane was injected directly in the reactor, above the preheating zone of glass beads, with a 30 cm<sup>3</sup> gastight syringe, Model BD-Multifit, from Becton, Dickinson and Co., Rutherford, New Jersey. Due to the high temperature in the reactor, the liquid hydrocarbon vapourized instantly. A Multispeed Transmission pump, 9, from Harvard Apparatus Co. displaced the plunger to keep a constant flow out of the syringe. Twelve different settings permitted varying the liquid flow rate in discrete steps from 0.00494 to 24.7 cm<sup>3</sup>/min. Calibrated flow rates were within 3.8% of the stated values.

#### 3.1.4 Analytical System

Analysis of the reactant and product gases was done with 2 gas chromatographs, using thermal conductivity cell detector, 14 and 15. Models 90-P and 920, built by Varian, Palo Alto, California. Hydrocarbons were separated in one of them, with a 2-meter long column packed with Porapak-Q (50-80 Mesh), using hydrogen as carrier gas because its thermal conductivity (471  $\mu\text{cal}/\text{sec}\cdot\text{cm}\cdot^{\circ}\text{C}$  at 40<sup>o</sup>C) is ten times higher than that of hydrocarbons (119). The second gas chromatograph separated H<sub>2</sub> from hydrocarbons, with a 80-cm long column packed with coconut charcoal (48-65 Mesh) using argon as carrier gas since its thermal conductivity (46  $\mu\text{cal}/\text{sec}\cdot\text{cm}\cdot^{\circ}\text{C}$ ) is very different from that of H<sub>2</sub>. Table 3.2 gives the settings for the 2 gas chromatographs.

A sampling device had to be designed to complete this analytical set-up. It consisted of 2 precision valves placed in series and manufactured by Carle Instruments, Inc., Anaheim, California. One was a

TABLE 3.2  
Settings of Gas Chromatographs

Analysis

- A) Hydrogen.
- B) Hydrocarbons in hydrogenolysis of isopentane.
- C) Hydrocarbons in hydrogenolysis of hexadecane.
- D) Hydrocarbons in hydrogenolysis of propane.
- E) Hydrocarbons in CO poisoning experiments.

	<u>A</u>	<u>B</u>	<u>C</u>	<u>D</u>	<u>E</u>
Temperature (°C)					
Injector	150	182	225	172	190
Detector	152	182	245	185	241
Column	98	153	205	111	67
Carrier Gas Flowrate (cm <sup>3</sup> /min)	105	60	60	82	135
Filament Current (mA)	100	200	200	200	200

sampling valve, 10, Model 2013, and the other, a switching valve, 13, Model 5521. The microvolume sampling valve, SV, had 8 ports and 2 sampling loops. While the gas sample in loop I was injected in the GC, loop II was filled by outlet gases, and vice-versa. This system did not limit the frequency of injections. With the 6-port switching valve, 13, H<sub>2</sub> or Ar was supplied to SV, as carrier gas for analysis of hydrocarbons or hydrogen. Between the reactor and the gas sampling device, there was a 3-way ball valve from Whitey, Oakland, California, which was opened before injection of a sample to decrease the pressure inside the loop to atmospheric level, for reproducibility in the GC analysis, on a daily basis.

The SV loops were put in a liquid nitrogen bath to accumulate hydrocarbon products which were in too small concentrations in the gas samples taken at room temperature. The vapour pressure of most hydrocarbons at -195°C is practically equal to 0.0 as shown in Table 3.3.

A 3-meter long copper tube (6.35 mm O.D.) was placed between the switching valve and the GC for hydrocarbon analysis to eliminate the pressure surge due to the injection of large gas samples, collected at -195°C.

A 3-way switch, 16, permitted sending the electrical signals from the GC detectors to an integrator-recorder, 17, HP-3380, from Hewlett-Packard, Cupertino, California. This integrator gave accurate values of the area of each GC peak which corresponds to a given component in the gas sample. These readings were easily converted to mole fractions with the calibration factors of each compound.

TABLE 3.3

## Physical Properties of Hydrocarbons (91).

Hydrocarbon	Melting Point (°K)	Boiling Point (°K)	Vapour Pressure (kPa)	
			At 77.4 K <sup>a</sup>	At 195 K <sup>b</sup>
CH <sub>4</sub>	90.7	111.7	1.53	-
C <sub>2</sub> H <sub>6</sub>	89.9	184.5	1.49x10 <sup>-5</sup>	-
C <sub>3</sub> H <sub>8</sub>	85.5	231.1	4.20x10 <sup>-10</sup>	50.93
i-C <sub>4</sub> H <sub>10</sub>	113.6	261.3	1.89x10 <sup>-14</sup>	11.50
n-C <sub>4</sub> H <sub>10</sub>	134.8	272.7	3.61x10 <sup>-16</sup>	6.263
i-C <sub>5</sub> H <sub>12</sub>	113.3	301.0	-	1.371
n-C <sub>5</sub> H <sub>12</sub>	143.4	309.3	-	.8159
n-C <sub>6</sub> H <sub>14</sub>	177.8	342.0	-	.1051
n-C <sub>7</sub> H <sub>16</sub>	182.6	371.7	-	1.32x10 <sup>-2</sup>
n-C <sub>8</sub> H <sub>18</sub>	216.4	398.9	-	1.55x10 <sup>-3</sup>
n-C <sub>9</sub> H <sub>20</sub>	219.7	424.1	-	1.66x10 <sup>-4</sup>
n-C <sub>10</sub> H <sub>22</sub>	243.5	447.4	-	1.56x10 <sup>-5</sup>
n-C <sub>11</sub> H <sub>24</sub>	247.6	469.2	-	1.35x10 <sup>-6</sup>
n-C <sub>12</sub> H <sub>26</sub>	263.6	489.6	-	-
n-C <sub>13</sub> H <sub>28</sub>	267.8	508.7	-	-
n-C <sub>14</sub> H <sub>30</sub>	279.1	526.8	-	-
n-C <sub>15</sub> H <sub>32</sub>	283.1	543.9	-	-
n-C <sub>16</sub> H <sub>34</sub>	291.1	560.1	-	-

a) Boiling point of liquid nitrogen.

b) Temperature of dry ice-acetone sludge.

Some modifications were made to the experimental set-up to collect the heavier products obtained during hydrogenolysis of hexadecane. As shown in Figure 3.1, a by-pass was built around the back-pressure regulator and a needle valve was used to control the reactor pressure at about 125 kPa. Downstream, a trap, 12, in a dry ice-acetone bath, collected all the liquid products. Special attachments permitted changing the glass bulb of the trap in a few seconds. Tubes and valves between the reactor, 1, and the cold trap, 12, were wrapped with heating tapes to prevent condensation of heavy hydrocarbons in the line. A thermocouple placed inside one of these tubes recorded temperatures of about 120°C.

The liquid products collected at -78°C were analyzed in the Department of Chemistry by gas chromatography and mass spectrometry, GC-MS, courtesy of Prof. M. Quilliam. Hydrocarbons in the C<sub>7</sub>-C<sub>16</sub> range were separated by temperature-programmed chromatography (from 30° to 220°C, at a rate of 4°C/min) with a 50 m x 32 mm ID capillary column coated with DB-5 (0.1 µm), which is a polar stationary phase made of silicone rubber with vinyl, phenyl and methyl groups. Injection of samples was done on-column. A mass spectrometer was used to identify the hydrocarbon corresponding to each GC peak. More details on GC-MS are found in Appendix C.

### 3.2 Catalysts

Hydrogenolysis of hydrocarbons was studied over reduced Fe and Fe carbides prepared from commercial NH<sub>3</sub> synthesis catalyst, D-3001, made

of fused magnetite promoted with 4.61 wt % MgO, 0.65% Cr<sub>2</sub>O<sub>3</sub>, 0.57% K<sub>2</sub>O and 0.71% SiO<sub>2</sub> (7). The particles of D-3001 were crushed and sieved in the 14-28 mesh or 1.19-0.595 mm range. Chen et al. (23) characterized D-3001 by electron probe microanalyzer and found that the catalyst was not homogeneous on a scale of microns. Iron crystallites were separated by bands containing mainly potassium and silica. Magnesium was dispersed throughout the catalyst as well as chromium.

Reduction of the fused magnetite was done for 45 hours at 450°C with a H<sub>2</sub> hourly space velocity of about 1000. During this operation, pores were formed by removal of oxygen atoms with hydrogen. The catalyst surface area measured by volumetric gas adsorption method, was about 11.2 m<sup>2</sup>/g, similar to values published in the literature (99). The average pore diameter was about 350 Å.

Pre-carbided catalysts were also used for hydrogenolysis experiments. Hägg carbide,  $\chi$ -Fe<sub>5</sub>C<sub>2</sub>, was prepared in a Pyrex U-shape tube containing a known weight of magnetite and glass beads. The tube was placed in an electric furnace and purged with H<sub>2</sub>. Reduction proceeded as described earlier. Carbon monoxide was then passed over the catalyst at a hourly space velocity of about 100, according to a method developed by Shultz et al. (98). The furnace temperature was slowly increased from 250 to 330°C, at a rate of about 10°C/hour. Concentration of CO in the outlet gases was monitored by gas chromatography and kept at less than 5% to prevent catalyst oxidation. Carburization was stopped when enough C has been laid down on the catalyst to form Fe<sub>5</sub>C<sub>2</sub> based on the CO<sub>2</sub> production according to



The carbided catalysts were handled under  $\text{CO}_2$  and  $n\text{-C}_6\text{H}_{14}$  to prevent oxidation. The bulk composition of the pre-carbided catalysts was checked by Mössbauer spectroscopy, in the Department of Chemistry.

### 3.3 Operating Procedures

One to three grams of catalyst were placed in the reactor over glass wool and a stainless steel gauze supported by a small tube, and they were covered with 15 to 20 glass beads. Then, the reactor was placed in the experimental set-up and the equipment was tested for leaks by pressurizing at 200 kPa. When all leaks were eliminated, pressure was reduced to about 125 kPa and air was flushed out completely with  $\text{H}_2$ . The temperature controller and the variac were then connected to the reactor.

After reduction of the catalyst, the reactor temperature and the  $\text{H}_2$  flow rate were decreased to experimental conditions. Reaction temperatures were usually 325 to 355°C, and pressure was about 125 kPa.

In most experiments,  $\text{H}_2$  was passed overnight at low space velocity to keep the catalyst surface free from amorphous carbon, and to avoid rapid deactivation. In tests where the catalyst was characterized by Mössbauer spectroscopy or where hydrogenolysis was done over Fe carbides, the catalyst bed was kept under an inert atmosphere of flowing Ar or He.

The GC's were calibrated periodically with pure gases to obtain the response factors of the different compounds. Pure  $\text{H}_2$  and  $\text{CH}_4$  were

injected every morning to correct the response factors for daily variations. At the beginning of an experiment, a feed mixture was prepared, using the reactor by-pass. Once the desired composition of inlet gases was reached, the reactor was put on stream.

To obtain one data point, three gas samples, taken downstream from the reactor, were injected in the GC's: two samples, collected at room and liquid nitrogen temperatures, were analyzed for the composition of hydrocarbons and a third one, for the hydrogen fraction. The injection of the products trapped in a sampling loop at  $-195^{\circ}\text{C}$  was necessary for quantitative analysis of the intermediate hydrocarbons which were in trace amounts in the outlet gases, like  $n\text{-C}_4\text{H}_{10}$  and  $i\text{-C}_4\text{H}_{10}$  in hydrogenolysis of  $i\text{-C}_5\text{H}_{12}$ . The time for a complete analysis by gas chromatography of each data point was quite large: more than 50 minutes. The first 10 minutes of analysis were reserved to  $\text{H}_2$  separation, to complete flushing of argon from the carrier gas lines of the sampling valve and to stabilization on the baseline, of the electric signal of the GC for hydrocarbon analysis. The second injection was also done at room temperature and the analysis lasted up to 20 minutes depending on the size of the hydrocarbons being analyzed. For the third injection, the sampling loop was put in a liquid nitrogen bath for about 30 seconds, and then immersed in water to rapidly vapourize its content just after injection.

For each data point, the reactor temperature and pressure were recorded as well as the gas flow rate measured with a bubble flow meter, and the room temperature and pressure. These data were used for the



calculations of mole fractions, conversion, selectivities and reaction rate, as described in Appendix D.

In recycle operations, the metal bellows pump was first turned ON and the reactant mixture was prepared using the reactor by-pass. When the desired gas composition was obtained, the reactor was put on stream.

When the feed composition was changed during a test, the reaction was assumed to have reached steady state and the outlet stream, its final composition, only after a lapse of time allowing the flow through the system, of a volume of gas equal to 5 times the volume of the experimental set-up which was estimated by step input to about  $180 \text{ cm}^3$  without the recycle loop or  $245 \text{ cm}^3$  with it.

Values of the Thiele modulus (95b) were calculated to verify that the tests were performed at conditions free of mass or heat transfer limitations. The experimental rates which were used for the calculation gave Thiele modulus values less than 0.04, indicating that the kinetic data were really intrinsic data.

At the end of an experiment, the catalyst bed was cooled to room temperature in  $\text{H}_2$  or He and the reactor was removed from the experimental set-up while passing carbon dioxide through the tube. Hexane was then used to wet the catalyst before removing it from the reactor.

Bulk compositions of the used catalysts were obtained from Mössbauer spectroscopy, MS, in the Department of Chemistry. Auger electron spectroscopy, AES, was also used to identify Fe carbides or elemental C on Fe foils placed in the reactor during some tests (powder and small particles are not suitable for AES characterization). Details

on MS and AES are found in Appendices A and B.

In experiments with hexadecane, the catalyst bed was heated at the reaction temperatures and the flow rate of  $H_2$  was set to the desired  $H_2$ :  $C_{16}H_{34}$  feed ratio and reactant conversion. The electric motor displacing the syringe plunger was turned ON and  $n-C_{16}H_{34}$  was injected in the reactor. After a few drops of liquid products condensed in trap 12, the glass bulb in 12 was changed and heavy hydrocarbons accumulated in the trap placed in a dry ice-acetone bath. The same operating conditions were kept for two hours to collect enough liquid samples. The dry ice-acetone bath was then removed, the glass bulb changed and a gas chromatographic analysis of the outlet gases was made.

In poisoning experiments, CO was added to the gas mixture only after appearance of liquid in the cold trap. A sample was then taken one hour later as steady state was reached.

## CHAPTER 4

### REACTION NETWORKS AND SELECTIVITY EQUATIONS

This chapter is based on a paper published in the Journal of Catalysis (82). It describes a new scheme for deriving selectivity equations for a reaction network. Relatively simple equations can be obtained as long as the network has no reversible reaction steps. Isomerization reactions can be included in the network, provided that the isomerization can be regarded as being irreversible.

#### 4.1 Description of a Reaction Network

Workers in this laboratory have developed useful selectivity equations based on reaction networks for the hydrogenolysis of propane, butanes, isopentane, and hexanes (59,60,73,74) such as is given for isopentane in Figure 4.1. These selectivity expressions plus the rate equation for the parent hydrocarbon provide a complete description of the course of the reaction. The network analysis provides considerably more pertinent information on the system than can be obtained in other ways.

The following assumptions were made (59, 60, 73, 74):

- a. Hydrocarbon molecule  $C_x$  in the gas phase adsorbs reversibly on the surface of the catalyst to form adsorbed species  $A_x$ .
- b. Splitting of species  $A_x$  is irreversible, no chain growth is possible, and no isomerization occurs.

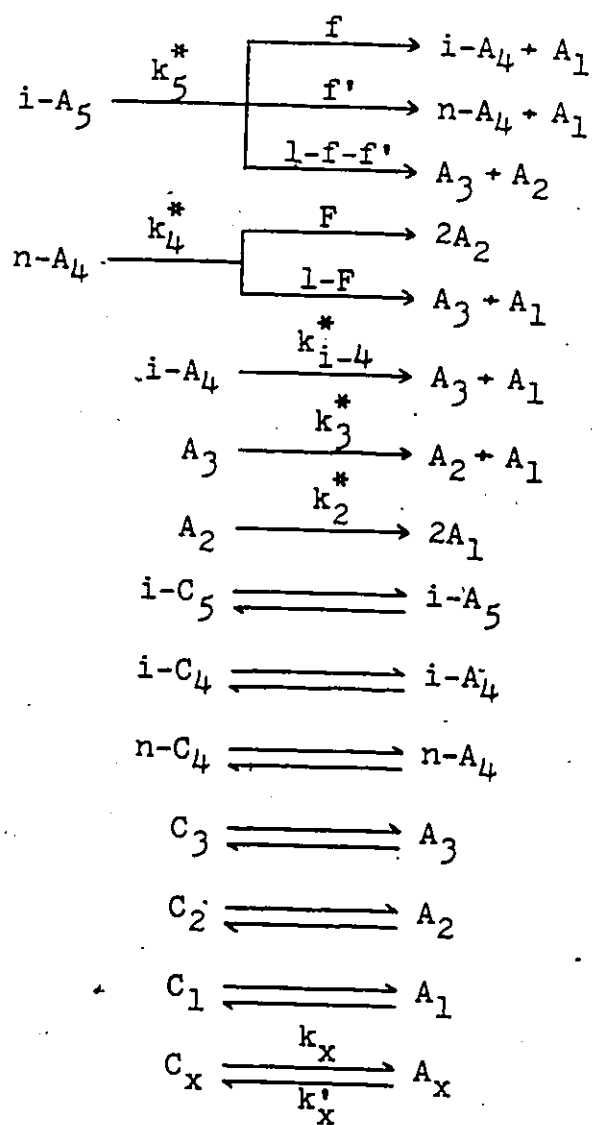


Figure 4.1 Reaction network for hydrogenolysis of isopentane.

c. Adsorption of hydrocarbons is first order in the gaseous hydrocarbons; splitting and desorption are first order in the adsorbed species.

d. Effects of the partial pressure of hydrogen on splitting and desorption are identical and the same for all  $A_x$  species.

Similarly, the  $H_2$  dependencies for the rate of adsorption of hydrocarbons are the same for all species.

e. No rate limiting step is assumed.

f. Only one carbon-carbon bond is split at a time.

The rate constants used in the reaction network are  $k_x$  for adsorption,  $k'_x$  for desorption and  $k_x^*$  for the irreversible breaking of C-C bonds. Splitting factors are probabilities of a molecule cracking at a particular C-C bond. As an example, iso- $A_5$  can be cracked into iso- $A_4$  and  $A_1$  with probability  $f$ , into n- $A_4$  and  $A_1$  with probability  $f'$  or into  $A_3$  and  $A_2$  with probability  $(1-f-f')$ .

The selectivity equation for a given product is derived from rate and mass balance equations for a differential reactor, and the selectivities are differential quantities defined for product P and reactant R as

$$S_P = -R_P/R_R \quad (4.1)$$

With this old-fashioned method, it is relatively easy to derive all the selectivity equations for the hydrogenolysis of propane or butane, but the derivation of networks for larger molecules are tedious, time consuming and chances of mistakes are large.

#### 4.2 A New Derivation of Selectivity Equations

A method for deriving selectivity equations is presented in this section. We also consider its application to networks involving isomerization. Mathematical derivation of the selectivity equation for product P by the old method indicates that  $S_P$  has the form:

$$S_P = \frac{Q_P \frac{k'_P}{k'_P + k^*_P}}{\left[1 + \frac{k''_P}{k''_R} \frac{X_R}{1 - X_R}\right]} \quad (4.2)$$

The ratio  $(k''_P/k''_R)$  compares the overall first order rate constants for product P and reactant R, respectively, which are defined the following way:

$$k''_x = k_x \frac{k^*_x}{k'_x + k^*_x} \quad (4.3)$$

The term  $Q_P$  represents the maximum amount of P formed by cracking of higher molecular weight hydrocarbons. The ratio  $(k'_P/(k'_P + k^*_P)) = j'_P$  measures the relative rates of cracking and desorption of adsorbed species P. If the rate controlling step is the surface splitting reaction, this parameter will be close to unity.

Equation 4.3 shows that any dependency on  $H_2$  for the overall rate constant  $k''_x$  is due to the adsorption step. Effects of  $H_2$  on splitting or desorption of  $A_x$  may cancel. Furthermore, in the selectivity equation, the dependency on  $H_2$  may cancel in terms like  $k''_P/k''_R$  and  $k'_P/(k'_P + k^*_P)$ .

The selectivity equation for  $CH_4$  becomes  $S_1 = Q_1$  since this molecule doesn't undergo cracking, and consequently,  $k'_1$  and  $k''_1$  are equal to 0.0.

In equation 4.2,  $Q_p$  is a summation of constants, the pertinent splitting factors, and of measurable variable quantities, the selectivities.  $Q_p$  equals the moles of P formed per mole of R consumed following the reaction network minus the moles of P produced if the observed intermediates react completely to P, as given by

$$Q_p = \left[ \begin{array}{l} \text{moles of P produced in} \\ R \rightarrow P \text{ for } X_{\text{int}} = 1 \end{array} \right] - \left[ \begin{array}{l} \text{moles of P produced in } J \rightarrow P \\ \text{for all J's for } X_{\text{int}} = 1 \end{array} \right]$$

where J denotes intermediates between R and P, and  $X_{\text{int}} = 1$  signifies that these intermediates react completely to P. The value of Q for a product of the  $N^{\text{th}}$  generation can be found by applying the algorithm of Figure 4.2.

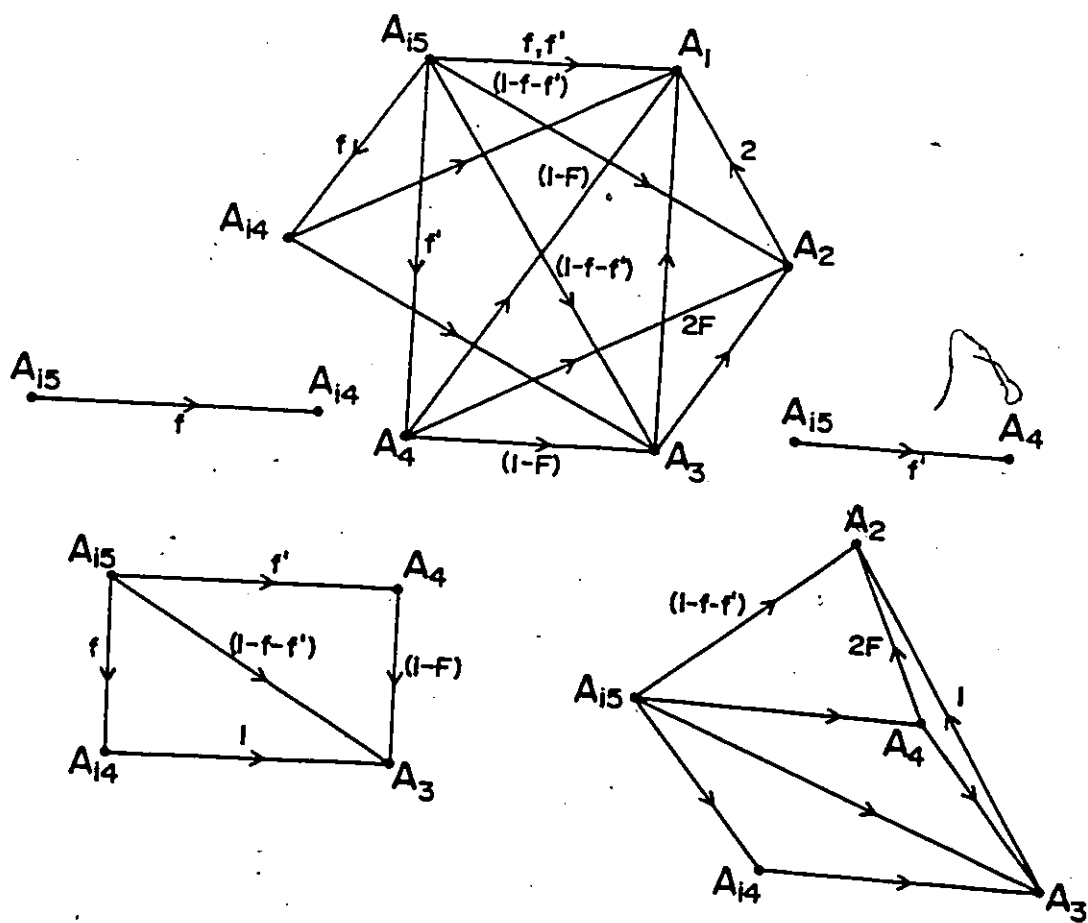
For example, isopentane can be split at 3 different bonds to give five products: iso-C<sub>4</sub>H<sub>10</sub>, n-C<sub>4</sub>H<sub>10</sub>, C<sub>3</sub>H<sub>8</sub>, C<sub>2</sub>H<sub>6</sub> and CH<sub>4</sub>. Figure 4.3 shows how to derive the Q factor for each selectivity equation. The pathways in Figure 4.3 represent all the possible ways of forming products, a genealogical tree for products. We find that  $Q_{14}$  is equal to the probability of cracking iso-C<sub>5</sub> to iso-C<sub>4</sub>,  $f$ , and  $Q_3$  is equal to the summation of probabilities of getting C<sub>3</sub> from reaction of iso-C<sub>5</sub> directly,  $(1-f-f')$ ; via n-C<sub>4</sub>,  $f'(1-F)$ ; and via i-C<sub>4</sub>,  $f$ .

Some correction terms are added to take account of the presence of n-C<sub>4</sub> and i-C<sub>4</sub> among the products,  $-(1-F)S_4 - S_{14}$ . The selectivity equations are given in Figure 4.4. These formula are easily derived. Furthermore, the value of Q can be explained physically as described with the algorithm.

$$\begin{aligned}
 Q_N &= \sum_{\text{All paths from } R \text{ to } I_N} \prod_{i=1}^N \left[ \begin{array}{l} \text{Probability factor in the } i^{\text{th}} \text{ reac-} \\ \text{tion of getting intermediate } I_i \\ \text{leading to product } I_N \end{array} \right] \\
 &= \sum_{\text{All paths from } I_i \text{ to } I_N} \left[ \begin{array}{l} \text{Selectivity of in-} \\ \text{termediate } I_i \text{ of} \\ \text{the } i^{\text{th}} \text{ reaction} \end{array} \right] \prod_{j=i-1}^N \left[ \begin{array}{l} \text{Probability factor in the} \\ j^{\text{th}} \text{ reaction of getting } I_j \\ \text{leading to product } I_N \end{array} \right]
 \end{aligned}$$

Figure 4.2: Algorithm for the calculation of the  $Q_N$  factor.





$$Q_{1-4} = f$$

$$Q_4 = f'$$

$$Q_3 = (1 - F)f' + f + 1 - f - f' - (1 - F)S_4 - S_{1-4}$$

$$Q_3 = 1 - Ff' - (1 - F)S_4 - S_{1-4}$$

$$Q_2 = (1 - F)f' + f + 1 - f - f' + 2Ff' + 1 - f - f' - S_3 - 2FS_4 - (1 - F)S_4 - S_{1-4}$$

$$Q_2 = 2 - f - f' + Ff' - S_3 - (1 + F)S_4 - S_{1-4}$$

Figure 4.3: Pathways for the derivation of Q factors for the hydrogenolysis of isopentane.

$$S_{i4} = M_{i4}f$$

$$S_{n4} = M_{n4}f'$$

$$S_3 = M_3(1 - S_{i4} - (1-F)S_{n4} - Ff')$$

$$S_2 = M(2 - S_{i4} - S_{n4}(1+F) - S_3 - f - f' + Ff')$$

$$S_1 = 5 - 2S_2 - 3S_3 - 4S_{n4} - 4S_{i4}$$

$$\text{where } M_h = \frac{\frac{k'_h}{(k'_{ih} + k'_h)}}{1 + \frac{k''_h}{k''_5} \frac{X_5}{(1 - X_5)}}$$

Figure 4.4: Selectivity equations for the hydrogenolysis of isopentane.

Numerical values of the parameters can be found by non-linear regression of experimental data. These parameters usually predict all the selectivity curves accurately. The splitting factors and the ratios of constants forming a given parameter, sometimes cannot be separated and their values cannot be found. In all cases, the ratio  $(k_p^n/k_R^n)$  is uniquely determined and values of  $k_p^i/(k_p^i + k_p^*)$  are obtained very often (73).

This algorithm has also been used for deriving selectivity equations for reactions involving isomerization. For example, Figure 4.5 shows the reaction network for the hydrogenolysis of isobutane with isomerization. We note that the reaction network can be solved only when all reaction steps are irreversible. In the present case, the isomerization is assumed to be so slow relative to hydrogenolysis that the formation of n-butane may be considered irreversible. Actually, this approximation is valid for most isomerizations. All the other assumptions for the hydrogenolysis network are still used. Two new ratios have been defined:

$$R_I = k_I / (k_R^* + k_I) \quad (4.4)$$

$$\text{and } R^* = 1 - R_I \quad (4.5)$$

where  $R^*$  represents the fraction of a converted reactant undergoing hydrogenolysis and  $R_I$ , the fraction being isomerized. By applying the algorithm, the selectivity equations can be derived for n-C<sub>4</sub>H<sub>10</sub>, C<sub>3</sub>H<sub>8</sub>, C<sub>2</sub>H<sub>6</sub>, and CH<sub>4</sub> (see Figure 4.6).

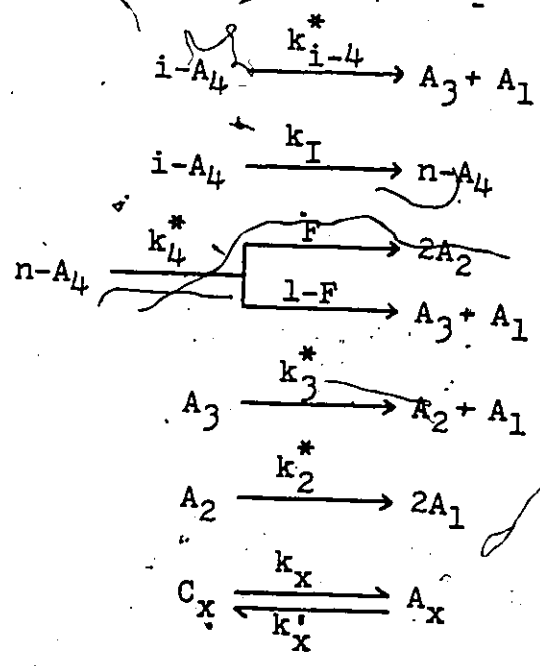
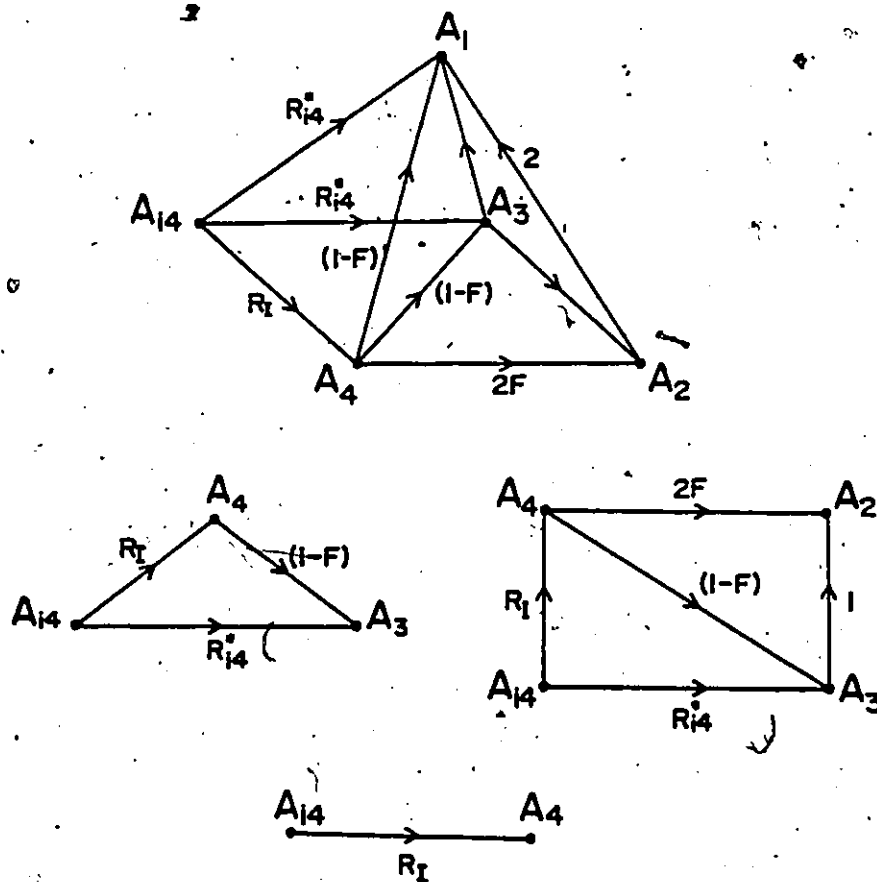


Figure 4.5: Reaction network for hydrogenolysis and isomerization of isobutane over Pt catalyst.



$$\begin{aligned}
 S_{n4} &= M_{n4} R_I \\
 S_3 &= M_3 (1 - FR_I - (1-F) S_{n4}) \\
 S_2 &= M_2 (1 - S_3 - (1+F) S_{n4} + FR_I) \\
 S_1 &= 4 - 2S_2 - 3S_3 - 4S_{n4}
 \end{aligned}$$

$$\text{where } M_h = \frac{\frac{k_h'}{(k_h' + k_h'')}}{1 + \frac{k_h''}{k_{14}''} \frac{X_{14}}{(1 - X_{14})}}$$

Figure 4.6: Pathways and selectivity equations for the reactions of isobutane over Pt catalyst.

### 4.3 An Example of Hydrogenolysis with Isomerization

To test the network analysis, these equations have been applied to kinetic data for hydrogenolysis and isomerization of isobutane on Pt on alumina. Pellets of Houdry hydrogenation catalyst were crushed to 14 to 25 mesh. The catalyst was reduced in situ for 1 hour at 430°C. The reaction temperature was 426°C and the reactant ratio was 3 H<sub>2</sub> to 1 i-C<sub>4</sub>H<sub>10</sub>. The pressure was kept at around 125 kPa.

Figure 4.7 shows selectivities as functions of conversion of i-C<sub>4</sub>H<sub>10</sub>. The selectivity of n-C<sub>4</sub>H<sub>10</sub> decreased monotonically as conversion increases. Initially, at zero-conversion, 41.5% of the converted i-C<sub>4</sub>H<sub>10</sub> was isomerized into n-C<sub>4</sub>H<sub>10</sub>. The other primary products (58.5%) were C<sub>3</sub>H<sub>8</sub> and CH<sub>4</sub>. Ethane, being formed by hydrogenolysis of n-C<sub>4</sub>H<sub>10</sub> and C<sub>3</sub>H<sub>8</sub>, was not initially found.

The selectivity equations (from Figure 4.6) have been fitted to the experimental data using a non-linear regression method, the Marquardt's compromise (35), which is a combination of the steepest descent method and the linearization method. The values of the parameters are found in Table 4.1. Figure 4.8 compares the experimental and the calculated values of selectivities. Although enough parameters are evaluated to satisfactorily represent the selectivity as a function of conversion, more information can be obtained in the present case by assigning values to  $j_4'$  and  $F$  to obtain those of  $R_I$  and  $j_3'$ , as they are multiplying each other in the numerator. The splitting factor  $F$  was assumed to be 0.3; the same as found for supported Ru (59,60). Furthermore,  $j_4'$  was set equal to 1.0, which seemed reasonable for a Pt

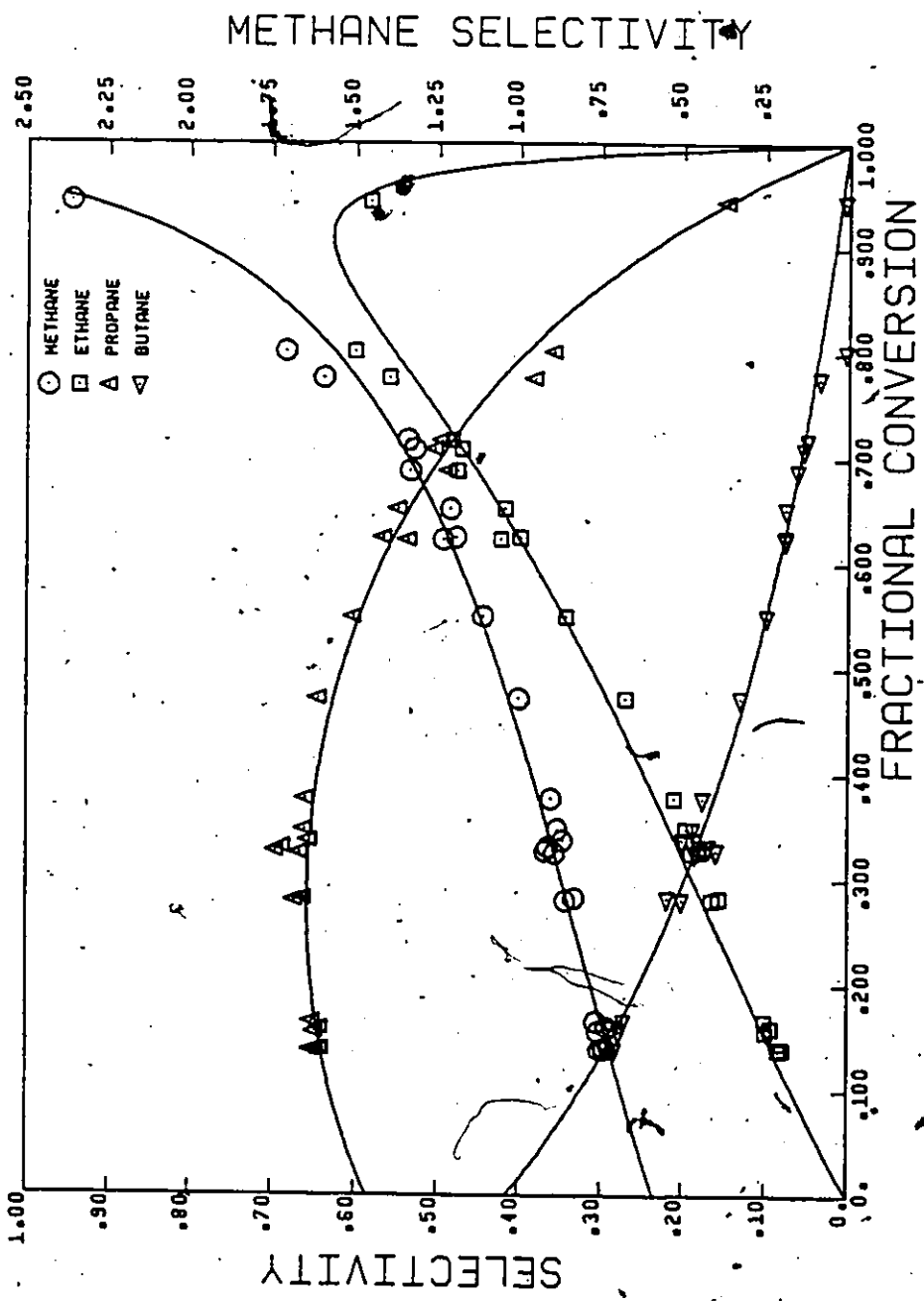


Figure 4.7: Product selectivity curves for the hydrolysis and isomerization of isobutane over Pt on alumina at 426°C.

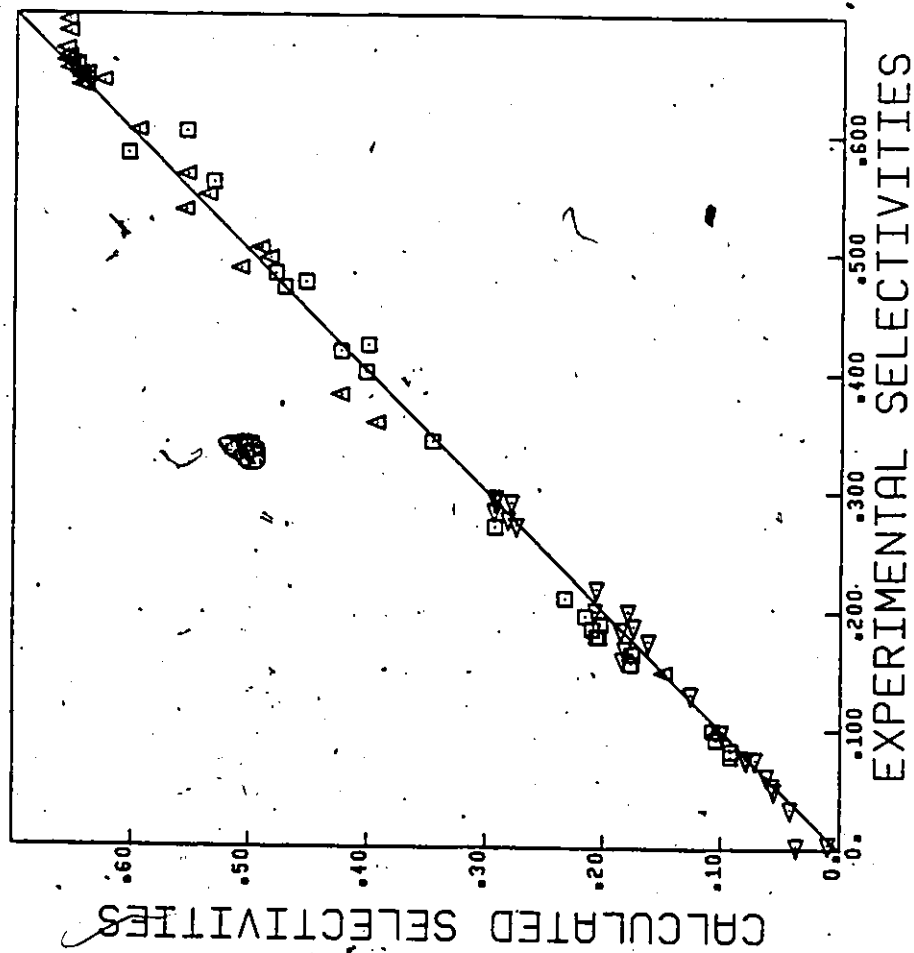


Figure 4.8: Calculated versus experimental selectivities in the hydrogenolysis-isomerization of isobutane over Pt on alumina.



Table 4.1  
 Parameters for the Hydrogenolysis-Isomerization of Isobutane  
 over Pt on Alumina at 426°C.

$n$	$J'_h$	$k_h^n/k_{14}^n$
n-C <sub>4</sub> H <sub>10</sub>	1.0	2.579
C <sub>3</sub> H <sub>8</sub>	1.0	0.289
C <sub>2</sub> H <sub>6</sub>	0.893	0.025
	$R_I = 0.415$	
	$F = 0.3$	

catalyst, i.e. the rate of cracking was much slower than the rate of desorption. Experimental values of  $j_3'$  and  $j_2'$  were close to 1.0 which confirms the validity of our assumption.

If  $j_4'$  is taken as 1.0,  $R_I$  is equal to 0.415, the fraction of reacted isobutane isomerized. The ratios of overall rates ( $k_x^n/k_{i4}^n$ ) were also compared:  $n\text{-C}_4\text{H}_{10}$  reacts 2.5 times faster than  $i\text{-C}_4\text{H}_{10}$  over Pt while  $\text{C}_3\text{H}_8$  cracks at about 1/3 the rate of  $i\text{-C}_4\text{H}_{10}$ . Ethane splits very much slower than the other hydrocarbons, and  $j_2'$  is close to 1.0.

#### 4.4 Selectivity Equations for Hydrogenolysis of Hexadecane

Network analysis has also been used to investigate the hydrogenolysis of normal hexadecane over reduced Fe catalyst. In the set of experiments described in Chapter 6, the possibility of hydrogenolysis exclusively by demethylation is examined. No splitting factors are involved in the reaction network, since only the C-C bonds adjacent to the terminal C's are broken. The assumptions used for the network of  $n\text{-C}_{16}\text{H}_{34}$  hydrogenolysis are similar to those described in section 4.1. Figure 4.9 presents the pathways for the derivation of the Q factor. By applying the algorithm of Figure 4.2, the following selectivity equations were obtained for  $\text{C}_2\text{-C}_{15}$  alkanes.

$$S_P = \left(1 - \sum_{i=P+1}^{15} S_i\right) \frac{j_P'}{Y_P} \quad (4.6)$$

$$\text{where } \frac{j_P'}{Y_P} = \frac{\frac{k_P'}{k_P' + k_P''}}{1 + \frac{k_P''}{k_{16}''} \frac{X_{16}}{1 - X_{16}}} \quad (4.7)$$

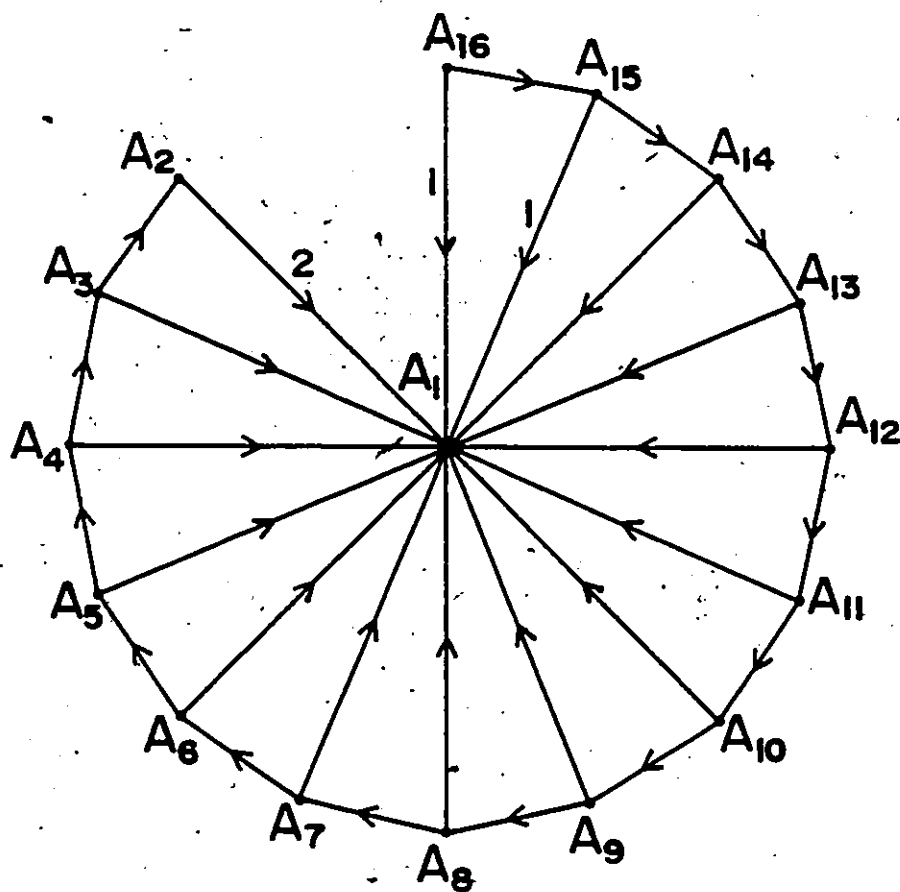


Figure 4.9: Pathways for hydrogenolysis of normal hexadecane, exclusively by demethylation.

and for  $\text{CH}_4$ ,

$$S_1 = 16 - \sum_{i=2}^{15} i S_i \quad (4.8)$$

These equations can be simplified further if the rate constants for adsorption, C-C bond splitting and desorption are assumed to have the same values for all hydrocarbons in a given range of intermediates, between  $C_{10}$  and  $C_{15}$  as an example. Equation 4.6 becomes

$$S_m = \frac{j}{Y} \left(1 - \frac{j}{Y}\right)^{16-(m+1)}, \quad (4.9)$$

and ratios of selectivities can be written as, carbon number  $m$  being smaller than  $n$ ,

$$\frac{S_m}{S_n} = \left(1 - \frac{j}{Y}\right)^{n-m} \quad (4.10)$$

where  $(1-j/Y)$  is a constant. Equation 4.10 will be used later in Chapter 6.

## CHAPTER 5

### HYDROGENOLYSIS OF ISOPENTANE

The present chapter deals with the hydrogenolysis of isopentane over iron catalysts. The first section presents a network analysis of the selectivity data permitting the identification of the slow step of the reaction mechanism. Section II discusses the influence of carbon on iron in relation to the selectivity and the rate of hydrogenolysis. Results from characterization of the used catalysts by Mössbauer spectroscopy, MS, and by Auger electron spectroscopy, AES, are reported in this section. The present chapter is adapted from 2 papers submitted to J. Catal. and to Can. J. Chem. Eng. (83, 84).

#### 5.1 Rate Determining Step in Hydrogenolysis Over Iron

Hydrogenolysis of isopentane was performed over reduced iron with a feed ratio, FR, of  $7H_2$  to  $1-i-C_5H_{12}$ , at  $355^\circ C$  and 125 kPa. Overnight, hydrogen was passed over the catalyst bed at the reaction temperature. The activity of the catalyst was constant throughout the experiment, which lasted 61 hours. Figure 5.1 presents a plot of selectivities as a function of conversion of isopentane. Methane accounted for 99 mole % of the products. Less than 0.02 mole of each intermediate hydrocarbon was formed per mole of isopentane converted. The selectivities were relatively constant over the range of conversions studied, although relatively scattered for the intermediate hydrocarbons due to the small quantities involved.

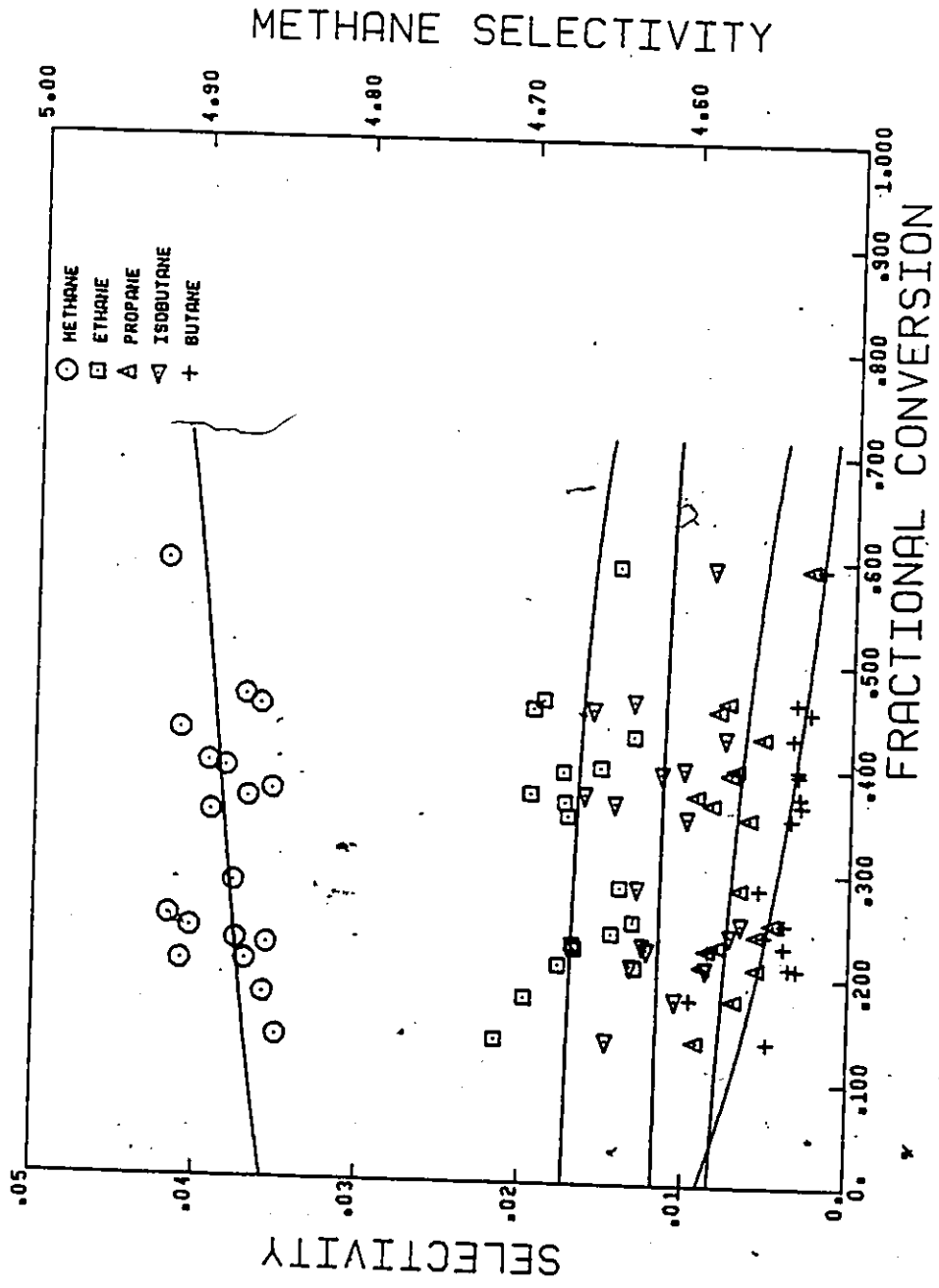


Figure 5.1: Selectivity curves for hydrogenolysis of  $i\text{-C}_5\text{H}_{12}$  over Fe at 355°C and 7.0 FR. (Test 5.3)

The complete derivation of selectivity equations for the reaction network applied to hydrogenolysis of isopentane is described in the previous chapter (Figures 4.1 to 4.4). Parameters of these equations were obtained by non-linear regression of the experimental data and are given in Table 5.1. The ratio  $k_h^n/k_{15}^n$  compares the overall rate of hydrogenolysis of a given product  $h$  with that of isopentane. Table 5.1 shows that n-butane reacts 2.5 times faster than isopentane, and is also more reactive than any other intermediate; isobutane has the lowest reactivity.

The splitting factors or probabilities for breaking a given C-C bond could not be obtained from the regression analysis, because the selectivities were relatively independent of conversion and they had very low values. Therefore, reasonable assumptions were made, based on the cracking patterns observed on nickel and ruthenium which may be regarded as 2 limiting cases. The reaction mechanism on Ni involves demethylation while on Ru, random splitting of the C-C bonds is observed. Nickel (74) forms about twice as much n-C<sub>4</sub>H<sub>10</sub> as i-C<sub>4</sub>H<sub>10</sub>. Splitting factors  $f$  and  $f'$  are, therefore, equal to 1/3 and 2/3, respectively. Since Ni removes only the terminal C atoms from straight chain paraffins,  $F$  is set equal to 0.0. On the other hand, ruthenium attacks with difficulty C-C bonds involving a ternary C atom (60). Therefore, isopentane is mostly broken into i-C<sub>4</sub>H<sub>10</sub> and CH<sub>4</sub>. Probabilities  $f$  and  $f'$  are then equal to 0.82 and 0.08, respectively. Random splitting of n-C<sub>4</sub>H<sub>10</sub> sets  $F$  equal to 1/3. Table 5.1 gives values of  $k_h^n/k_h^i$  for the intermediate hydrocarbons, the ratio of the rate of breaking of C-C bonds to the rate of desorption of the adsorbed species.

TABLE 5.1

Parameters for the hydrogenolysis of isopentane  
over Fe at 355°C and 7.0 FR.

h	$k_h^n/k_{15}^n$	$k_h^n/k_h^i$ for Fe		Observed $k_h^n/k_h^i$	
		Pattern A <sup>a</sup>	Pattern B <sup>b</sup>	Ni	Ru
n-C <sub>4</sub> H <sub>10</sub>	2.516	73	8	0.45	0.11
i-C <sub>4</sub> H <sub>10</sub>	0.033	27	69	0.33	
C <sub>3</sub> H <sub>8</sub>	0.382	119	115		0.18
C <sub>2</sub> H <sub>6</sub>	0.067	57	65		

- a) Same splitting pattern as nickel.
- b) Same splitting pattern as ruthenium.



Even with the widely different assumptions for the splitting factor, the  $k_h^*/k_h'$  values are quite similar and large. By assuming equal values of  $k_h^*/k_h'$  for all intermediate hydrocarbons, the splitting factors may be eliminated from the selectivity equations. This approximation gave an average splitting-desorption ratio of 64. Also given in Table 5.1 are values of  $k_h^*/k_h'$  obtained from hydrogenolysis on Ni and Ru (60, 74); these numbers are less than 0.45. Therefore, product desorption is the rate determining step in the hydrogenolysis reactions on iron. Hydrocarbon species adsorbed on the surface of the catalyst are largely completely hydrocracked to  $CH_4$  before they desorb.

## 5.2 Effect of Carbon on Iron in Hydrogenolysis

### 5.2.1 Selectivity, Rate and Feed Ratio of $H_2$ to Isopentane

This section reports the results of  $1-C_5H_{12}$  hydrogenolysis over reduced Fe at  $325^\circ C$  where the  $H_2$  to isopentane feed ratio was varied to determine how it affected selectivity and reaction rate. The activity of the catalyst was nearly constant during the 90 hours of this experiment. The ranges of partial pressures were:  $H_2$ , 50.45 to 117.2 kPa and  $1-C_5H_{12}$ , 9.91 to 80 kPa. The rate data were treated as differential although conversion varied between 5.5% and 10%. Parameters of the power rate law were calculated by non-linear regression. The following expression was obtained:

$$\text{Rate} = 3.73 P_{H_2}^{1.66} \times P_{1-C_5H_{12}}^{0.91} \quad (5.1)$$

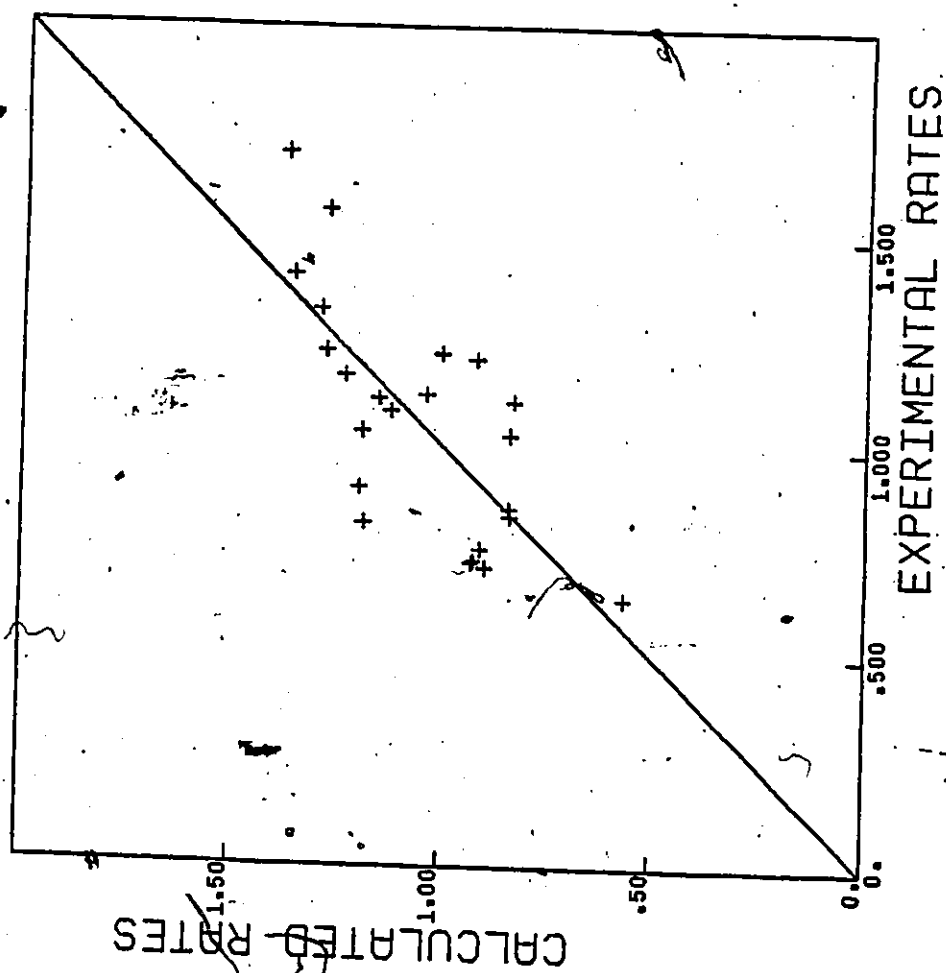


Figure 5.2: Experimental and calculated rates of hydrogenolysis of isopentane at 325°C.

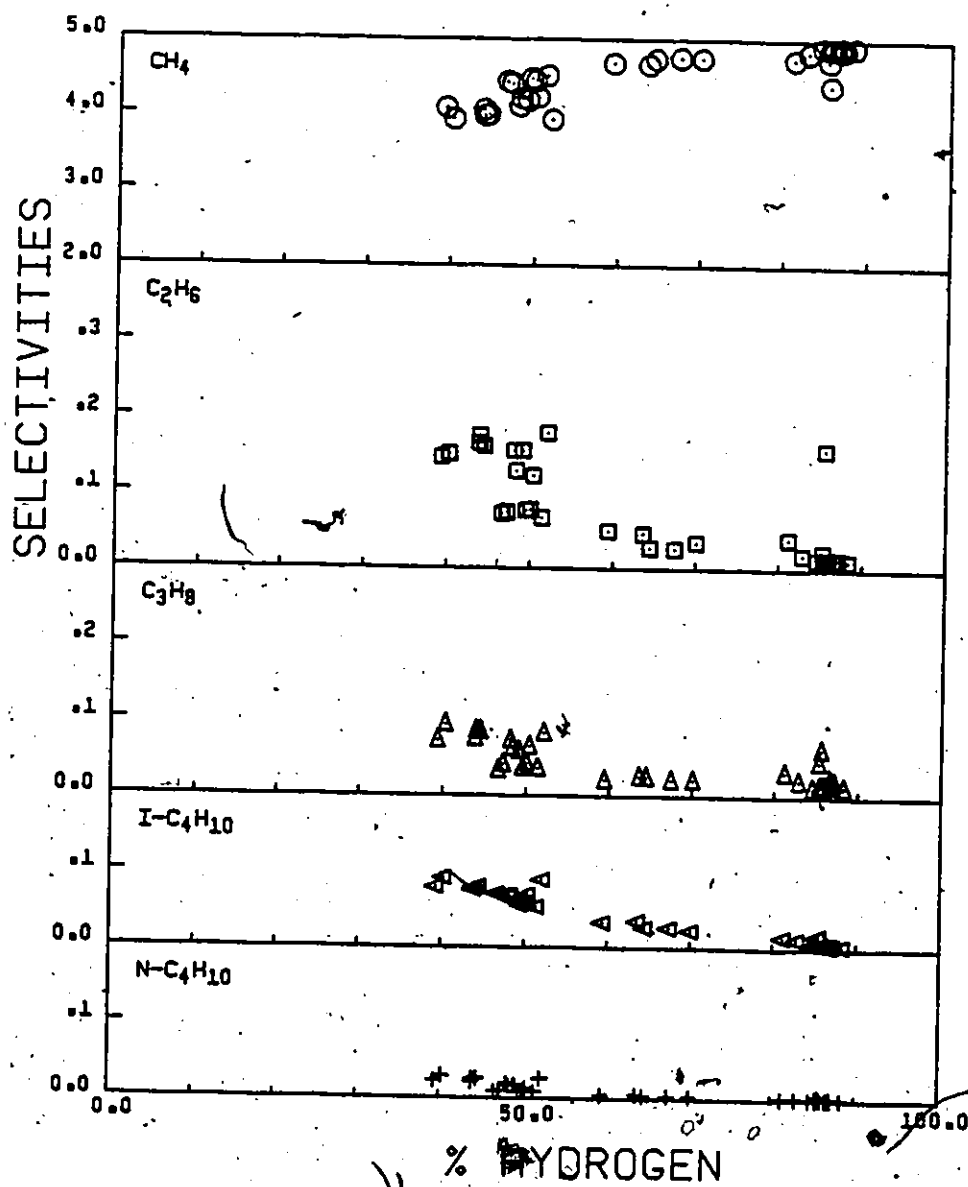


Figure 5.3: Product selectivities as a function of mole %  $H_2$  in the feed during hydrogenolysis at 325 C.

where P's are in atm. This rate equation fits the data reasonably well; The predicted values agree with the experimental data within 20%. Figure 5.2 compares the calculated and experimental rates. Both powers are positive, in agreement with Sinfelt's work (106) in which Fe was the only Group VIII metal with a positive  $H_2$  exponent for the hydrogenolysis of  $C_2H_6$ .

Selectivity data were also obtained in the same experiment. Selectivities at conversion of about 7% are plotted in Figure 5.3 as a function of %  $H_2$  in the feed. They are quite constant at high  $H_2$  partial pressure in the feed. However, for FR less than 1.8 - 1.9 (65 mole %  $H_2$ ), the selectivity for  $CH_4$  drops rapidly with decreasing %  $H_2$  while it increases sharply for the other products. If the partial pressures of  $H_2$  and  $i-C_5H_{12}$  are varied at constant total pressure, the power rate expression has a maximum at about 1.8 FR for total pressures in the range of 122 to 192 kPa. The feed ratio for this maximum rate is also the point below which selectivities change significantly.

### 5.2.2 Selectivity and Formation of Bulk Carbides

Tables 5.2 and 5.3 give selectivities, conversions and rates for  $i-C_5H_{12}$  hydrogenolysis on reduced Fe at  $325^\circ C$  and 2.8 FR, in Test 5.1, and at  $355^\circ C$  and 7.0 as well as 0.8 FR, in Tests 5.3 and 5.4.

Selectivity data obtained at 0.8 FR are plotted as a function of conversion in Figure 5.4 for conversions less than 10% and in Figure 5.5, for those less than 1%.

TABLE 5.2

Product Selectivities and Reaction Rates for Hydrogenolysis of Isopentane over Fe Catalysts at 325°C and 2.8 FR.

Test	Phase Initially Present	Selectivity, moles per mole $i-C_4H_{10}$ consumed	Conversion	Rate <sup>b</sup>	Used Catalyst <sup>a</sup>				
		$C_4H_4$ $C_2H_6$ $C_3H_8$ $C_4H_{10}$ $1-C_4H_{10}$							
5.1-	$\alpha$	4.414 <sup>c</sup> .099 <sup>d</sup>	.050 .005	.029 .003	.023 .008	.076 .012	.034-.107	.055-.169	$\alpha$
5.2.1	X	3.754	.057	.064	.204	.032	.002-.008	1.5 - 2.3	[ 33% $\theta$ 67% $\alpha$ ]
5.2.2		4.353	.083	.038	.064	.027	.012-.028		
5.2.3		4.615	.056	.022	.028	.024	.031-.064		

a)  $\alpha$  =  $\alpha$ -Fe, X = Hägg carbide,  $Fe_5C_2$ ,  $\theta$  = cementite,  $Fe_3C$  (characterized by Mössbauer spectroscopy).

b) in  $\mu$ mole/g sec.

c) average value of product selectivity over the complete range of conversions.

d) standard deviation of the average value described in c.

TABLE 5.3

Product Selectivities and Reaction Rates for Hydrogenolysis of Isopentane over Reduced Fe Catalysts at 355°C.

Test	FR <sup>a</sup>	Selectivity, moles per mole i-C <sub>5</sub> H <sub>12</sub> consumed					Conversion	Rate <sup>b</sup>	Used Catalyst <sup>c</sup>
		CH <sub>4</sub>	C <sub>2</sub> H <sub>6</sub>	C <sub>3</sub> H <sub>8</sub>	C <sub>4</sub> H <sub>10</sub>	i-C <sub>4</sub> H <sub>10</sub>			
5.3	7.0	4.882 <sup>d</sup>	.017	.007	.004	.012	.17 - .59	.12 - .99	α
		.008 <sup>e</sup>	.003	.002	.002	.003			
	0.8	3.566	.141	.156	.080	.091			
		.296	.020	.041	.040	.019	.003-.008	.05 - .27	
5.4	0.8	3.895	.155	.082	.051	.087			θ
		.157	.043	.022	.022	.015	.011-.090	.09 - .33	

a) feed ratio of H<sub>2</sub> to i-C<sub>5</sub>H<sub>12</sub>.

b) in μmole/g sec.

c) α = α-Fe, θ = cementite, Fe<sub>3</sub>C (characterized by Mössbauer spectroscopy).

d) average value of product selectivity over the complete range of conversions.

e) standard deviation of the average value described in d.

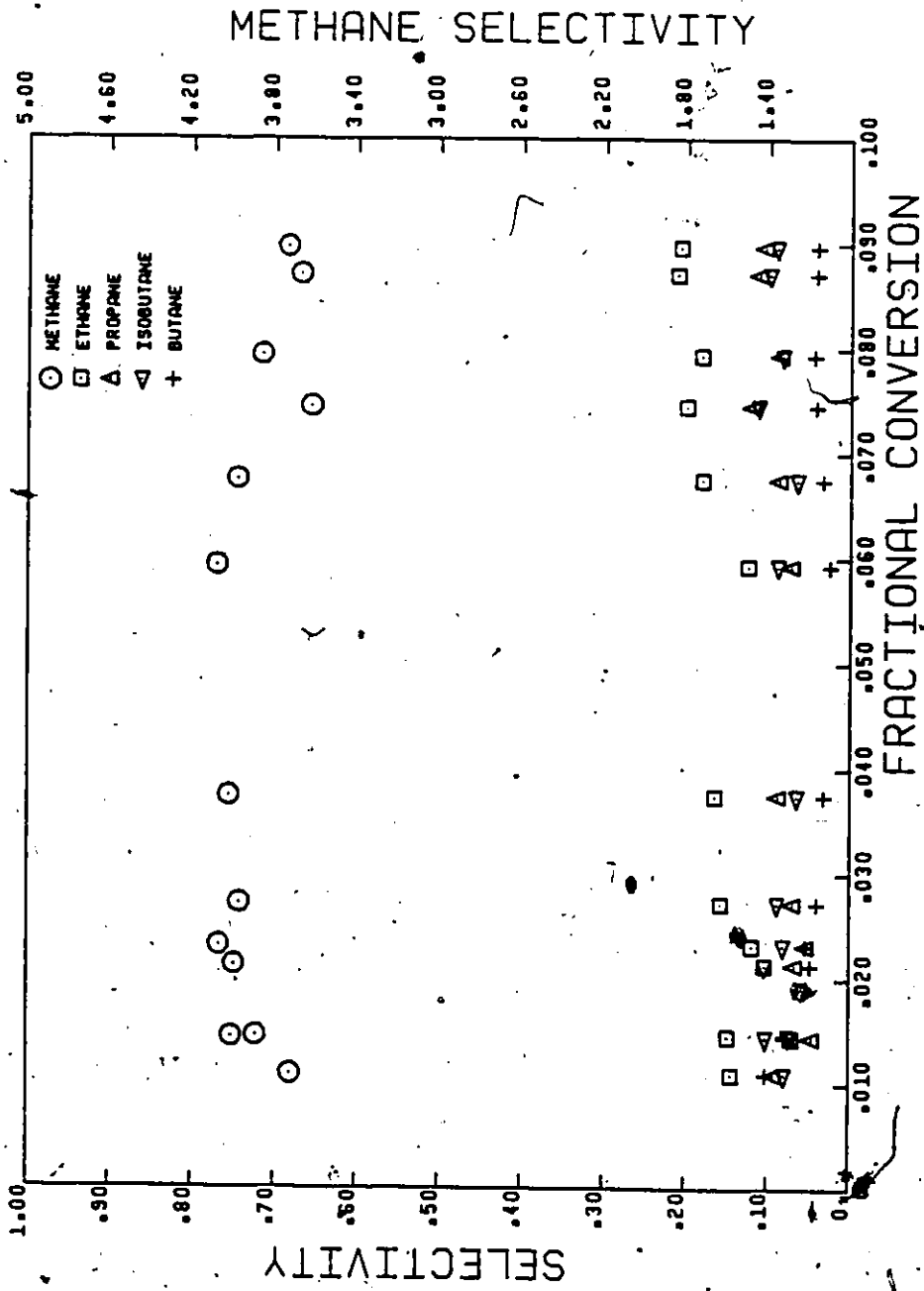


Figure 5.4: Selectivity curves for hydrogenolysis of  $i\text{-C}_5\text{H}_{12}$  over Fe at  $355^\circ\text{C}$  and 0.8 FR (Test 5.4), conversion less than 10%.

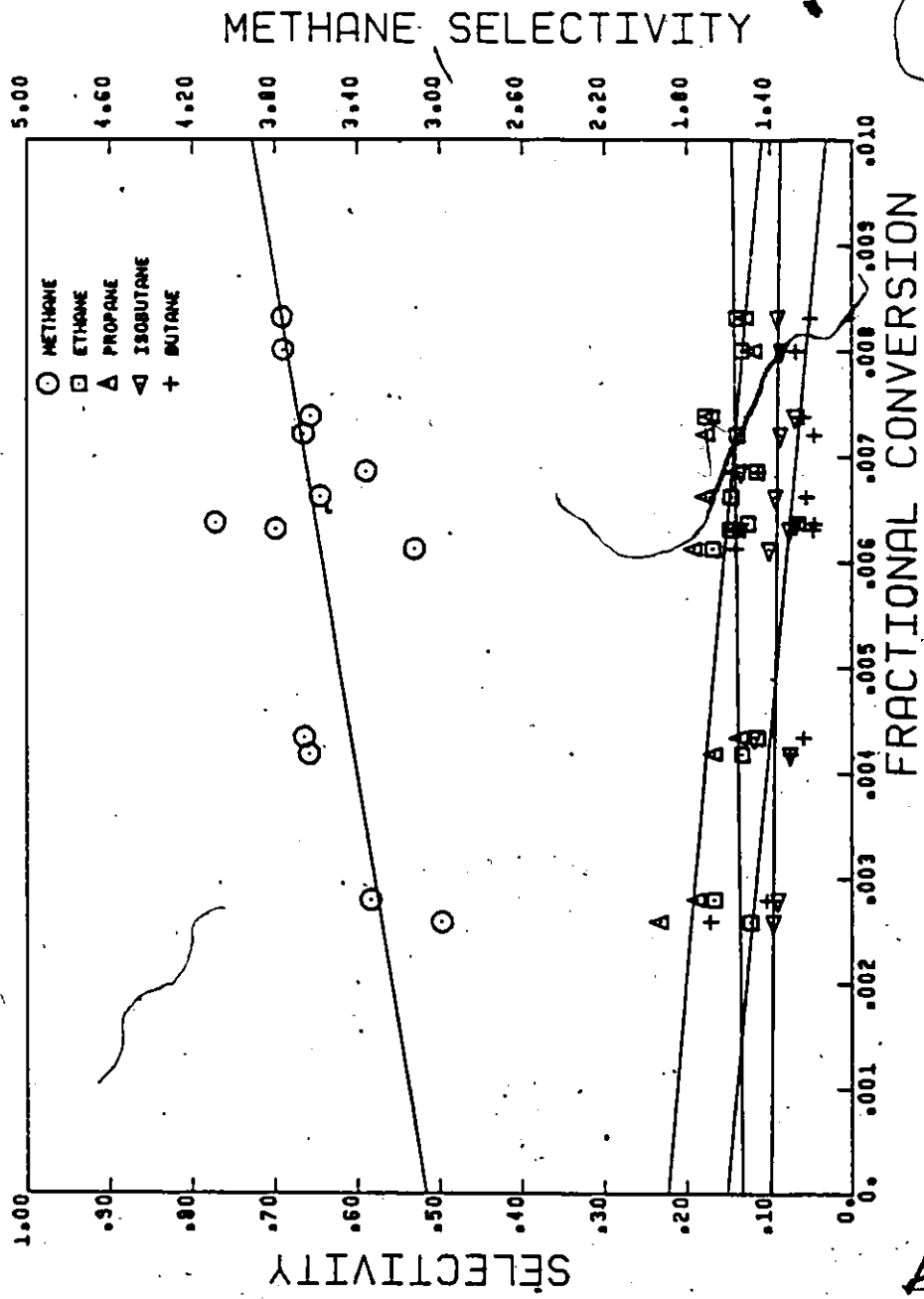


Figure 5.5: Selectivity curves for hydrogenolysis of  $i\text{-C}_8\text{H}_{12}$  over Fe at  $355^\circ\text{C}$  and 0.8 FR (Test 5.4), conversion less than 1%.



Table 5.2 also gives results from an experiment at 325°C with a catalyst converted to Hägg carbide, Fe<sub>5</sub>C<sub>2</sub>. Preparation and handling of Fe<sub>5</sub>C<sub>2</sub> has been described in Chapter 3. Overnight, either argon or helium was passed over the catalyst bed to keep it under inert atmosphere.

Average values are presented in Tables 5.2 and 5.3 because the experimental data are relatively constant throughout the range of conversions studied, as shown by Figures 5.1, 5.4 and 5.5 and by the standard deviations given in these Tables. Furthermore, selectivities are relatively independent of catalyst activities.

Pre-carbided and used catalysts were characterized by Mössbauer spectroscopy, MS, for identification of the bulk phase. Dr. Georges Dénès from the Department of Chemistry operated the MS equipment and interpreted the data. The Mössbauer spectra and the parameters of the fits are given in Appendix A.

#### 5.2.2.1 Hydrogenolysis at a Feed Ratio of 2.8 H<sub>2</sub>: 1.1-C<sub>5</sub>H<sub>12</sub>

Iron catalysts produce mostly CH<sub>4</sub> during hydrogenolysis reactions as shown in test 5.1 of Table 5.2. In fact, CH<sub>4</sub> was at least 96.1 mole % of the products and no other hydrocarbons accounted for more than 1.6 mole %.

Mössbauer spectroscopic characterization of the used catalyst in test 5.1 indicated only α-Fe. Examination by Auger electron spectroscopy of the Fe foil showed the presence at its surface, of elemental C which gives peaks different from those of carbidic C.

Selectivities of test 5.2.3 over a catalyst containing Hägg carbide are similar to those of test 5.1. The pre-carbided catalyst, after being used for more than 90 hours, contained 67 weight %  $\alpha$ -Fe and 33% cementite. Thus, carbidic carbon in the catalyst had decreased by 75% and the Hägg carbide was converted to  $\alpha$ -Fe and cementite,  $\theta$ -Fe<sub>3</sub>C. Cementite is probably found only in the core of the Fe crystallites, the selectivity being similar on Hägg carbide and  $\alpha$ -Fe, at 2.8 FR. At these experimental conditions, the catalyst may be carbided due to the high concentration of isopentane while carbides may be reduced in H<sub>2</sub> due to the low level of CH<sub>4</sub>, or thermally decomposed. The stability of Fe<sub>3</sub>C in a 2.8 FR mixture is discussed later in this chapter.

The activity of the pre-carbided catalyst in 5.2 was quite high compared to that of  $\alpha$ -Fe in 5.1 since the rate of hydrogenolysis varied between 1.5 and 2.0  $\mu$ mole/g sec, which is equivalent to 15-20 times that of 5.1.

#### 5.2.2.2 Hydrogenolysis at a Feed Ratio of 0.8 H<sub>2</sub>:1 i-C<sub>5</sub>H<sub>12</sub>

Experiments were done on a reduced Fe catalyst at 0.8 FR and 355°C. Selectivity data are given in Table 5.3, test 5.4, and can be compared with those of test 5.3, at 7.0 FR. In the 0.8 FR mixture, the selectivity for methane decreased by 20% while it increased 10-fold for intermediate hydrocarbons. Similarly, less CH<sub>4</sub> was produced in test 5.4 than during hydrogenolysis with the next lowest feed ratio, 2.8 FR, even though the latter one was at lower temperature. Selectivities of test 5.4 for conversion less than 1% are plotted in Figure 5.4. Because of

small conversions, selectivity values are erratic, particularly for  $\text{CH}_4$ . Characterization by MS of the used catalyst of test 5.4 indicates that only  $\text{Fe}_3\text{C}$  is present.

The formation of cementite in the bulk catalyst is reversible as shown by another experiment where the reduced catalyst, first transformed completely to  $\text{Fe}_3\text{C}$  by using it for 27 hours with a 0.8 FR mixture at  $325^\circ\text{C}$ , was changed back to  $\alpha\text{-Fe}$  after 25 hours in 2.8 FR, at  $355^\circ\text{C}$ . The change in feed composition affected selectivities which were similar to those in test 5.1. Consequently, the cementite formed at 0.8 FR, decomposes into  $\alpha\text{-Fe}$  and elemental C when used at 2.8 FR. Direct hydrogenation to  $\text{CH}_4$  is also possible. The carbon content measured by chemical analysis (combustion at high temperature in excess of  $\text{O}_2$ ) was 0.795 weight % of total solid, corresponding to a decrease of carbon by 88% from cementite.

### 5.3 Discussion

Product desorption is the rate determining step in hydrogenolysis of hydrocarbons on iron, as shown in the first part of this chapter. Splitting of C-C bonds is much faster than desorption, making hydrocarbon species adsorbed on the catalyst, largely completely hydrocracked to  $\text{CH}_4$  before they desorb. These results confirm the conclusions of Dowie et al. (34): Furthermore, the overall rate of hydrogenolysis,  $k_h''$ , decreases with the size of the straight chain alkane.

Our results demonstrate also that bulk Fe carbides are detected only at very low  $\text{H}_2$  to hydrocarbon feed ratio. In the temperature range

studied, the reactant ratio is the main factor determining the presence of carbides; they presumably result from the competition between diffusion in the bulk catalyst and hydrogenation to  $\text{CH}_4$  of the surface carbon species. For FR less than 1.8, the excess surface carbon dissolves and diffuses in the Fe lattice until a saturation point is reached and cementite forms. For FR larger than 1.8, there is enough  $\text{H}_2$  present for hydrogenation of all carbon species. According to the carbon-iron phase diagram, cementite starts forming at  $355^\circ\text{C}$  when more than 0.008% C is dissolved in Fe. The density of Fe being lower than that of other transition metals (7.82 g/cc for Fe at  $20^\circ\text{C}$  compared to 8.85 and 8.93 for  $\alpha\text{-Co}$  and  $\beta\text{-Ni}$ ), carbon can diffuse more easily in Fe than in Ni and Co, and the Fe lattice can dissolve more C. At low  $\text{H}_2$  to hydrocarbon feed ratio, Fe may be envisioned as a reservoir for C, mainly in carbidic form.

The change of selectivity at  $\text{H}_2/1\text{-C}_5\text{H}_{12}$  ratios less than 1.8 can be explained by the conversion of the metallic iron to carbides. Under conditions that produce bulk  $\text{Fe}_3\text{C}$ , the presence of surface carbides is insured and the surface iron atoms probably chemisorb less strongly hydrocarbons than those of  $\alpha\text{-Fe}$ , due to Fe-C bonds in the carbides. This change is also suggested by the magnetic properties of  $\alpha\text{-Fe}$  and cementite, given in Table 2.3. Thus, intermediate hydrocarbons like  $1\text{-C}_4\text{H}_{10}$ ,  $n\text{-C}_4\text{H}_{10}$  or  $\text{C}_3\text{H}_8$  should therefore be more readily desorbed, as shown by their increased selectivity at 0.8 FR.

## CHAPTER 6

### HYDROGENOLYSIS OF PROPANE AND HEXADECANE

The present chapter is divided into 2 sections. The first reports selectivities and a power rate expression for hydrogenolysis of propane at various feed ratios of  $H_2$  to propane while keeping the conversion constant. The second section presents experimental results obtained from hydrogenolysis of a high molecular weight alkane, n-hexadecane.

#### 6.1 Hydrogenolysis of Propane: Rate and Selectivity

Propane was used as reactant in a series of experiments, because the composition of the feed mixture could be more accurately set with an electronic mass flow controller, than with the saturator used for

$i-C_5H_{12}$ .

Hydrogenolysis of propane was studied at  $325^\circ C$  and 125 kPa, with different molar  $H_2$  to  $C_3H_8$  feed ratios, FR. Hydrogen partial pressure was varied from 66.5 to 199 kPa and  $C_3H_8$  pressure, from 6.2 to 49.7 kPa. The conversion ranged from 4.0 to 6.5%. The activity of the catalyst was constant during the 40 hours of this experiment. The following power rate expression was obtained:

$$\text{Rate} = 0.81 P_{H_2}^{0.43} \times P_{C_3}^{1.08}$$

(6.1)

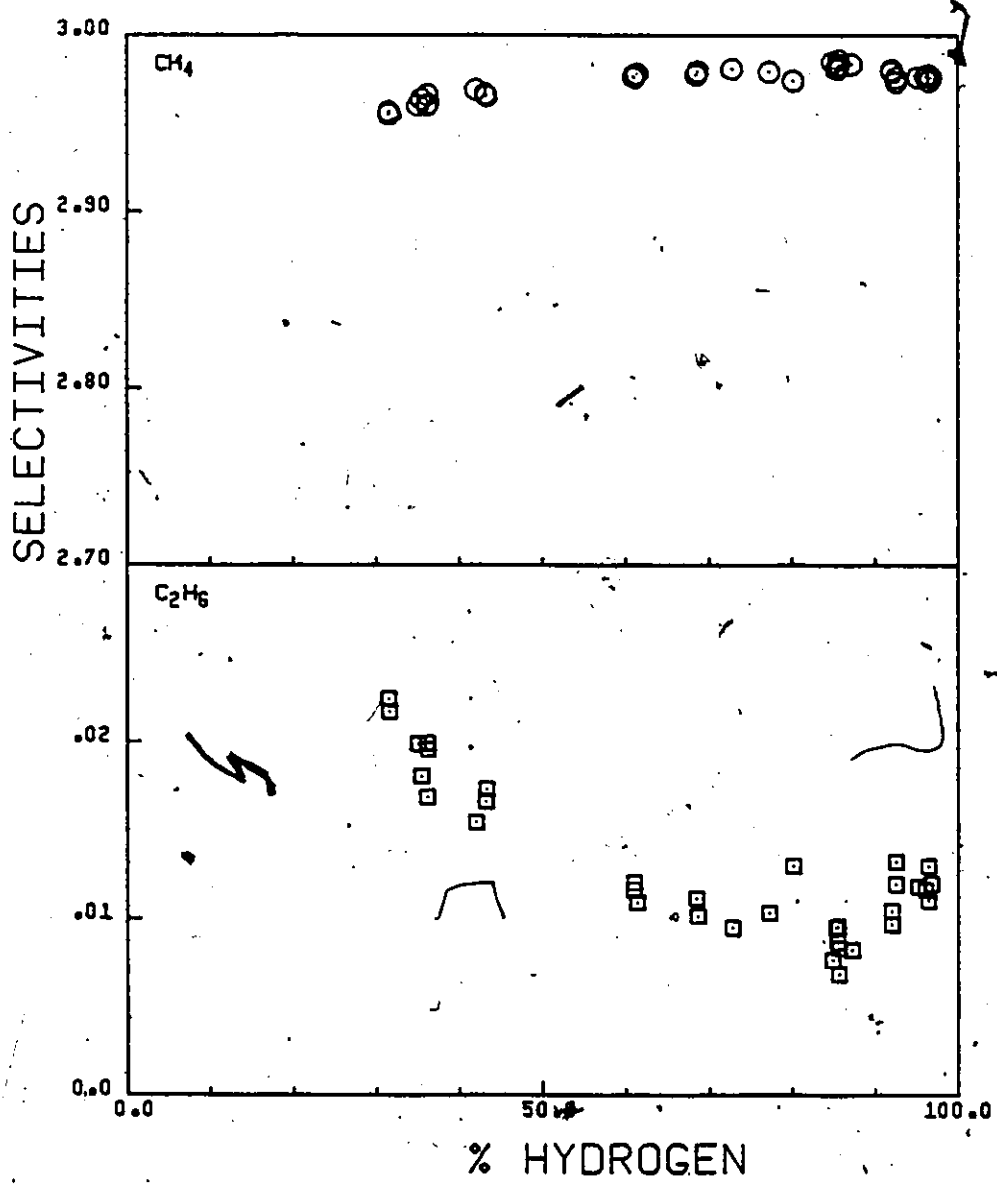


Figure 6.1: Product selectivities as a function of mole % H<sub>2</sub> in the feed during hydrogenolysis of propane at 325°C.

76

where the pressures are in atm. The experimental data, given in Appendix D, were fitted reasonably well with equation 6.1, since experimental and calculated rate values agree within 20%. The exponents of the partial pressures are both positive, which is characteristic of power rate expressions for hydrogenolysis reactions over Fe, as shown in Chapter 5.

Selectivity data were collected in the same experiment. They are plotted in Figure 6.1 as a function of the concentration of  $H_2$  in the feed. The formation of methane is quite high, accounting for more than 99 mole % of the products. Selectivities change appreciably when the  $H_2$  fraction in the feed is less than 65 mole % which corresponds to a 1.8 FR. A similar result was obtained in hydrogenolysis of isopentane.

## 6.2 Hydrogenolysis of Hexadecane

This section investigates the effect on product selectivity of the length of the carbon chain in a paraffinic reactant. Previous sections of this thesis indicated that over iron, the formation of methane is very high in hydrogenolysis of short molecules like  $C_3H_8$  and  $i-C_5H_{12}$ , which is in agreement with the literature. But will the selectivity for intermediate products increase if hexadecane,  $n-C_{16}H_{34}$ , is the reactant? The present section deals with this question.

Hydrogenolysis of hexadecane was studied at 325 and 355°C over a reduced Fe catalyst. Details of the modifications to the experimental set-up were described earlier in Chapter 3. The molar feed ratio of hydrogen to hexadecane was about 9.1, and the pressure, 125 kPa. Light

hydrocarbons from  $C_1$  to  $C_7$  were analyzed on-line while the  $C_8^+$  products with 8 carbons or more, were separated using capillary column gas chromatography and identified by mass spectrometry in the Department of Chemistry, courtesy of Prof. Michael Quilliam.

The purity of the  $n-C_{16}H_{34}$  feed stock was checked by gas chromatographic analysis and was found to be higher than 99%. More details on the experimental procedures and the product analysis are provided in Chapter 3 and in Appendix C.

#### 6.2.1 Hydrogenolysis of Hexadecane at 355°C

In test 6.1, the hydrogenolysis of hexadecane at 355°C and 3.7% conversion produced mainly methane which accounted for 94 mole % of all products. Figure 6.2 presents a chromatogram of the  $C_8^+$  products obtained by GC analysis with a capillary column and a flame ionization detector and Figure 6.3, the same chromatogram after a 10-fold magnification of the Y-axis and an expansion of the time axis. Examination of the 2 chromatograms shows that the peaks form a pattern which is repeated at fixed time intervals. After identification of the large peaks (peak numbers 1, 2, 15, 29, 42, 54, 65, 75, 83, 86) as normal alkanes, ranging from  $C_7H_{16}$  to  $C_{16}H_{34}$ , retention indices were calculated for all of the other peaks, based on their retention time, using a cubic spline interpolation method (49). Homologous series were then formed by grouping together peaks with the same relative position between 2 normal alkanes. Each series includes compounds with a common structural feature but with a different number of carbon atoms. Since most of the



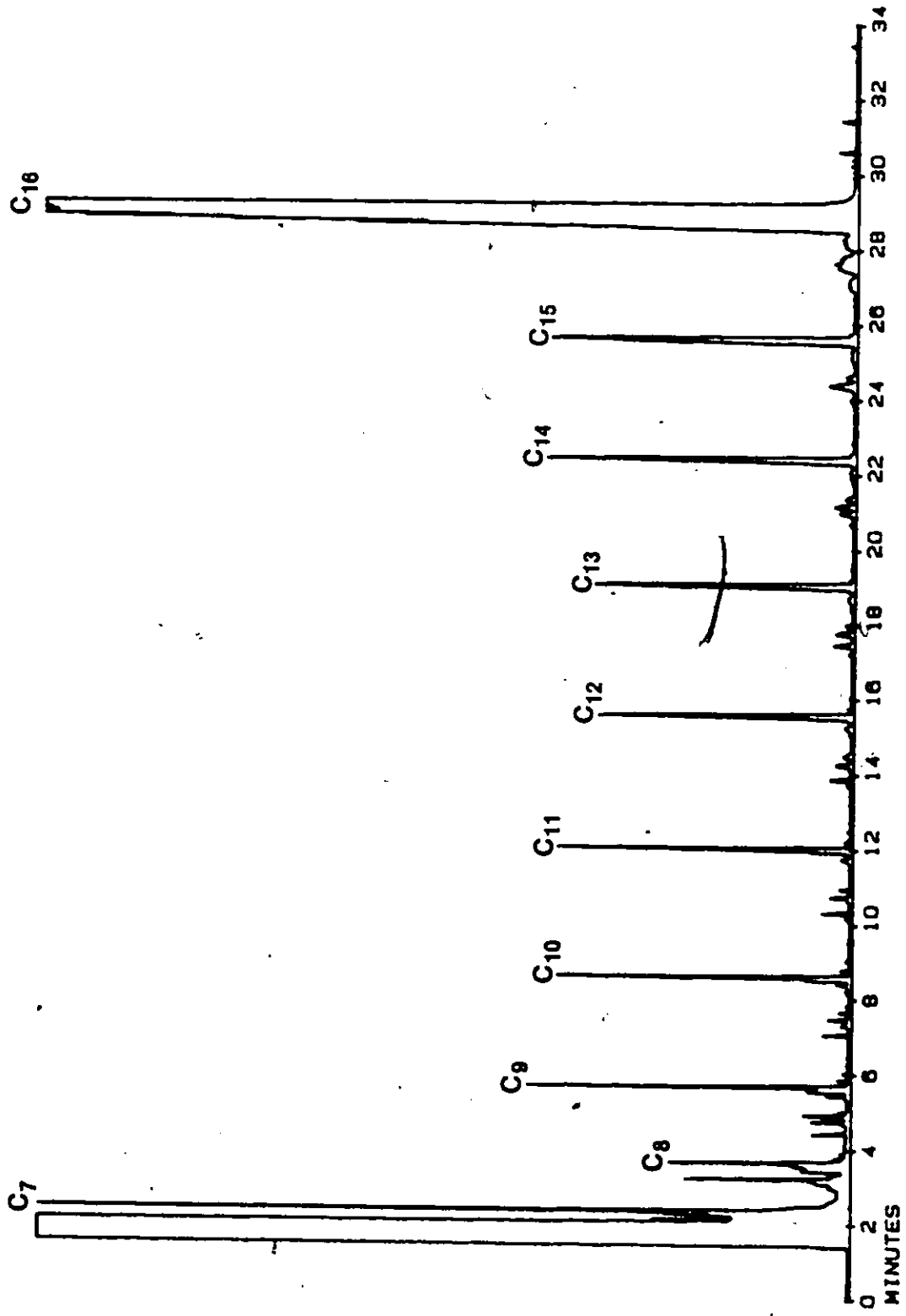


Figure 6.2: Gas chromatogram of C7 products in hydrogenolysis of hexadecane at 355°C and 9.1 FR. (Test 6.1)

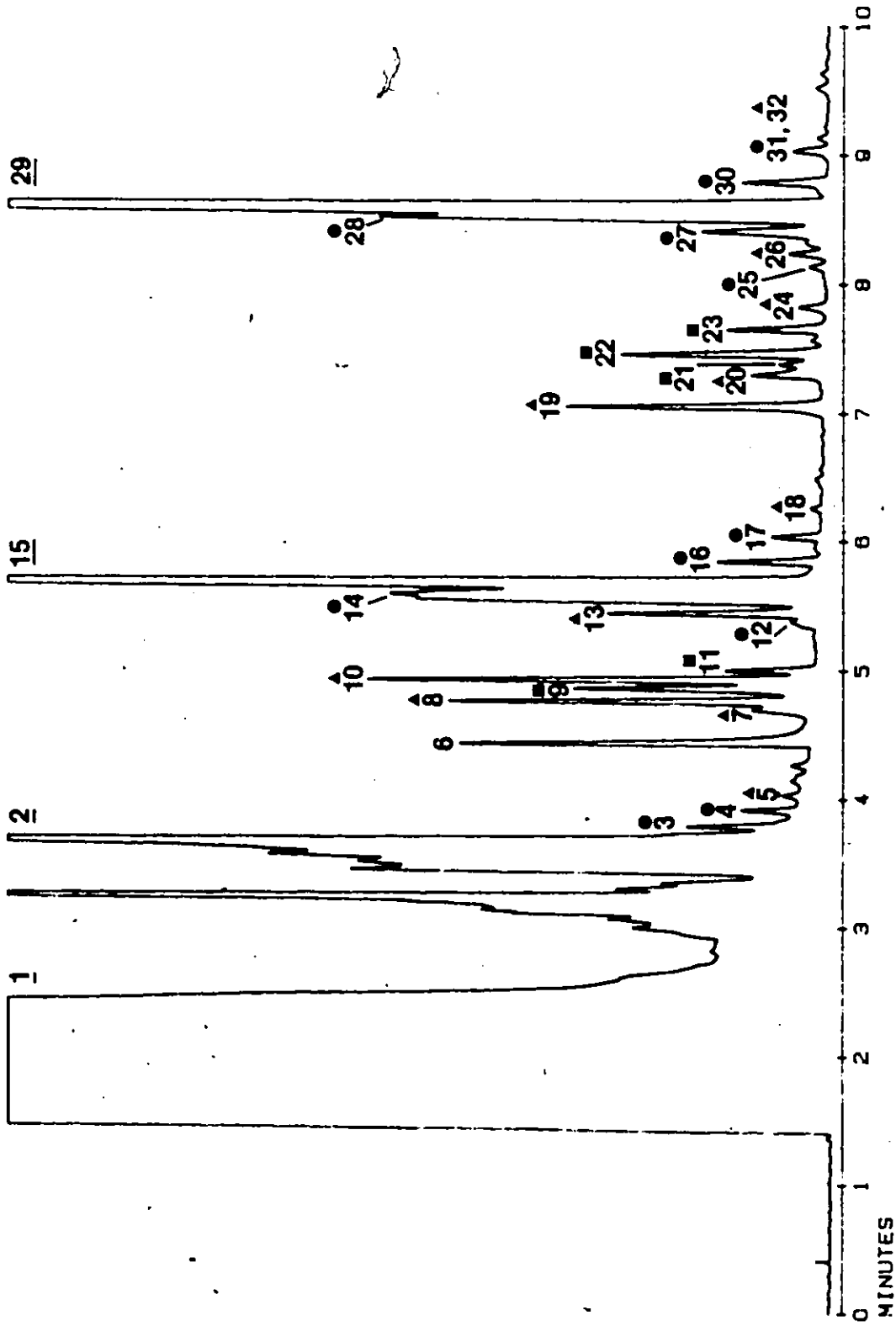


Figure 6.3: Gas chromatogram of C<sub>7</sub><sup>+</sup> products in hydrolysis at 355°C (Test 6.1) after 10-fold magnification of Figure 6.2 and expansion of time axis:

— = n-alkane, ● = olefin, ▲ = alkylbenzene, ■ = branched alkane

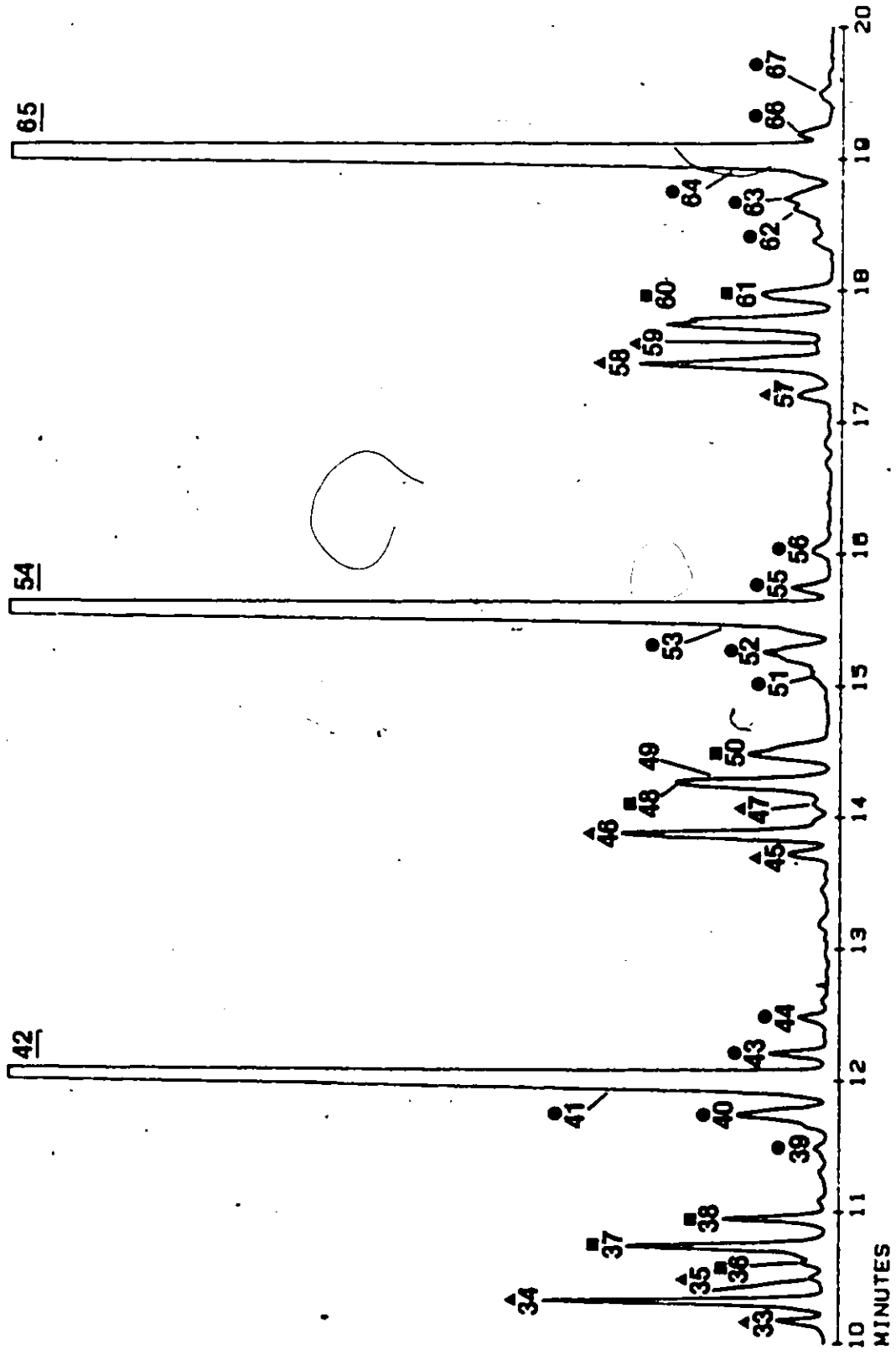


Figure 6.3 (continued)

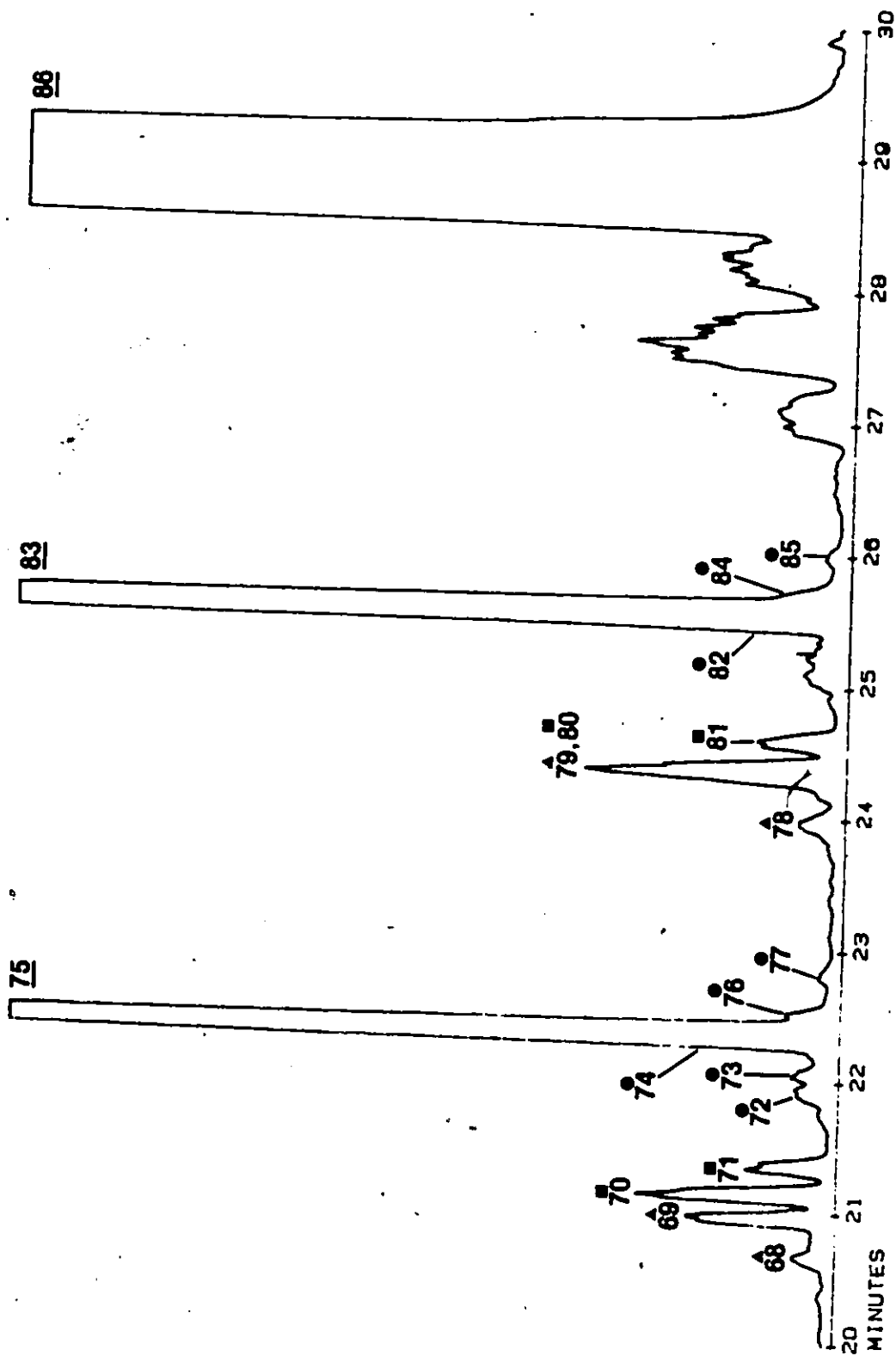


Figure 6.3 (continued)

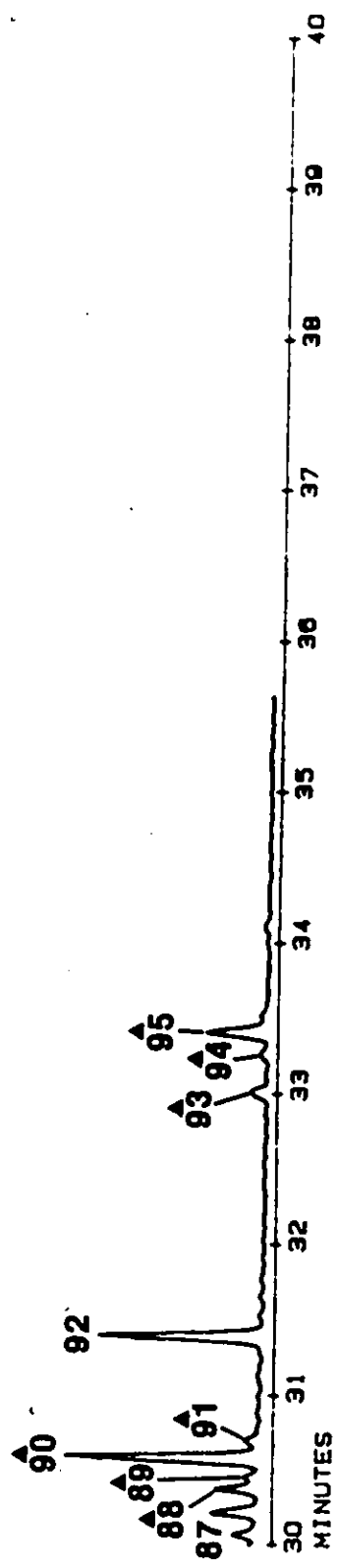


Figure 6.3 (continued)

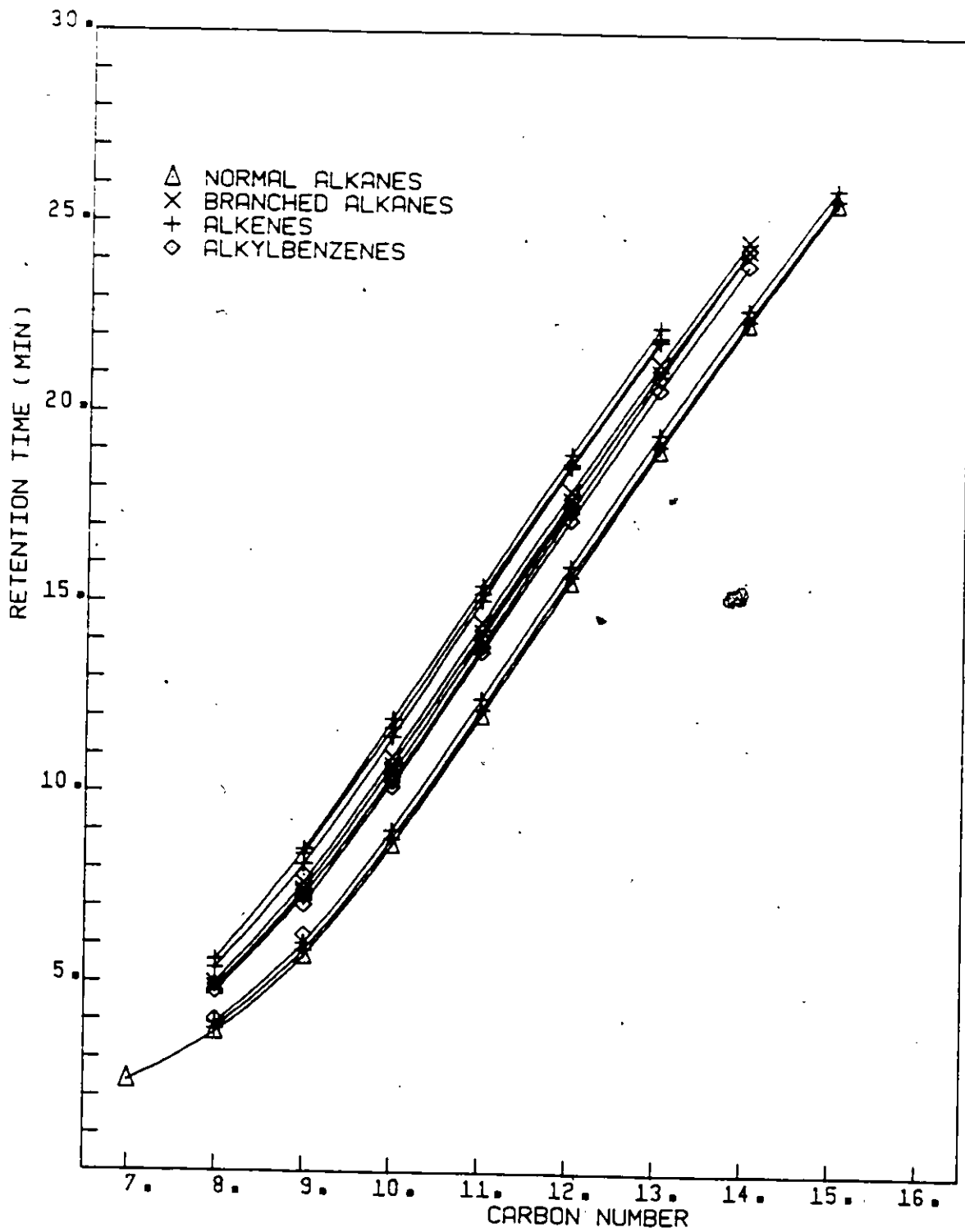


Figure 6.4: Homologous series for  $C_7^+$  products in hydrogenolysis of hexadecane at 355 °C and 9.1 FR (test 6.1).

TABLE 6.1: SUMMARY OF COMPOUNDS IDENTIFIED BY CAPILLARY COLUMN GC-MS ANALYSIS, IN HYDROGENOLYSIS OF  $n\text{-C}_{16}\text{H}_{34}$  (TEST 6.1)

Homologous Series:

A - Normal Alkanes	H - Branched Alkanes
B - Alkenes	I - Alkenes
C - Alkenes	J - Alkylbenzenes
D - Alkylbenzenes	K - Alkenes
E - Alkylbenzenes	L - Alkenes
F - Alkylbenzenes	M - Alkylbenzenes
G - Branched Alkanes	

Peak <sup>a</sup> No.	$t_R^b$	RI <sup>c</sup>	MW <sup>d</sup>	Formula		Homol. Series	Tentative Identity	Peak Area	ID <sup>e</sup>
				C	H				
1	2.39	7.00	100	7	16	A	n-heptane	185792	C
2	3.68	8.00	114	8	18	A	n-octane	137007	A,C,D
3	3.79	8.07	112	8	16	B	octene	1597	B,C
4	3.92	8.15	112	8	16	C	octene	1218	B,C
5	4.03	8.21	106	8	10	M	C <sub>2</sub> -alkylbenzene	250	B,C
6	4.43	8.43	111	-	-		-	12608	*
7	4.70	8.56	106	8	10		C <sub>2</sub> -alkylbenzene	2556	B,C
8	4.76	8.59	106	8	10	E	n-ethylbenzene	11378	A,B,C,D
9	4.86	8.64	128	9	20	G	branched nonane	7960	B,C
10	4.93	8.67	106	8	10		m,p-xylene	13952	A,B,C,D*
11	5.00	8.70	128	9	20	H	branched nonane	2283	B,C
12	5.39	8.87	126	9	18	I	nonene	1131	B,C
13	5.45	8.90	106	8	10	J	o-xylene	6973	A',B,C,D*
14	5.60	8.96	126	9	18	L	nonene	(32935) <sup>f</sup>	B,C

- a) Peak number from Figure 6.3.
- b) Retention time, in minutes.
- c) Retention index, ratio of retention times =  $((A_i - P)/(A_i - A_{i+1})) + i$ .
- d) Molecular weight.
- e) Identification:
- A - retention time matches with a standard.
  - B - Homologous series match.
  - C - Molecular ion and selected fragment ions of correct mass observed (but "pure" mass spectrum not acquired).
  - D - Mass spectrum matches with that of a library spectrum.
  - \* - Mass spectrum in Appendix C.
- f) Merging with homologous series A.

TABLE 6.1 (continued)

Peak No.	$t_R$	RI	MW	Formula		Homol. Series	Tentative Identity	Peak Area	ID
				C	H				
15	5.70	9.00	128	9	20	A	n-nonane	102308	A,C,D*
16	5.85	9.06	126	9	18	B	nonene	3185	B,C*
17	6.04	9.13	126	9	18	C	nonene	1481	B,C*
18	6.26	9.21	120	9	12	M	C <sub>3</sub> -alkylbenzene	243	B,C,D
19	7.05	9.50	120	9	12	E	n-propylbenzene	8798	A,B,C,D*
20	7.30	9.58	120	9	12	F	C <sub>3</sub> -alkylbenzene	3213	B,C,D*
21	7.38	9.61	142	10	22		branched decane	1765	B,C
22	7.46	9.63	142	10	22	G	branched decane	7087	B,C*
23	7.65	9.69	142	10	22	H	branched decane	3106	B,C*
24	7.83	9.75	120	9	12		C <sub>3</sub> -alkylbenzene	1005	B,C,D
25	8.13	9.85	140	10	20	I	decene	641	B,C
26	8.24	9.88	120	9	12	J	C <sub>3</sub> -alkylbenzene	1366	B,C,D*
27	8.41	9.94	140	10	20	K	decene	5987	B,C*
28	8.52	9.97	140	10	20	L	decene	(16740) <sup>a</sup>	B,C*
29	8.62	10.00	142	10	22	A	n-decane	123368	A,C,D
30	8.79	10.05	140	10	20	B	decene	3082	B,C
31	9.03	10.12	140	10	20	C	decene	} 1489	B,C
32	9.03	10.12	120	9	12		C <sub>3</sub> -alkylbenzene		B,C
33	10.18	10.46	134	10	14	D	C <sub>4</sub> -alkylbenzene	1932	B,C,D*
34	10.32	10.50	134	10	14	E	n-butylbenzene	10645	A,B,C,D*
35	10.50	10.56	134	10	14	F	C <sub>4</sub> -alkylbenzene	749	B,C,D
36	10.62	10.59	156	11	24		branched undecane	936	B,C
37	10.74	10.63	156	11	24	G	branched undecane	9432	B,C
38	10.95	10.69	156	11	24	H	branched undecane	3936	B,C
39	11.48	10.84	154	11	22	I	undecene	678	B,C
40	11.74	10.91	154	11	22	K	undecene	6831	B,C
41	11.95	10.97	154	11	22	L	undecene	(-) <sup>a</sup>	B,C

a) Merged with peak of homologous series A.



TABLE 6.1 (continued)

Peak No.	$t_R$	RI	MW	Formula		Homol. Series	Tentative Identity	Peak Area	ID
				C	H				
42	12.05	11.00	156	11	24	A	n-undecane	157234	A,C,D*
43	12.21	11.05	154	11	22	B	undecene	2575	B,C
44	12.49	11.12	154	11	22	C	undecene	1420	B,C
45	13.72	11.47	148	11	16	D	C <sub>5</sub> -alkylbenzene	2057	B,C,D*
46	13.87	11.52	148	11	16	E	C <sub>5</sub> -alkylbenzene	11944	B,C,D*
47	14.10	11.58	148	11	16	F	C <sub>5</sub> -alkylbenzene	703	B,C,D
48	14.27	11.63	170	12	26	G	branched dodecane naphthalene	10980	B,C* B,C*
49	14.27	11.63	128	10	8				
50	14.49	11.69	170	12	26	H	branched dodecane	6806	B,C
51	15.08	11.86	168	12	24	I	dodecene	1009	B,C
52	15.26	11.91	168	12	24	K	dodecene	6225	B,C
53	15.47	11.97	168	12	24	L	dodecene	(-) <sup>a</sup>	B,C
54	15.57	12.00	170	12	26	A	n-dodecane	175322	A,C,D
55	15.75	12.05	168	12	24	B	dodecene	2136	B,C
56	16.01	12.12	168	12	24	C	dodecene	1212	B,C
57	17.21	12.47	162	12	18	D	C <sub>6</sub> -alkylbenzene	2106	B,C,D*
58	17.45	12.53	162	12	18	E	n-hexylbenzene	12370	A,B,C,D*
59	17.60	12.58	162	12	18	F	C <sub>6</sub> -alkylbenzene	1279	B,C,D
60	17.75	12.62	184	13	28	G	branched tridecane	13066	B,C
61	17.98	12.69	184	13	28	H	branched tridecane	5371	B,C
62	18.62	12.87	182	13	26	I	tridecene	6681	B,C B,C
63	18.70	12.89	182	13	26				
64	18.97	12.97	182	13	26	L	tridecene	(-) <sup>a</sup>	B,C

a) Merged with peak of homologous series A.

TABLE 6.1 (continued)

Peak No.	$t_R$	RI	MW	Formula		Homol. Series	Tentative Identity	Peak Area	ID
				C	H				
65	19.07	13.00	184	13	28	A	n-tridecane	207319	A,C,D*
66	19.19	13.03	182	13	26	B	tridecene	2199	B,C
67	19.50	13.13	182	13	26	C	tridecene	942	B,C
68	20.67	13.47	176	13	20	D	C <sub>7</sub> -alkylbenzene	4203	B,C,D*
69	20.98	13.56	176	13	20	E	C <sub>7</sub> -alkylbenzene	11844	B,C,D*
70	21.14	13.61	198	14	30	G	branched tetradecane	15648	B,C
71	21.36	13.68	198	14	30	H	branched tetradecane	6469	B,C
72	21.95	13.86	196	14	28	I	tetradecene	8062	B,C
73	22.04	13.89	196	14	28	K	tetradecene		B,C
74	22.31	13.97	196	14	28	L	tetradecene		(-) <sup>a</sup>
75	22.41	14.00	198	14	30	A	n-tetradecane	252480	A,C,D*
76	22.52	14.03	196	14	28	B	tetradecene	-	B,C
77	22.81	14.13	196	14	28	C	tetradecene	1159	B,C
78	23.95	14.48	190	14	22	D	C <sub>8</sub> -alkylbenzene	42206	B,C*
79	24.36	14.61	190	14	22		C <sub>8</sub> -alkylbenzene		B,C*
80	24.36	14.61	212	15	32	G	branched pentadecane		B,C
81	24.59	14.67	212	15	32	H	branched pentadecane		B,C
82	25.37	14.97	210	15	30	L	pentadecene	(-) <sup>a</sup>	B,C
83	25.61	15.00	212	15	32	A	n-pentadecane	313945	A,C,D
84	25.70	15.03	210	15	30	B	pentadecene		B,C
85	25.98	15.11	210	15	30	C	pentadecene	1542	B,C
86	28.90	16.00	226	16	34	A	n-hexadecane		A,C,D*

a) Merged with peak of homologous series A.

TABLE 6.1 (continued)

Peak No.	$t_R$	RI	MW	Formula		Homol. Series	Tentative Identity	Peak Area	ID
				C	H				
87	30.22	-	224(226)	16	32(34)	-	hexadecene (or branched hexadecane)	1660	C
88	30.38	-	218	16	26	-	C <sub>10</sub> -alkylbenzene	9263	C
89	30.46	-	218	16	26	-	C <sub>10</sub> -alkylbenzene		C
90	30.59	-	218	16	26	-	C <sub>10</sub> -alkylbenzene		C
91	30.70	-	218	16	26	-	C <sub>10</sub> -alkylbenzene		C
92	31.39	-	240(238)	17	36(34)	-	branched heptadecane (or heptadecene)	5976	C
93	33.02	-	232	17	28	-	C <sub>11</sub> -alkylbenzene	4278	C
94	33.25	-	232	17	28	-	C <sub>11</sub> -alkylbenzene		C
95	33.41	-	232	17	28	-	C <sub>11</sub> -alkylbenzene		C

peaks are part of homologous series, compound identification by mass spectrometry was done over a representative region of the chromatogram of Figure 6.3. Mass spectra obtained in the  $C_9-C_{11}$  region are presented in Appendix C. Tentative identities of the products from hydrogenolysis at  $355^\circ C$ , are given in Table 6.1, which also includes their molecular weight, molecular formula, retention time, retention index, peak area and the homologous series to which they belong. Although normal alkanes are the main products, alkenes, alkylbenzenes and branched alkanes are also identified. Figure 6.4 shows the different homologous series in a plot of retention time of GC peaks as a function of the carbon number of the preceding normal alkane.

Alkylbenzenes and aliphatic hydrocarbons with 16 C atoms, are found in peaks 87 to 92 of Figure 6.3, and traces of  $C_{17}$  hydrocarbons, mostly alkylbenzenes, are positively identified in 93, 94, 95 and 96. Naphthalene is present as traces in peak 49.

The alkylbenzenes that are found consist mainly of long carbon chains with a benzene or a toluene group at one end, according to their mass spectra given in Appendix C.

Olefins, aromatics and branched alkanes account for about 4.9, 7.9 and 7.1 mole % of the  $C_9-C_{13}$  products, as shown in Table 6.2, which also gives the hydrocarbon composition at each carbon number. Difficulty in separating the olefins of homologous series L from the normal alkanes, led to a smaller overall area for the alkenes and a larger area for the normal alkanes.

TABLE 6.2

Product distribution for hydrogenolysis of hexadecane  
(C<sub>9</sub>-C<sub>14</sub> range) in mole % of carbon number fraction.

	<u>Normal Alkanes</u>		<u>Alkenes</u>		<u>Alkylbenzenes</u>		<u>Branched Alkanes</u>	
	Test: 6.1 <sup>a</sup>	6.4 <sup>b</sup>	6.1	6.4	6.1	6.4	6.1	6.4
C <sub>9</sub>	81.00	81.95	3.53	0.51	9.34	7.75	6.13	9.78
C <sub>10</sub>	78.91	82.06	6.40	1.14	7.95	5.51	6.74	11.29
C <sub>11</sub>	79.14	81.26	5.87	1.24	7.80	5.95	7.20	11.55
C <sub>12</sub>	79.57	82.05	4.86	1.13	7.50	5.50	8.07	11.32
C <sub>13</sub>	82.12	83.58	3.93	0.84	6.65	5.16	7.30	10.42
C <sub>14</sub>	-	86.07	-	0.83	-	3.08	-	10.03
Avg.	80.15	82.83	4.92	0.95	7.85	5.49	7.09	10.73

a) Test 6.1 at 355°C and 3.7% conversion.

b) Test 6.4 at 325°C and 15.9% conversion.

Furthermore, the selectivities of  $\text{CH}_4$ ,  $\text{C}_2\text{H}_6$ ,  $\text{C}_3\text{H}_8$ ,  $n\text{-C}_4\text{H}_{10}$ ,  $n\text{-C}_5\text{H}_{12}$  and  $n\text{-C}_6\text{H}_{14}$  are respectively equal to 11.971, 0.191, 0.109, 0.102, 0.092 and 0.058 moles per mole of hexadecane converted and none of the heavier hydrocarbons had a selectivity larger than 0.027 (as shown in Table 6.3). The presence of products other than normal alkanes in  $\text{C}_{16}\text{H}_{34}$  hydrogenolysis over Fe will be discussed later in this chapter.

### 6.2.2 Hydrogenolysis of Hexadecane at 325°C

Hydrogenolysis of hexadecane was also studied at 325°C, with a feed ratio of 9.1  $\text{H}_2$  to 1  $n\text{-C}_{16}\text{H}_{34}$  and at 3 different conversions: 0.7, 7.7 and 15.9%, corresponding to tests 6.2, 6.3 and 6.4. Figures 6.5 and 6.6 are the chromatograms of the  $\text{C}_7^+$  products of tests 6.2 and 6.3, while hydrocarbons obtained at the highest conversion are presented in Figure 6.7 and with a 10-fold magnification and an expansion of the time axis, in Fig. 6.8. The distribution of peaks in these 4 figures is similar to the pattern observed earlier in Figures 6.2 and 6.3. Consequently, product identification is possible using the homologous series of Table 6.1. Selectivities of tests 6.3 and 6.4 are given in Table 6.3.

The proportion of alkenes, alkylbenzenes and branched alkanes in the higher hydrocarbons of test 6.4 is given in Table 6.2: on average, olefins account for less than 1% of the total hydrocarbons in the region examined, aromatics, about 5.5% and branched alkanes, more than 10%.

The catalyst was quite active during hydrogenolysis of hexadecane as the reaction rate reached 0.33  $\mu\text{mole/g sec}$ , which is about 2 to 5 times higher than the rates observed in test 5.1 for hydrogenolysis of

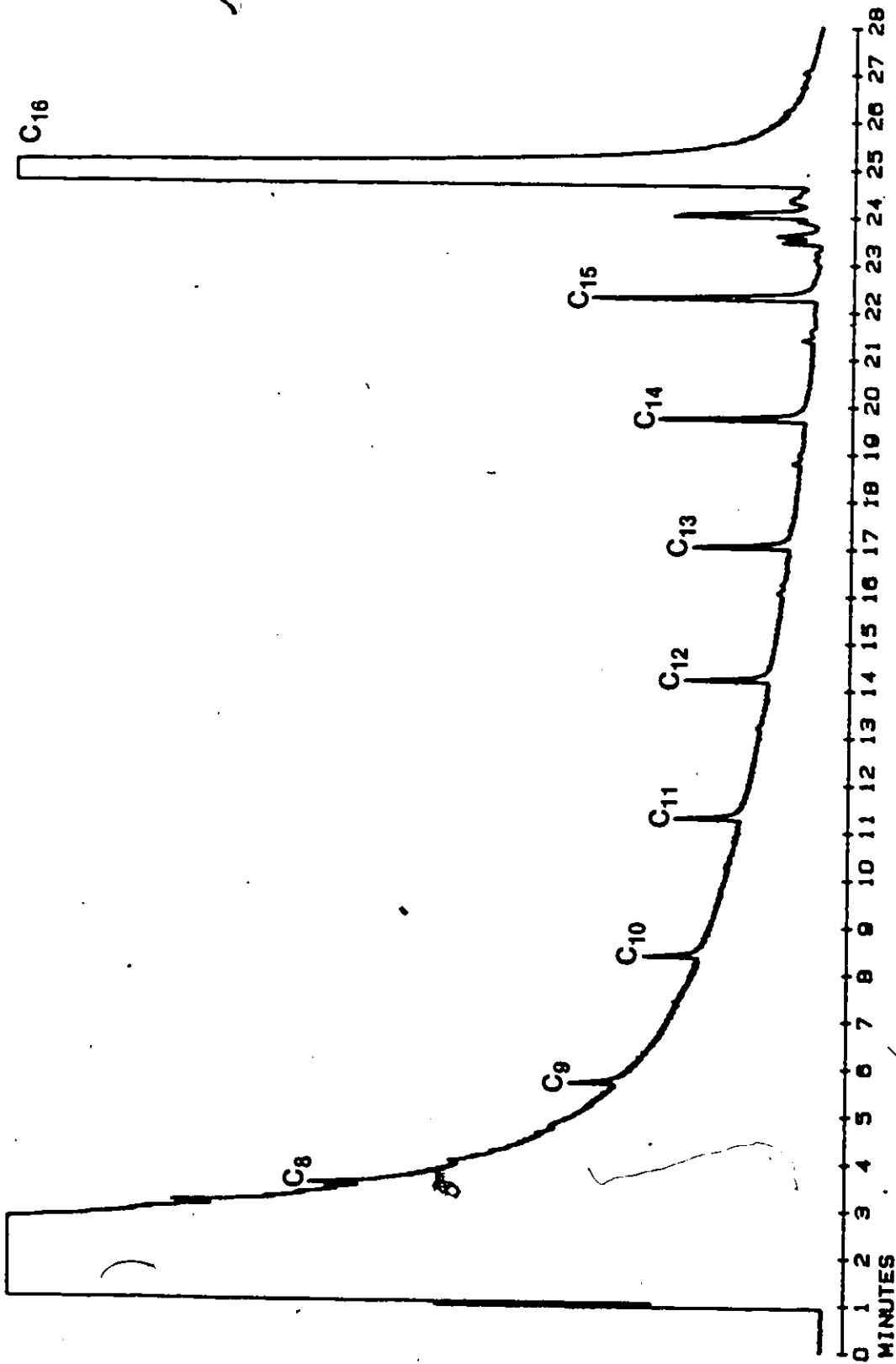


Figure 6.5: Gas chromatogram of C<sub>7</sub> products in hydrogenolysis of hexadecane at 325°C and 0.7% conversion. (Test 6.2)

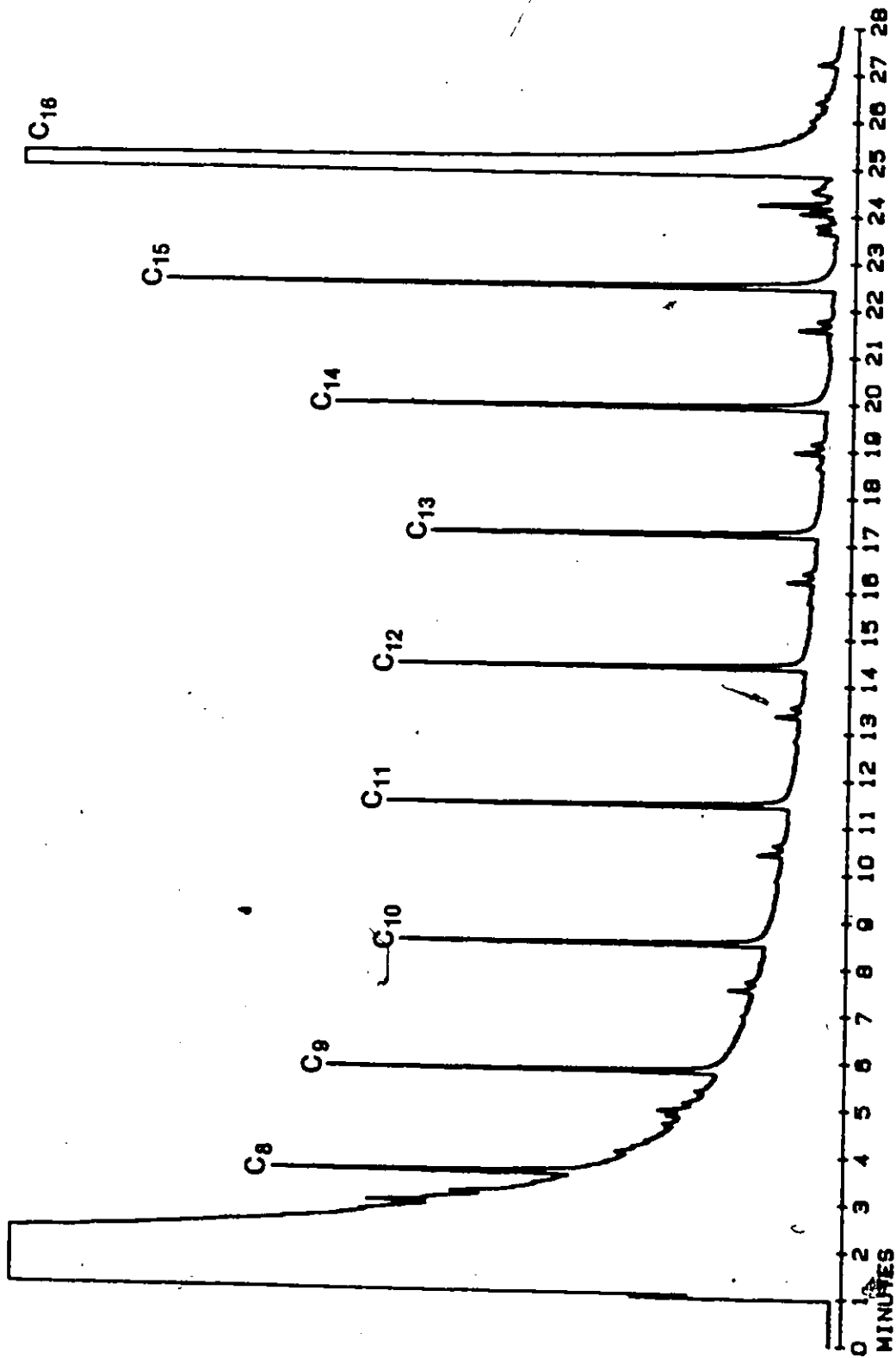


Figure 6.6: Gas chromatogram of C<sub>7</sub> products in hydrogenolysis of hexadecane at 325°C and 7.7% conversion. (Test 6.3)



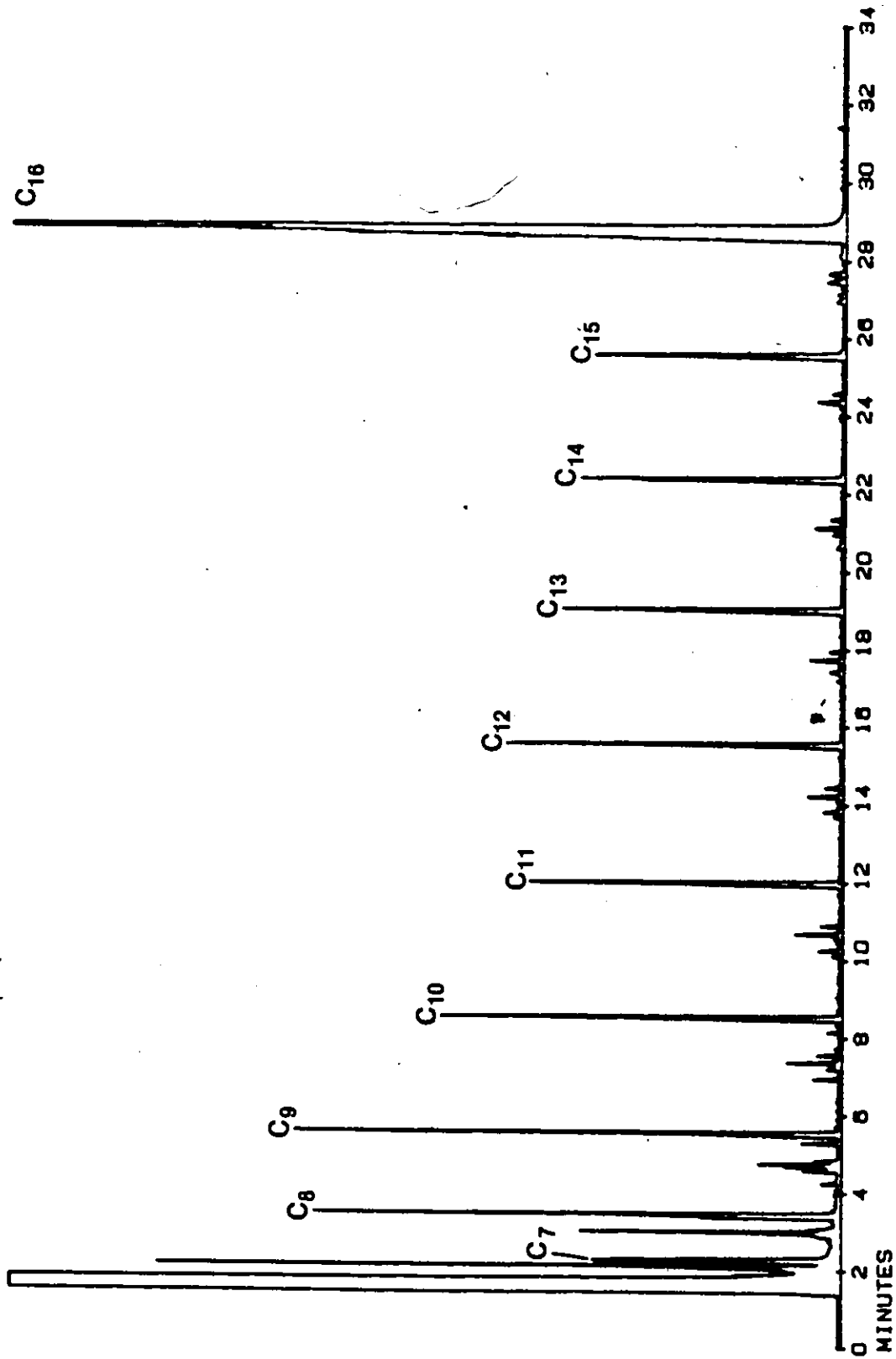


Figure 6.7: Gas chromatogram of C<sub>7</sub> products in hydrogenolysis of hexadecane at 325°C and 15.9% conversion. (Test 6.4)

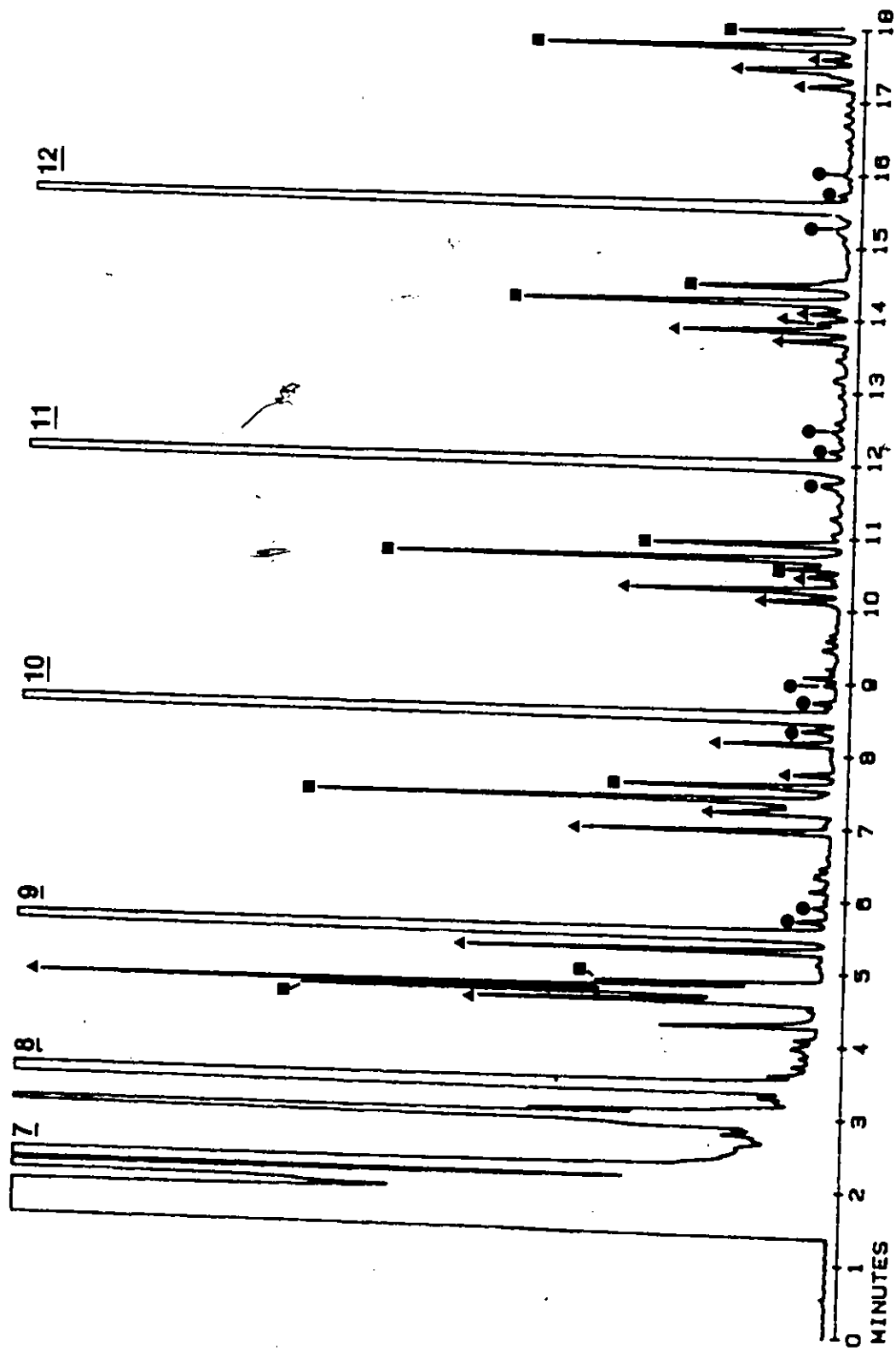


Figure 6.8: Gas chromatogram of C<sub>7</sub> products in hydrogenolysis of hexadecane at 325°C and 15.9% conversion (Test 6.4), after a 10-fold magnification of Figure 6.7 and expansion of time axis:

— = n-alkane, ● = olefin, ▲ = alkylbenzene, ■ = branched alkane.

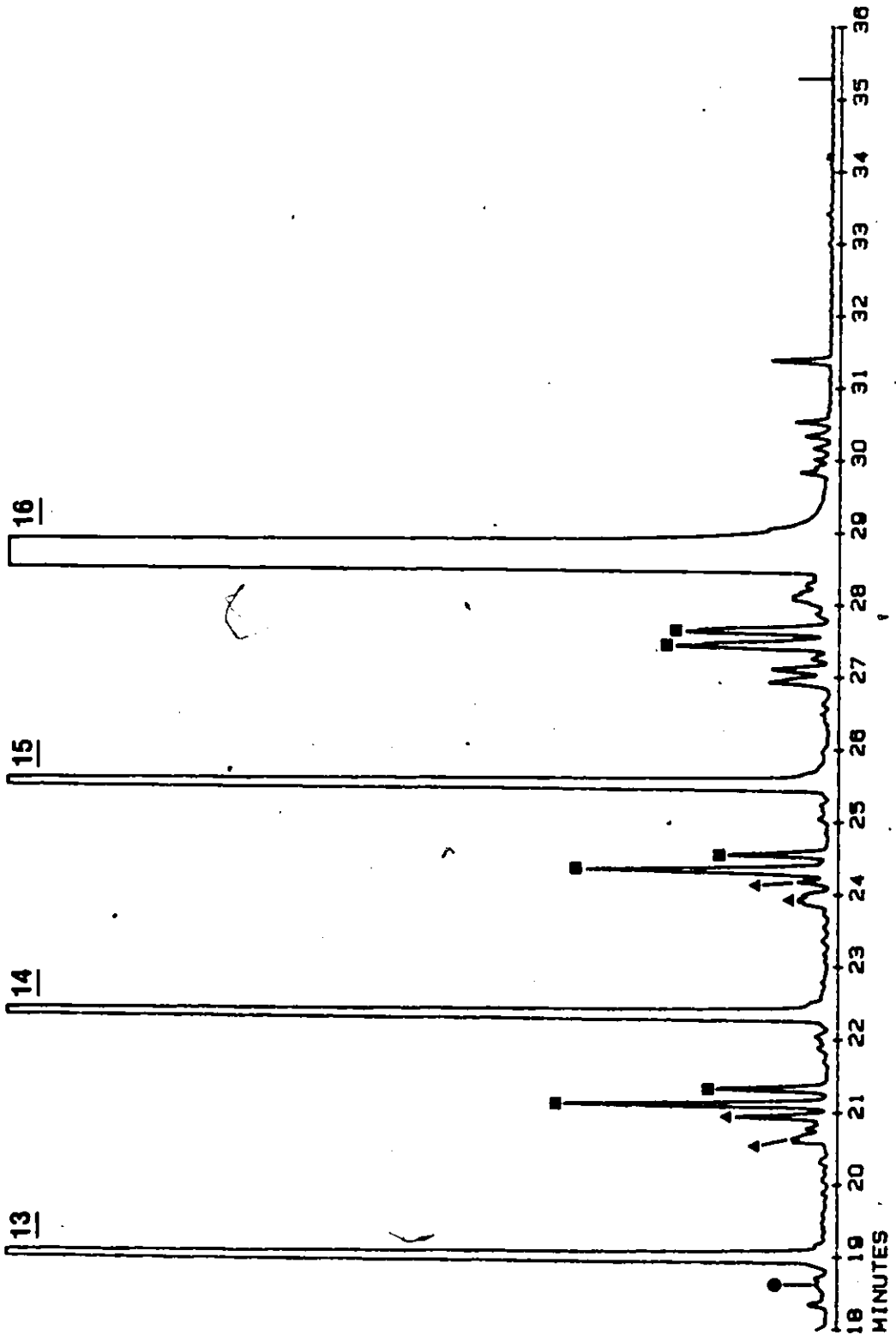


Figure 6.8 (continued)

5

isopentane at 325°C. However, deactivation of the catalyst was noticeable over an one-day experiment. Overnight H<sub>2</sub> treatment was therefore necessary. The used catalyst characterized by Mössbauer spectroscopy contained 93 weight % Fe<sub>3</sub>C and 7% Fe. Only the catalyst contributed to the hydrogenolytic activity since none of the hexadecane reacted in a blank experiment.

### 6.3 Discussion

Hydrogenolysis of hexadecane produces large amounts of methane which accounted for at least 87 mole % of all products in tests 6.1, 6.3 and 6.4, reported in Table 6.3.

Generally, the response of the flame ionization detector used in the gas chromatographic analysis of the C<sub>8</sub><sup>+</sup> products, is proportional to the weight of the substances passing through it, varying slightly with the unsaturation of the molecules. Therefore, the number of moles of a given compound is approximately calculated by dividing the corresponding peak area by its molecular weight.

The carbon number distributions of the 3 tests performed at 325°C are presented in Figure 6.9 where the logarithm of the number of moles of a given n-alkane in the C<sub>8</sub>-C<sub>15</sub> range is plotted as a function of carbon number. These data are also given in Table 6.4, where A is the weight (peak area) of C<sub>i</sub>-alkane and B, its number of moles. Hydrocarbons other than straight chain paraffins were not included in these calculations because their peak area could not be estimated accurately in the chromatograms of the low conversion samples.

TABLE 6.3

Product selectivities in hydrogenolysis of hexadecane at 9.1 FR.

Carbon Number		Selectivity <sup>a</sup>		
Test		6.1	6.3	6.4
Temperature (°C)		355	325	325
Conversion (%)		3.7	7.7	15.9
1		11.971	9.058	10.743
2		.190	.323	.379
3		.109	.213	.250
4		.102	.176	.201
5		.092	.143	.110
6		.058	.085	.073
7		.027	.037	.027
8		.021	.041	.035
9		.019	.038	.030
10		.0176	.036	.024
11		.0180	.033	.020
12		.0184	.032	.016
13		.020	.033	.014
14		.023	.038	.013
15		.026	.050	.013
$\sum_{i=2}^{15} S_i$		.741	1.278	1.205

a) Moles per mole of n-C<sub>16</sub>H<sub>34</sub> consumed.

TABLE 6.4

Carbon number distribution for hydrogenolysis of hexadecane at 325°C

Carbon Number	Test 6.2 (0.7%) <sup>a</sup>		Test 6.3 (7.7%)		Test 6.4 (15.9%)	
	A <sup>b</sup>	B <sup>c</sup>	A	B	A	B
8	3508 <sup>d</sup>	30.8	43402 <sup>d</sup>	381	241997 <sup>d</sup>	2123
9	4094	32.0	44941	351	230841	1803
10	4665	32.9	47389	334	207309	1460
11	5141	33.0	48101	308	186100	1193
12	6851	40.3	50620	298	168802	993
13	9088	49.4	55716	303	160807	874
14	13603	68.7	69523	351	161462	815
15	21742	102.6	97178	458	170107	802

a) conversion.

b) peak area.

c) number of moles (peak area/molecular weight).

d) discrepancies in areas are due to different integrators and different quantities injected.



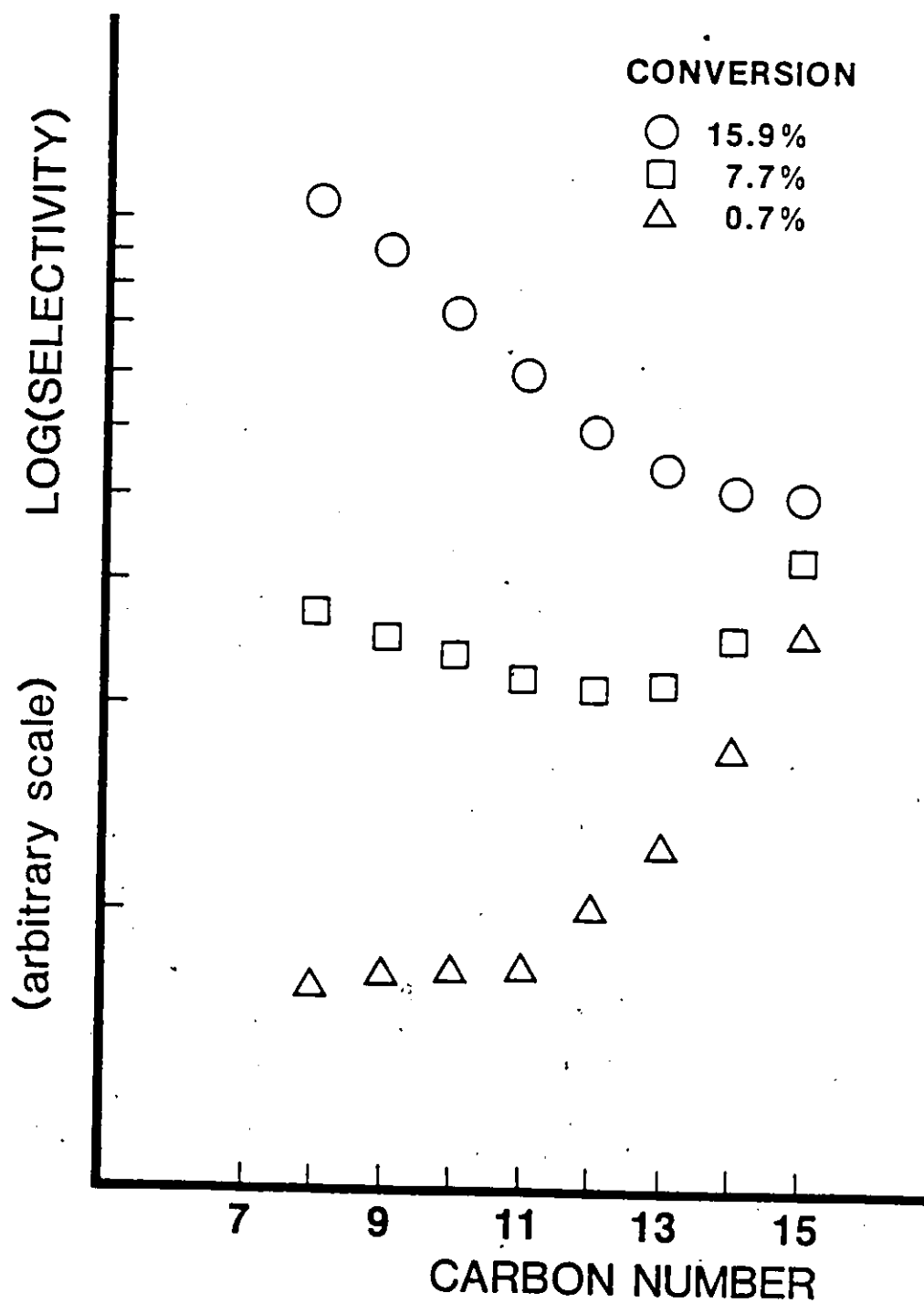


Figure 6.9: Carbon number distribution curves for  $C_7-C_{15}$  hydrocarbons in hydrogenolysis of hexadecane at 325 °C (tests 6.2, 6.3 and 6.4).

The carbon number distribution is affected by conversion, as demonstrated by Figure 6.9. At 15.9% conversion, the amount of n-alkanes increases with decreasing carbon number. However, in tests 6.2 and 6.3, the distribution curve first diminishes, reaches a minimum and then increases. Furthermore, the carbon number at which this minimum occurs, decreases with conversion, being 12 at 7.7% conversion and 8 at 0.7%.

Semi-logarithmic plots of this kind are also used in hydrogenation of carbon monoxide where hydrocarbon chains are growing by addition of 1 carbon atom at a time, which gives a linear plot (9). In the case of hydrogenolysis reactions, a straight line of similar slope may indicate the removal of one carbon at a time from the hydrocarbons.

The  $C_{11} - C_{15}$  segment of the distribution curve of test 6.2 was fitted to a straight line by linear least squares and a ratio of selectivities was obtained:

$$\frac{S_i}{S_{i+1}} = .755 \quad (6.6)$$

or

$$S_i = 0.755 S_{i+1} \quad (6.7)$$

where  $i$  and  $i+1$  are carbon numbers.

Based on equation 4.10 which was derived earlier from the network of  $n-C_{16}H_{34}$  hydrogenolysis involving only demethylation reactions, a general equation is obtained to represent selectivities in the  $C_{11} - C_{15}$  range:

$$S_m = (.755)^{n-m} S_n \quad (6.8)$$



where carbon number  $\underline{m}$  is smaller than  $\underline{n}$ .

Equation 6.8 is similar in form to the expression developed by the Bureau of Mines, which represents the growth of carbon chains in the Fischer-Tropsch synthesis:

$$\phi_m = \alpha^{m-n} \phi_n \quad (6.9)$$

where  $\phi_m$  is the number of moles of product of carbon number  $\underline{m}$ , and  $\underline{n}$  is smaller than  $\underline{m}$ .

In the hydrogenolysis network analysis, the ratio  $k_p^*/k_p'$  compares the rates of splitting and desorption of product P, and is calculated with equations 4.7, 4.10 and 6.8. To evaluate this ratio, values for  $k_p^n/k_{16}^n$  are required, but in the present case,  $k_p^*/k_p'$  is relatively insensitive to this parameter. The ratio  $k_p^*/k_p'$  varies between 3.06 and 3.09, depending on the value of  $k_p^n/k_{16}^n$ , assumed in equation 4.7: 1.0 or 0.01, which are reasonable limiting cases, since the overall rate of hydrogenolysis,  $k_p^n$ , normally drops with decreasing carbon number. This result indicates that C-C bond splitting is more than 3 times faster than desorption. In test 6.3, the initial selectivity ratio of equation 6.9 is equal to 0.766 and  $k_p^*/k_p'$  varies between 2.95 and 3.27. All these values confirm the previous results for 1-C<sub>5</sub>H<sub>12</sub> hydrogenolysis that product desorption is the slow step. However,  $k_p^*/k_p'$  in test 6.2 is 20 to 25 times smaller than in 1-C<sub>5</sub>H<sub>12</sub> hydrogenolysis and this is reflected by the smaller fraction of CH<sub>4</sub> in the products. Therefore, the length of C chain seems to have an effect on the reaction mechanism.

Slopes were also estimated from carbon number distributions of Fischer-Tropsch products published in the literature and the values of

$\alpha$ , in equation 6.9, were similar to those of the selectivity ratios in hydrogenolysis of  $n\text{-C}_{16}\text{H}_{34}$  over cobalt catalysts,  $\alpha$  was about 0.757 (9) and over Fe, 0.671 (9).

Therefore, at high carbon numbers, between  $\text{C}_{11}$  to  $\text{C}_{15}$ , the mechanism of hydrogenolysis seems to involve demethylation, the removal of 1 C atom at a time from the hydrocarbon chain: the converse of the FT synthesis where one C is added at a time.

However, as the carbon number decreases, the selectivity increases, as shown in Table 6.3, and consequently equation 4.10 is not suitable anymore. Apparently the simple demethylation mechanism with parameters independent of carbon number has limited validity.

If hydrogenolysis involves only demethylation, a hypothetical value of  $\text{CH}_4$  selectivity,  $S_1^*$  can be calculated from the selectivities of the intermediate products, based on each C-C bond splitting producing 1 molecule of  $\text{CH}_4$ :

$$S_1^* = \sum_{i=2}^{15} (16 - i) S_i \quad (6.10)$$

Since the summation of the selectivities,  $\sum_{i=1}^{15} iS_i$ , is equal to 16.0 if  $S_1^* = S_1$ , equation 6.2 can be simplified to

$$SS = \sum_{i=2}^{15} S_i = 1.0 \quad (6.11)$$

The validity of equation 6.11 was checked with experimental data from the Ph.D. thesis of J. Machiels, former graduate student in this laboratory, who investigated the hydrogenolysis of normal hexane over nickel and ruthenium catalysts (71). Since the reaction mechanism over

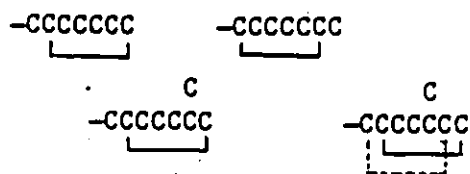
Ni involves demethylation, the summation of selectivities in equation 6.3, SS, is close to 1.0, varying between 0.89 and 0.95. However, for ruthenium, SS is between 1.54 and 1.69 since this metal breaks the C-C bonds of a molecule at random.

At 355°C on Fe, one mole of hexadecane was converted into 11.97 moles of CH<sub>4</sub> while formation of intermediate hydrocarbons by removal of terminal C atoms would produce only 7.86 moles of CH<sub>4</sub>. The summation SS was equal to 0.741. Demethylation is therefore possible in this case and the reason for the rather low value of SS will be discussed later in this section. However, in tests 6.3 and 6.4, performed at 325°C, the calculated values of CH<sub>4</sub> selectivity, respectively equal to 13.47 and 14.03, are much larger than the actual values of 9.06 and 10.74. And SS is larger than 1.0: 1.28 and 1.21 respectively, suggesting that Fe breaks also internal C-C bonds in the molecule. The carbon chain of hexadecane is probably long enough to permit adsorption on the catalyst surface at carbon atoms relatively distant from each other, which may change the splitting pattern of the reaction.

In hydrogenolysis of isopentane, SS is equal to 0.178 for test 5.1 at 2.8 FR and 325°C, and 0.04, for 5.3 at 7.0 FR and 355°C. These low values are probably due to the strong adsorption of hydrocarbons to the catalyst surface which leads to a rapid demethylation of the molecules, before desorption. In the extreme case, where all C-C bonds are broken, only CH<sub>4</sub> is produced and SS equals 0.0. However, in test 5.4 where α-Fe became Fe<sub>3</sub>C due to the low H<sub>2</sub> to i-C<sub>5</sub>H<sub>12</sub> feed ratio, the value of SS is increased to between 0.375 and 0.468. The formation of

iron carbide affected probably SS by changing the strength of the hydrocarbon adsorption as discussed in Chapter 5. The larger value of SS in test 6.1 compared to 5.1 and 5.3 is probably due to larger hydrocarbon coverage of the catalyst surface in hydrogenolysis of hexadecane compared to that of isopentane, as discussed later in this chapter.

The formation of alkylbenzenes probably involves dehydrocyclization of a paraffin. Similarly, adsorbed species with a 5-carbon ring can also be formed as intermediates in isomerization reactions, as discussed later in this section. Cyclization reaction is possible if the long alkane is bonded to the catalyst surface at positions 1 and 6, or 2 and 7, and undergoes ring closure as depicted in the following diagram:



The presence of methyl groups in the chain does not interfere with the mechanism.

This reaction mechanism was suggested by Weitkamp and co-workers (18, 120) to explain the formation of aromatics and alicyclic hydrocarbons in the Fischer-Tropsch synthesis on iron.

Although the formation of alkylbenzenes is not expected during hydrogenolysis reactions, since it involves ring formation, creation of C-C bonds, and evolution of H<sub>2</sub>, their existence is probably due to the high stability of the benzene ring. At 600 K, the Gibbs free energy of

formation,  $\Delta G_f^\circ$ , expressed per carbon atom is smaller for alkylbenzenes than for alkanes and alkenes, varying from 6.9 kcal/mole for  $C_7H_8$  to 8.1 for  $C_{14}H_{22}$ , about 5.7% less than for n-alkanes, between 7.5 and 8.4 respectively. Normal alkenes have values of  $\Delta G_f^\circ$  of about 9.2 and those of cycloalkanes are even higher.

Branched alkanes are probably formed by skeletal isomerization, as described by Gates et al (41). A five-membered ring hydrocarbon, obtained by cyclization of an alkane on the catalyst surface, has one of its C-C bond broken by hydrogenolysis, leading to a branched species. As an example, 2-methylpentane and 3-methylpentane can be formed via cyclic isomerization of n-hexane, as observed on Pt catalyst by Gault and co-workers (11). Furthermore, formation of 2-methyl groups may also occur via the breaking of a C-C bond in an adsorbed intermediate with a 3-carbon ring (41).

Examination of the product distribution of tests 6.1 and 6.4 given in Table 6.2 indicate that the proportion of alkenes is small at 325°C compared to 355°C while that of branched alkane decreases from 10.7 mole % in 6.4 to 7.0%.

Cady et al. (18) characterized the products from CO hydrogenation on Fe in a fluidized bed reactor operated at 315°C and 18 atm with a feed ratio of  $2H_2$  to 1 CO. Paraffins accounted for 12.8 volume % of all  $C_6$  hydrocarbons and 16.5% of the  $C_{14}$ 's while the proportion of olefins dropped from 86.9 to 63.6%. However, the fraction of aromatics increased from 0.3% for  $C_6H_6$  to 19.9% for  $C_{14}H_{22}$ . These figures indicate that much more  $C_8$ - $C_{14}$  olefins are produced in CO hydrogenation

than in hydrogenolysis.

If the coverage of the catalyst surface by adsorbed  $C_1$  species follows the same trend as the virtual pressure of methane,  $P_M^*$ , as suggested by Dowie et al. (34), one can expect a much higher surface coverage with  $n-C_{16}H_{34}$  hydrogenolysis than with  $C_3H_8$  or  $i-C_5H_{12}$ . Based on equation 1.11, one can calculate  $P_M^*$  in hydrogenolysis of  $n-C_{16}H_{34}$  using

$$P_M^* = (K_E P_{C_{16}} P_{H_2}^{15})^{1/16} \quad (6.4)$$

where  $P$ 's are in atm and  $K_E$  is the equilibrium constant of the following reaction



Calculations of  $P_M^*$  indicate that the surface coverage by  $C_1$  hydrocarbons with a molar feed ratio of 9.1  $H_2$  to 1  $n-C_{16}H_{34}$ , at  $325^\circ C$ , and a total pressure of 1.27 atm, is about 7 times larger than that at a ratio of 3  $H_2$  to 1  $i-C_5H_{12}$ . This is not surprising since the used  $\alpha$ -Fe catalyst was mostly transformed into  $Fe_3C$  after reaction with hexadecane while remaining  $\alpha$ -Fe with  $i-C_5H_{12}$  in test 1.1 of Chapter 5.

The higher concentration of hydrocarbon species on the surface may also explain the traces of  $C_{17}$  hydrocarbons among the products. Formation of products with a higher carbon number than the parent molecule has also been observed in hydrogenolysis of hydrocarbons on Pt (3,6).

## CHAPTER 7

### EFFECT OF WATER, POTASSIUM PROMOTER AND CARBON MONOXIDE IN

#### HYDROGENOLYSIS

The present chapter discusses the possible effects of  $H_2O$ ,  $K_2O$  and CO on selectivity and rate of hydrogenolysis on iron for the following reasons: carbon monoxide is hydrogenated to hydrocarbons in the Fischer-Tropsch Synthesis on Fe,  $K_2O$  is present as a chemical promoter in the catalysts used in the previous tests, and  $H_2O$  can be a source of adsorbed oxygen species which may inhibit the reaction. Propane was chosen as hydrocarbon reactant to simplify the experiments. Normal hexadecane is also used in the tests with the addition of CO in the feed.

#### 7.1 Hydrogenolysis of Propane in Presence of Water

This section describes the effect of water on hydrogenolysis reactions over iron. Water was added to a feed mixture of 4.7  $H_2$ : 1  $C_3H_8$ , using the saturator described in Chapter 3; its concentration was about 0.5 mole %. The reaction temperature was  $330^\circ C$  and the pressure, 125 kPa. When  $H_2O$  was added, both reaction rate and conversion decreased drastically, 30 to 50 times, as shown in Table 7.1. The rate was not more than 0.0033  $\mu\text{mole/g sec}$ . Selectivities were also affected:  $CH_4$  production decreased and  $C_2H_6$  increased.

The logarithm of the selectivity for ethane is plotted in Figure 7.1, as a function of conversion, with or without addition of water in the feed. A straight line is obtained which demonstrates that the

TABLE 7.1

Product Selectivities and Reaction Rates for Hydrogenolysis of  $C_3H_8$  over Reduced Fe Catalyst with or without Addition of  $H_2O$ , at  $330^\circ C$  and 4.7 FR.

Test	Selectivity <sup>a</sup>		Conversion	Rate <sup>b</sup>	Water
	$CH_4$	$C_2H_6$			
7.1	2.978	.011	.025 - .101	.056 - .182	No
7.2	2.551	.225	.0004 - .0033	.0014 - .0034	Yes

a) Moles per mole of  $C_3H_8$  consumed.

b) in  $\mu\text{mole/g sec.}$



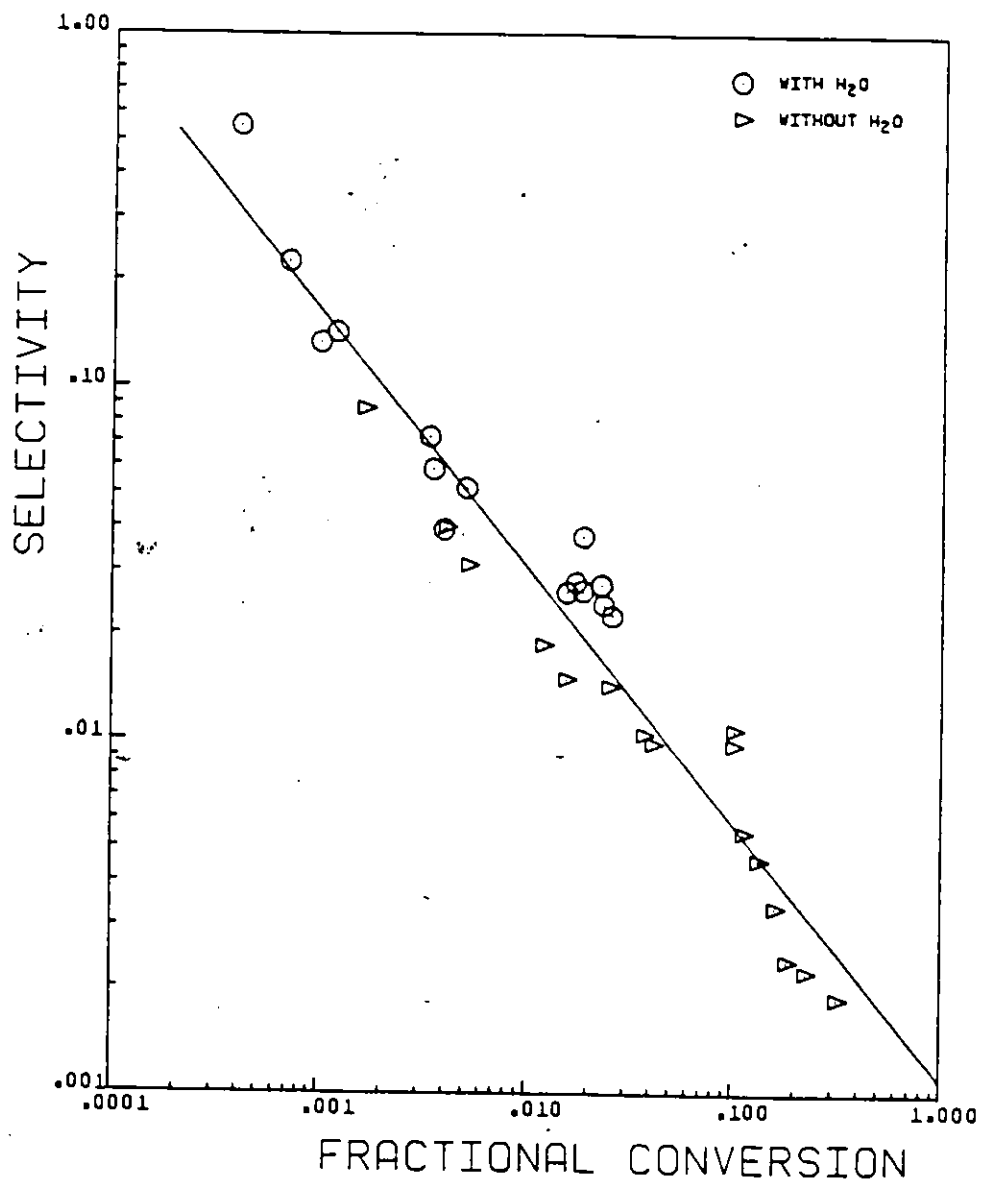


Figure 7.1: Selectivity for ethane in hydrogenolysis of propane at 330°C with or without H<sub>2</sub>O as a function of conversion of propane.

reaction mechanism is not modified by the presence of  $H_2O$  and that any effect on selectivity is due to lower conversion.

The inhibiting effect of  $H_2O$  is probably due to the adsorption of  $H_2O$  on the catalytic sites which would be used otherwise for hydrogenolysis. Thus, addition of  $H_2O$  to the feed effectively shortens the catalyst bed. Figure 7.1 indicates also that the selectivity for ethane is a function of the conversion to the power 0.72. Catalytic activity returns to its initial levels on stopping the addition of  $H_2O$ . Therefore, water poisons iron only temporarily, which agrees with the results of Almquist on poisoning experiments during  $NH_3$  synthesis over Fe catalysts (1).

## 7.2 Hydrogenolysis of Propane over Potassium-Enriched Catalyst

This section describes the effect of a chemical promoter, potassium oxide, on rate and selectivity in hydrogenolysis of propane. A potassium-enriched catalyst was prepared by impregnating with a solution of 0.27 M KOH in methanol, a reduced magnetite catalyst, D-3001. After placing the particles in an evacuation tube and covering them with a pre-determined volume of KOH solution,  $CH_3OH$  was evaporated under vacuum, without decanting the excess. The evacuation left the alkali promoter on the catalyst surface. The modified catalyst was then handled under hexane to prevent oxidation. Before the experiment, the potassium-enriched catalyst was reduced over-night at  $450^\circ C$ . A quantitative analysis by atomic absorption spectrophotometry indicated that the concentration of  $K_2O$  increased from 0.57 g  $K_2O$ /100 g Fe in the initial magnetite, to 1.60 g  $K_2O$ /100 g Fe.

TABLE 7.2  
 Product Selectivities and Reaction Rates for Hydrogenolysis  
 of  $C_3H_8$  with a 4.8 FR.

Test	Potassium Content <sup>a</sup>	$T_R$ (°C)	Selectivity <sup>b</sup>		Conversion	Rate <sup>c</sup>
			$CH_4$	$C_2H_6$		
7.3	1.6	325	2.840	0.080	.0004	.0005
7.4	1.6	337	2.972 <sup>d</sup>	0.014 <sup>d</sup>	.0013 - .019	.0003 - .0041
7.5	1.6	358	2.991	0.0045	.0022 - .014	.0029 - .0041
7.6	0.57	327	2.977	0.012	.025 - .041	.0096 - .0181

a) g  $K_2O$ /100 g Fe.

b) moles per mole of  $C_3H_8$  consumed.

c) in  $\mu\text{mole/g sec.}$

d) average value of product selectivity over the complete range of conversion.

In the hydrogenolysis, the feed ratio of  $H_2$  to  $C_3H_8$  was about 4.8 and the pressure, 125 kPa. Because of poor catalytic activity at  $325^\circ C$ , experimental values of rates and selectivities were also obtained at  $335$  and  $355^\circ C$ , all of them given in Table 7.2. Data from hydrogenolysis over an original reduced Fe catalyst, test 7.6, are also presented in Table 7.2.

A dramatic drop in activity is observed for the catalyst with increased K-content. The original catalyst was 7 to 10 times more active than the alkalized catalyst in test 7.5, performed at  $30^\circ C$  higher than 7.6. Furthermore, the selectivity for methane in tests 7.3, 7.4 and 7.5 was slightly smaller compared to 7.6 and for  $C_2H_6$ , a bit larger.

These results indicate that potassium does not seem to modify the mechanism of reaction or the splitting pattern. However, it may influence the rate of adsorption of hydrocarbon reactant as the overall rate of reaction changes. This drop in activity is also observed in hydrogenation of carbon monoxide over a Fe catalyst with a K-content larger than  $0.6 \text{ g } K_2O/100 \text{ g Fe}$  (111).

### 7.3 Effect of Carbon Monoxide on Hydrogenolysis over Iron

This section investigates the effect of carbon monoxide on hydrogenolysis of propane and hexadecane in relation to selectivity and reaction rate. CO was added to the reactant mixture either at low concentration or as pulses.

### 7.3.1 Effect of Carbon Monoxide on Hydrogenolysis of n-Hexadecane

Hydrogenolysis of n-hexadecane was studied with a low concentration of carbon monoxide in the feed to investigate the inhibiting effect of carbon monoxide. Craxford (29) observed that wax which had accumulated on cobalt after 3 weeks of hydrogenation of carbon monoxide, could be removed in less than 3 hours by passing hydrogen over the catalyst bed. Furthermore, workers at the Bureau of Mines (54) found  $\text{CH}_4$  and higher hydrocarbons, up to wax, in the hydrogenation of carbon monoxide over ruthenium but only  $\text{CH}_4$  in  $\text{CO}_2$  hydrogenation over the same metal. Since ruthenium is also a very good hydrogenolysis catalyst (114), these results suggest that carbon monoxide inhibits this reaction. But will small CO concentrations in the feed inhibit hydrogenolysis over iron catalysts? The present section deals with this question.

An electronic mass flow meter was used to deliver accurately a predetermined flow of CO. The molar feed ratio of  $\text{H}_2$  to  $\text{n-C}_{16}\text{H}_{34}$  was about 9.4 and the CO concentration in the feed, 5.7 mole %. The reaction temperature was  $325^\circ\text{C}$  and the pressure, 125 kPa. Figure 7.2 presents 2 gas chromatograms obtained on a capillary column, of the  $\text{C}_8^+$  products in hydrogenolysis of  $\text{n-C}_{16}\text{H}_{34}$  without (test 7.7) or with addition of CO (test 7.8); chromatogram II (with CO) is inverted. The size of the sample injected in the gas chromatograph was larger for II than for I.

Chromatogram I (without CO) is similar to those described in Section 6.2 of Chapter 6, where the main products are normal alkanes and the small peaks, alkylbenzenes, olefins or branched alkanes. However,

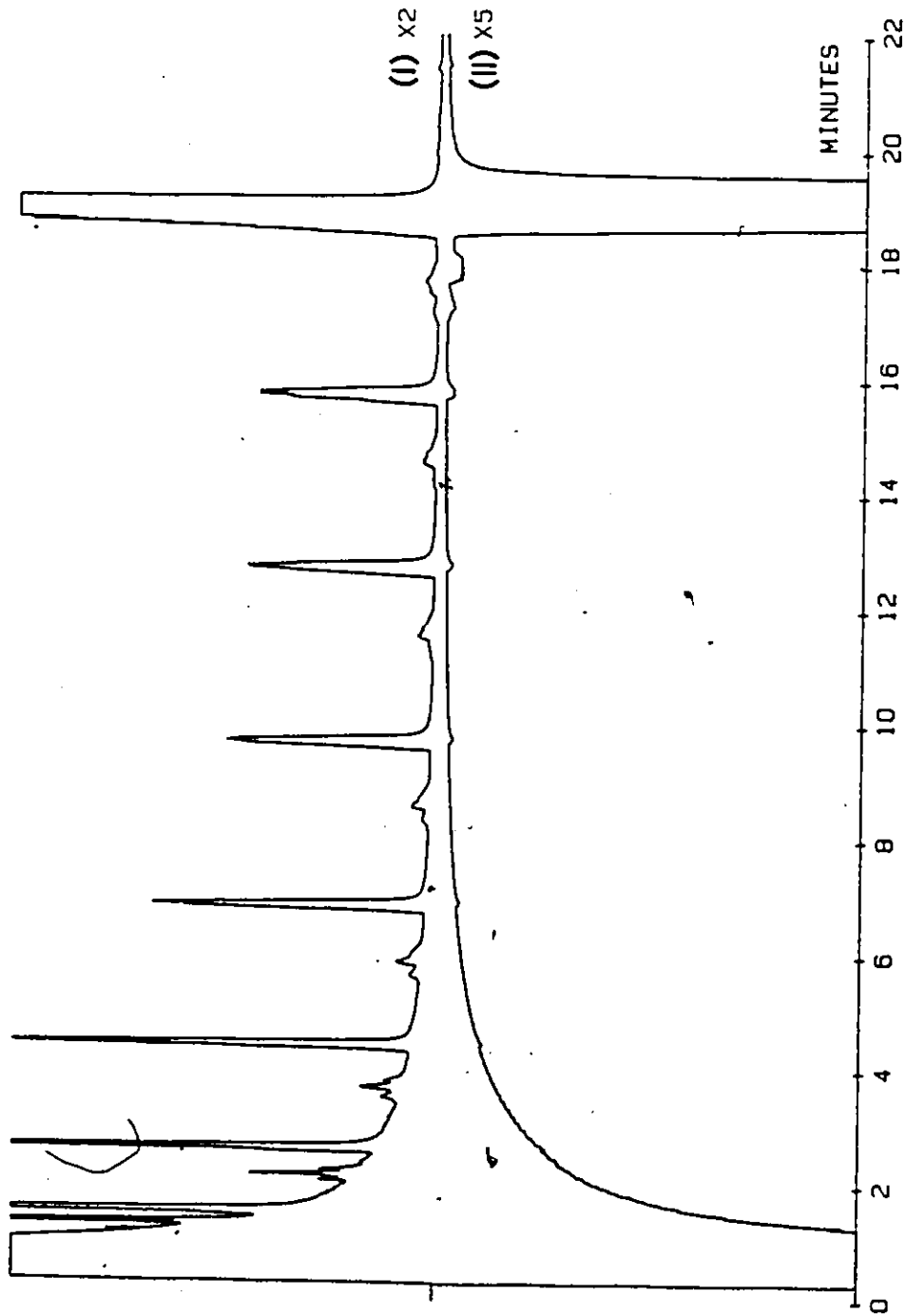
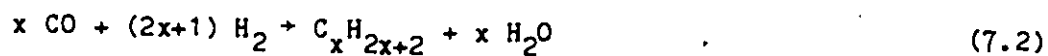


Figure 7.2: Gas chromatogram of  $C_8$  products in hydrogenolysis of hexadecane at  $325^\circ C$  without (I) or with (II) 5.7 mole % CO in the feed. Chromatogram II is inverted.

chromatogram II (with CO) shows only traces of straight chain alkanes in the  $C_8$  to  $C_{15}$  hydrocarbon range, even after a 5-fold magnification of the Y-axis. But the gas chromatographic analysis of the outlet gases indicates the presence of methane, ethane and propane. Ethylene, carbon dioxide and water were also found among the products, although not present in tests 6.1 - 6.4. The composition in mole fractions of the outlet gases in test 7.8 was the following: CO, .0056,  $CH_4$ , .0271,  $CO_2$ , .0096,  $C_2H_4$ , .0017,  $C_2H_6$ , .0018,  $H_2O$ , .025-.028 (approximately),  $H_2$ , .8637, and  $n-C_{16}H_{34}$ , .0902.

Chromatogram II shows that hydrogenolysis of  $n-C_{16}H_{34}$  is stopped completely when carbon monoxide is added to the feed mixture. Furthermore, the presence of water and carbon dioxide among the products as well as the large drop in CO concentration in the catalyst bed indicate that hydrogenation of CO is taking place in the reactor. Carbon monoxide is probably more strongly adsorbed on iron than hydrocarbons, leading to the occupation by CO of active sites which would be otherwise used for hydrogenolysis. Methane and the other products are therefore obtained from the hydrogenation of CO:



and from the water gas shift reaction:



The presence of ethylene in the outlet gases indicates that the reactions of hydrogen are inhibited by CO, since olefins should be hydrogenated under these conditions. Consequently, carbon monoxide acts

like a poison for the hydrogenolysis of hydrocarbons; these data explain why during the Fischer-Tropsch synthesis, the  $C_2^+$  hydrocarbons, formed via CO hydrogenation, are not broken down to methane, further along the catalyst bed.

Carbon monoxide was more than 90% converted in test 7.8 and the concentration of water in the outlet gases reached 2.8 mole %. However, as shown in Section 7.1, a concentration of water of 0.5 mole % in the feed drastically reduced the rate of hydrogenolysis. One may ask if in test 7.8,  $H_2O$  is interfering with the hydrogenolysis of  $n-C_{16}H_{34}$  and the hydrogenation of CO. However, the reaction rate was about 0.564  $\mu$ mole CO/g sec, which is 200 times larger than the rates obtained for  $C_3H_8$  in  $H_2O$  poisoning tests, given in Table 7.1. Therefore, the inhibiting effect of water does not seem important in this system. Carbon monoxide is probably more strongly adsorbed on the catalyst than water which reacts with CO to form  $CO_2$  via the water-gas-shift reaction (equation 7.3).

### 7.3.2 Effect of Carbon Monoxide on Hydrogenolysis of Propane

Different concentrations of CO were added to the feed in hydrogenolysis of propane. The molar feed ratio of  $H_2$  to  $C_3H_8$  was about 4.3, the temperature,  $335^\circ C$  and the pressure, 125 kPa. Tests 7.9 to 7.12 were done at 1.1, 3.5, 4.85 and about 10 mole % CO in the feed. Carbon monoxide was also injected in pulses containing about 50% CO, 42%  $H_2$  and 8%  $C_3H_8$ . The pulse experiments are described later in this section.

Gas chromatographic analysis of the outlet gases showed that when



TABLE 7.3

Hydrogenolysis of Propane at 335°C and 4.3 FR,  
with Different Concentrations of CO in the Feed

Test:	7.9	7.10	7.11	7.12	7.13
% CO <sup>a</sup>	1.1	3.5	4.85	10.0	0.0
<u>MOLE FRACTION<sup>b</sup></u>					
CH <sub>4</sub>	.0092-.0115	.0181-.0217	.0218	.0230-.0270	.0070-.0161
C <sub>2</sub> H <sub>6</sub>	.0010-.0012	.0023-.0025	.0034	.0026-.0035	< .00009
C <sub>3</sub> H <sub>8</sub>	.1928-.1964	-	.1866	-	.1666-.1924
C <sub>3</sub> H <sub>8</sub> <sup>a</sup>	.1948	-	.1758	-	.1722-.1948
<u>RATE<sup>c</sup></u>					
CO	.372	.252	.319	.588	0
C <sub>3</sub> H <sub>8</sub>	-	0	0	0	.059-.107
<u>MOLAR RATIOS IN PRODUCT</u>					
C <sub>1</sub> /(C <sub>1</sub> +C <sub>2</sub> )	.903	.891	.866	.892	.996
C <sub>2</sub> /C <sub>2</sub>	.115	.154	.158	.756	0
CO <sub>2</sub> /CH <sub>4</sub>	.003	.020	.034	1.02	0
<u>CONVERSION<sup>d</sup></u>					
(%)	>99.9	99.9	99.8	86.4-92.2	.012-.05 <sup>e</sup>

a) in the feed.

b) in the outlet gases.

c) in  $\mu$ mole CO or C<sub>3</sub>H<sub>8</sub>/g sec.

d) conversion of CO.

e) conversion of C<sub>3</sub>H<sub>8</sub>.

CO was added to the feed, ethylene,  $\text{CO}_2$  and  $\text{H}_2\text{O}$  were produced as well as methane and ethane. Table 7.3 gives molar ratios of products,  $\text{CH}_4/(\text{C}_2\text{H}_6 + \text{CH}_4)$ ,  $\text{C}_2\text{H}_4/\text{C}_2\text{H}_6$ , and  $\text{CO}_2/\text{CH}_4$  for tests 7.9 - 7.12.

The presence of CO in the feed increased the concentration of  $\text{C}_2\text{H}_6$  30 to 50 times, while keeping that of methane constant. The production of ethylene and  $\text{CO}_2$  increased with the amount of CO in the feed. With less than 5 mole % CO, 0.10 to 0.15 mole of  $\text{C}_2\text{H}_4$  was formed per mole of  $\text{C}_2\text{H}_6$  and with 10% CO, 0.75 mole. Furthermore, only traces of CO were found in the outlet gases. However, propane did not seem to be consumed, based on values of initial and final concentrations given in Table 7.3. Therefore, all of the products probably came from hydrogenation of carbon monoxide and from the water-gas-shift reaction, like in test 7.8. The conversion of carbon monoxide was larger than 99.8% in tests 7.9 - 7.11, while at high CO concentration, it varied between 86.4 and 92.2%. Discrepancies between data for propane in test 7.11 may be due to the contraction of the gas volume in hydrogenation reactions.

Pulses of carbon monoxide were added to the feed while hydrogenolysis of propane was in progress, test 7.14, or while pure  $\text{H}_2$  was passed through the reactor, test 7.15.

The pulses of CO were produced by opening the solenoid valve of the CO flow controller to obtain a predetermined flow rate during 30 seconds. The pulse composition was about 50 mole % CO, 42%  $\text{H}_2$  and 8%  $\text{C}_3\text{H}_8$  in test 7.14, and 53% CO, 47%  $\text{H}_2$  in test 7.15. Both tests were performed over reduced Fe catalyst at  $340^\circ\text{C}$  and 125 kPa. The molar feed

TABLE 7.4

Molar Ratios of Products from CO Pulse Experiments  
during Hydrogenolysis of Propane at 340°C and 4.9 FR.

Time <sup>a</sup>	Mole Fraction		Molar Ratio in Product		
	CH <sub>4</sub>	C <sub>2</sub> H <sub>6</sub>	CH <sub>4</sub> /C <sub>2</sub> H <sub>6</sub>	CO <sub>2</sub> /CH <sub>4</sub>	C <sub>2</sub> H <sub>4</sub> /C <sub>2</sub> H <sub>6</sub>
(50/60)	.00492	.00036	13.6	9.1	1.98
1.0	.00586	.00043	13.6	18.4	1.56
1.25	.00440	.00065	6.7	41.9	1.93
	(.00175) <sup>b</sup>	(.00035) <sup>b</sup>	(5.1) <sup>b</sup>	(43.9) <sup>b</sup>	(1.70) <sup>b</sup>
1.50	(.00608)	(.00067)	(9.0)	(23.2)	(1.55)
2.00	.00534	.00047	11.4	11.4	1.40
	(.00847)	(.00200)	(4.2)	(43.9)	(1.05)
6.00	.01157	.00006	193.	.066	-
20.00	.01027	.00005	201.	.019	-

a) time interval after injection of a pulse of CO, in minutes.

b) (ratio), from CO pulse experiments, without C<sub>3</sub>H<sub>8</sub> in the feed (test 7.15).

ratio of  $H_2$  to  $C_3H_8$  in test 7.14 was about 4.9. Samples of the outlet gases were taken at different time intervals after the closing of the CO valve.

In both tests, alkanes ( $CH_4$ ,  $C_2H_6$ ), ethylene, water and carbon monoxide were identified among the products as in tests 7.9 - 7.12. Table 7.4 gives values of the molar ratios of  $CH_4$  to  $C_2H_6$ ,  $C_2H_4$  to  $C_2H_6$  and  $CO_2$  to  $CH_4$ , at different time intervals following pulses of CO. Data from test 7.15, without  $C_3H_8$  in the feed, are presented in brackets.

Similar results were obtained in tests with or without propane in the feed. Large fluctuations in the product distribution were observed in the first 3 minutes. Ethylene was present in the outlet gases only for a few minutes indicating that after its formation from CO, it does not react further due to the inhibiting effect of CO. The production of ethylene was quite large as shown by samples containing up to 1.9 times more  $C_2H_4$  than  $C_2H_6$ . Very large quantities of  $CO_2$  were made in the first minutes following the injection of a pulse. In some particular samples, the  $CO_2$  concentration was more than 40 times that of  $CH_4$ . Traces of water and carbon dioxide were still found 30 minutes after a pulse of CO. In test 7.14, the ratio of  $CH_4$  to  $C_2H_6$  became larger than 100 after 6 minutes, indicating that hydrogenolysis had resumed.

## CHAPTER 8

### CONCLUSIONS

The present chapter gives the main findings of my research on the mechanism of hydrogenolysis of hydrocarbons over iron.

Iron catalysts produce a large amount of methane in hydrogenolysis of hydrocarbons, compared to other Group VIII metals. The network analysis of the selectivity data from hydrogenolysis of isopentane and n-hexadecane, indicates that product desorption is the slow step of the reaction mechanism. The ratio of splitting to desorption,  $k_s^*/k_p^*$ , varies with the length of the hydrocarbons and is equal to about 3.0 for  $C_{10}^+$  alkanes, and 64 for  $C_2$  to  $C_5$ 's, on average. The hydrocarbon species adsorbed on the catalyst surface are largely completely broken to methane before desorbing, since the splitting of C-C bonds is much faster than desorption. Network analysis also indicates that the overall rate of hydrogenolysis,  $k_p^*$ , increases with the carbon number.

Characterization of the used catalysts by Mössbauer spectroscopy has shown that bulk Fe carbides are present only at very low ratios of  $H_2$  to hydrocarbon in the feed. Bulk carbides presumably result from the competition between diffusion in the catalyst and hydrogenation to methane for surface carbon species. At low feed ratios, the excess surface carbon dissolves in the bulk and precipitates as  $Fe_3C$ ; iron becomes a reservoir for carbon, mainly in carbidic form. The formation

of bulk iron carbides in the catalyst is reversible since high ratios of  $H_2$  to hydrocarbon leads to their hydrogenation to  $CH_4$ .

Under conditions that form bulk  $Fe_3C$ , the presence of surface carbides is insured and the products contain less  $CH_4$  and more intermediates due to the presence of Fe-C bond in the carbides, which probably makes the hydrocarbons less-strongly chemisorbed on Fe atoms of cementite than on those of  $\alpha$ -Fe. Intermediate hydrocarbons should therefore be more readily desorbed, leading to an increase of their selectivity.

Although normal alkanes are the main products of  $n-C_{16}H_{34}$  hydrogenolysis, alkylbenzenes, branched alkanes and alkenes are also found. These side products account for about 20 mole % of the  $C_9$  to  $C_{14}$  hydrocarbons. The alkylbenzenes that are found, consist of long carbon chains with either a benzene or a toluene group at one end. These aromatics are presumably obtained by dehydrocyclization of alkanes, and the branched alkanes, by ring opening of adsorbed alicyclic species.

Iron catalysts apparently break the hydrocarbon molecules by demethylation, as indicated by the network analysis applied to the low conversion selectivity data for  $C_{11}$ - $C_{15}$  alkanes in  $n-C_{16}H_{34}$  hydrogenolysis. However, with short hydrocarbon chains, demethylation is too rapid to be observed in the carbon number distribution. At high conversion of  $n-C_{16}H_{34}$ , iron may also break the C-C bonds which are not adjacent to terminal C atoms.

The hydrogenolysis of hydrocarbons is completely inhibited when carbon monoxide is added to the feed, even at concentration as low as 4

mole %. Furthermore, CO is hydrogenated to light alkanes and ethylene with production of water and carbon dioxide via the water-gas-shift reaction. The poisoning effect of CO probably explains why  $C_2^+$  alkanes and olefins, formed during Fischer-Tropsch synthesis, are not broken down to methane, further along the catalyst bed. An increase in the ethylene production is observed with increasing CO content in the feed. Experiments, involving pulses of CO, gave similar results with or without propane in the feed, confirming the inhibiting effect of CO.

Traces of water in the feed reduce the rate of hydrogenolysis on Fe. An increase in the  $K_2O$  content of Fe catalyst decreases the reaction rate without affecting the selectivity.

A new method of deriving selectivity equations for reaction network, using graphical pathways, was developed. The network analysis was shown to apply to irreversible reactions for hydrogenolysis and isomerization.

## REFERENCES

1. Almquist, J.A. and Black, C.A., J. Amer. Chem. Soc., 48, 2814 (1926).
2. Amelse, J.A., Butt, J.B. and Schwartz, L.H., J. Phys. Chem., 82 (5), 558 (1978).
3. Anderson, J.R. and Baker, B.G., Proc. Roy. Soc., Ser. A, 271, 402 (1963).
4. Anderson, J.R. and Avery, N.R., J. Catal., 7, 315 (1967).
5. Anderson, J.R. and Baker, B.G., "Chemisorption and Reactions on Metallic Films", ed. J.R. Anderson, Academic Press, New York, 1971, Chapter 8.
6. Anderson, J.R., Adv. Catal., 23, 1 (1973).
7. Anderson, R.B., Hofer, L.J.E., Cohn, E.M. and Seligman, B., J. Amer. Chem. Soc., 73, 944 (1951).
8. Anderson, R.B., from "Catalysis IV", ed. P.H. Emmett, Reinhold Publishing Corporation, New York, 1956, Chapter 1.
9. Anderson, R.B., from "Catalysis IV", ed. P.H. Emmett, Reinhold Publishing Corporation, New York, 1956, Chapter 2.
10. Barbier, J., Morales, A. and Maurel, R., Bull. Soc. Chim. Fr., I-31 (1978).
11. Barron, Y., Maire, G., Muller, J.M. and Gault, F.G., J. Catal., 5, 428 (1966).
12. Berkowitz, A.E. and Kneller, E., eds., "Magnetism and Metallurgy", Academic Press, New York, 1969.
13. Boitiaux, J.-P., Martino, G. and Montarnal, R., C.R. Acad. Sci., Paris, Ser. C, 280, 1451 (1975).
14. Bokhoven, C., Van Heerden, C., Westrik, R. and Zwietering, P., from "Catalysis III", ed. P.H. Emmett, Reinhold Publishing Corporation, New York, 1955, Chapter 7.
15. Boudart, M., Adv. Catal., 20, 153 (1969).



16. Browning, L.C., De Witt, T.W. and Emmett, P.H., J. Amer. Chem. Soc., 72, 4211 (1950).
17. Brucker, C. and Rhodin, T., J. Catal., 47, 214 (1977).
18. Cady, W.E., Launer, P.J. and Weitkamp, A.W., Ind. Eng. Chem., 45 (2), 350 (1953).
19. Carter, J.L. and Sinfelt, J.H., J. Phys. Chem., 70 (9), 3003 (1966).
20. Carter, J.L., Cusumano, J.A. and Sinfelt, J.H., J. Catal., 20, 223 (1971).
21. "Cobalt Monograph", Centre d'information du cobalt, Brussels, 1960.
22. Chang, C.C., from "Characterization of Solid Surfaces", eds. P.F. Kane and G.B. Larrabee, Plenum Press, New York, 1974, Chapter 20.
23. Chen, H.C. and Anderson, R.B., J. Colloid Interfac. Sci., 38, 535 (1972).
24. Chevreau, T. and Gault, F.G., J. Catal., 50, 124, 143 (1977).
25. Chikazumi, S. and Charap, S.H., "Physics of Magnetism", John Wiley and Sons, New York, 1964.
26. Cimino, A., Boudart, M. and Taylor, H., J. Phys. Chem., 58, 796 (1954).
27. Corolleur, C., Tomanova, D. and Gault, F.G., J. Catal., 24, 401 (1972).
28. Craxford, S.R. and Rideal, E.K., J. Chem. Soc., 1604 (1939).
29. Craxford, S.R., Fuel, 26, 119 (1947).
30. Darken, L.S. and Gurry, R.W., "Physical Chemistry of Metals", McGraw-Hill Book Company, New York, 1953.
31. Dénès, G., "GMFP5", A Revised Version of GMFP (92) for Fitting Mössbauer Spectra with up to 5 Hyperfine Sites.
32. Dowie, R.S., Gray, M.C., Whan, D.A. and Kemball, C., Chem. Commun., 883 (1971).
33. Dowie, R.S., Kemball, C., Kempling, J.C. and Whan, D.A., Proc. Roy. Soc., Ser. A, 327, 491 (1972).

34. Dowie, R.S., Kemball, C. and Whan, D.A., *J. Phys. Chem.*, 80 (26), 2900 (1976).
35. Draper, N.R. and Smith, H., "Applied Regression Analysis", John Wiley and Sons, New York, 1966.
36. Dry, M.E., from "Catalysis, Science and Technology", eds. J.R. Anderson and M. Boudart, Vol. 1, Springer-Verlag, Berlin, 1981, Chapter 4, p. 196.
37. Dumesic, J.A. and Topsoe, H., *Adv. Catal.*, 26, 121 (1977).
38. Dutartre, R. and Martin, G.A., *C.R. Acad. Sci., Paris, Ser. C*, 288, 65 (1979).
39. Everhart, J.L., "Engineering Properties of Nickel and Nickel Alloys", Plenum Press, New York (1971).
40. Fischer, F. and Tropsch, H., *Brennstoff-Chem.*, 7, 97 (1926).
41. Gates, B.C., Katzer, J.R. and Schuit, G.C.A., "Chemistry of Catalytic Processes", McGraw-Hill Book Company, New York, 1979, p. 266.
42. Grant, J.T., in "Characterization of Metal and Polymer Surfaces", ed. L.-H. Lee, Vol. 1, Acad. Press, New York, 1977, p. 133.
43. Greenwood, N.N. and Gibb, T.C., "Mössbauer Spectroscopy", Chapman and Hall, London, 1971.
44. Grübmler, P., Schleyer, P. and McKervey, M., *Tetrahedron Letters*, 2, 181 (1979).
45. Guczi, L., Gudkov, B.S. and Tétényi, P., *J. Catal.*, 24, 187 (1972).
46. Guczi, L., Sárkány, A. and Tétényi, P., "Catalysis", ed. J.W. Hightower, Vol. 2, Elsevier, Amsterdam, 1973, p. 1111.
47. Guczi, L. and Ujszászi, K., *React. Kinet. Catal. Lett.*, 8 (4), 489 (1978).
48. Haas, T.W., Grant, J.T. and Dooley, G.J., *J. Appl. Phys.*, 43 (4), 1853 (1972).
49. Halang, W.A., Langlais, R. and Kugler, E., *Anal. Chem.*, 50 (13), 1829 (1978).
50. Heller, S.R. and Milne, G.W.A., eds., "EPA/NIH, Mass Spectral Data Base", U.S. Department of Commerce, Washington, 1978.

51. Hobson, M.C., from "Experimental Methods in Catalytic Research", eds. R.B. Anderson and P.T. Dawson, Vol. 2, Academic Press, New York, 1976, Chapter 5.
52. Hofer, L.J.E., "Catalysis IV", ed. P.H. Emmett, Reinhold Publishing Corporation, New York, 1956, Chapter 4.
53. Joshi, A., Davis, L.E. and Palmberg, P.W., from "Methods of Surface Analysis", eds. S.P. Wolsky and A.W. Czanderna, Elsevier, Amsterdam, 1975, Chapter 5, p. 159.
54. Karn, F.S., Shultz, J.K. and Anderson, R.B., Ind. Eng. Chem., Prod. Res. Develop., 4, 265 (1965).
55. Kemball, C. and Taylor, H.S., J. Amer. Chem. Soc., 70, 345 (1948).
56. Kemball, C., Discuss. Faraday Soc., 41, 190 (1966).
57. Kemball, C., Catal. Rev., 5 (1), 33 (1971).
58. Kemball, C. and Kempling, J.C., Proc. Roy. Soc., Ser. A, 329, 391 (1972).
59. Kempling, J.C. and Anderson, R.B., Ind. Eng. Chem., Process Des. Develop., 11, 146 (1972).
60. Kempling, J.C. and Anderson, R.B., "Catalysis", ed. J.W. Hightower, Vol. 2, Elsevier, Amsterdam, 1973, p. 1099.
61. Kikuchi, E., Morita, Y. and Yamamoto, K.J., Bull. Jap. Petr. Inst., 11, 34 (1969).
62. Kikuchi, E., Tsurumi, M. and Morita, Y., J. Catal., 22, 226 (1971).
63. Kochloefl, K. and Bazant, V., J. Catal., 10, 140 (1968).
64. Larsson, R., Chemica Scripta, 12, 78, 87, 89 (1977).
65. Le Caër, G., Dubois, J.M. and Sénateur, J.M., J. Solid State Chem., 19, 19 (1976).
66. Le Caër, G., Dubois, J.M., Pijolat, M., Perrichon, V. and Bussière, P., J. Phys. Chem., 86, 4799 (1982).
67. Leclercq, L., Leclercq, G. and Maurel, R., Séminaire soviétique-français de Kiev (1974).
68. Lee, C.B., Machiels, C.J. and Anderson, R.B., Can. J. Chem. Eng.,

- 54, 590 (1976).
69. Logan, S.R., Moss, R.L. and Kembal, C., Trans. Faraday Soc., 54, 922 (1958).
  70. Logan, S.R. and Kembal, C., Trans. Faraday Soc., 56, 144 (1960).
  71. Machiels, C.J., Ph.D. Thesis, McMaster University (1978).
  72. Machiels, C.J. and Anderson, R.B., J. Catal., 58, 253 (1979).
  73. Machiels, C.J. and Anderson, R.B., J. Catal., 58, 260, 268 (1979).
  74. Machiels, C.J. and Anderson, R.B., J. Catal., 60, 339 (1979).
  75. Maire, G., Plouidy, G., Prudhomme, J.C. and Gault, F.G., J. Catal., 4, 556 (1965).
  76. Martin, G.-A., Vide 1978 (numéro spécial), 199 (1978).
  77. Matsumoto, H., Saito, Y. and Yoneda, Y., J. Catal., 19, 101 (1970).
  78. Matsumoto, H., Saito, Y. and Yoneda, Y., J. Catal., 22, 182 (1971).
  79. Matsumoto, H. and Bennett, C.O., J. Catal., 53, 331 (1978).
  80. McFadden, W.H., "The Technique of Combined Gas Chromatography - Mass Spectroscopy", Wiley and Sons, New York, 1973.
  81. McLafferty, F.W., "Interpretation of Mass Spectra - An Introduction", W.A. Benjamin, New York, Amsterdam, 1967.
  82. Monnier, J. and Anderson, R.B., J. Catal., 78, 419 (1982).
  83. Monnier, J. and Anderson, R.B., accepted for publication by J. Catal.
  84. Monnier, J., Dénès, G. and Anderson, R.B., submitted to Can. J. Chem. Eng.
  85. Morikawa, K., Benedict, W.S. and Taylor, H.S., J. Amer. Chem. Soc., 58, 1445 (1936).
  86. Morikawa, K., Benedict, W.S. and Taylor, H.S., J. Amer. Chem. Soc., 58, 1795 (1936).
  87. Niemantsverdriet, J.W., van der Kraan, A.M., van Dijk, W.L. and

- van der Baan, H.S., *J. Phys. Chem.*, 84, 3363 (1980).
88. Paal, Z. and Tétényi, P., *Nature*, 267, 234 (1977).
89. Pauling, L., *Proc. Roy. Soc., Ser. A*, 196, 343 (1949).
90. Raupp, G.B. and Delgass, W.N., *J. Catal.*, 58, 348 (1979).
91. Reid, R.C., Prausnitz, J.M. and Sherwood, T.K., "The Properties of Gases and Liquids", McGraw-Hill Book Company, 1977, Appendix A.
92. Rhodin, T.N., Brucker, C.F. and Anderson, A.B., *J. Phys. Chem.*, 82 (8), 894 (1978).
93. Ruebenbauer, K. and Birchall, T., *Hyperfine Interact.*, 7, 125 (1979).
94. Sárkány, A., Matusek, K. and Tétényi, P., *Trans. Faraday Soc.*, 73 (11), 1699 (1977).
95. Sárkány, A. and Tétényi, P., *React. Kinet. Catal. Lett.*, 3, 315 (1978).
- 95b. Satterfield, C.N., "Mass Transfer in Heterogeneous Catalysis", Massachusetts Institute of Technology, 1977, Chapter 3, p. 142.
96. Selwood, P.W., "Chemisorption and Magnetization", Academic Press, New York, 1975.
97. Shephard, F.E., *J. Catal.*, 14, 148 (1969).
98. Shultz, J.F., Hall, W.K., Seligman, B. and Anderson, R.B., *J. Amer. Chem. Soc.*, 77, 213 (1955).
99. Shultz, J.F., Hofer, L.J.E., Cohn, E.M., Stein, K.C. and Anderson, R.B., "Cobalt and Iron Catalysts: Preparation and Characterization", US Bureau of Mines, Bulletin 578, Washington, 1959.
100. Sinfelt, J.H., Taylor, W.F. and Yates, D.J.C., *J. Phys. Chem.*, 69 (1), 95 (1965).
101. Sinfelt, J.H. and Yates, D.J.C., *J. Catal.*, 8, 82 (1967).
102. Sinfelt, J.H. and Taylor, W.F., *Trans. Faraday Soc.*, 64, 3086 (1968).
103. Sinfelt, J.H. and Yates, D.J.C., *J. Catal.*, 10, 362 (1968).

104. Sinfelt, J.H., Catal. Rev., 3 (2), 175 (1969).
105. Sinfelt, J.H., J. Amer. Inst. Chem. Eng., 19 (4), 673 (1973).
106. Sinfelt, J.H., Adv. Catal., 23, 91 (1973).
107. Smith, M.A., Sinharoy, S. and Levenson, L.L., J. Vac. Sci. Technol., 16 (2), 462 (1979).
108. Somorjai, G.A., Adv. Catal., 26, 1 (1977).
109. Somorjai, G.A., Pure Appl. Chem., 50, 963 (1978).
110. Somorjai, G.A., Plenary Lecture, 6th Canadian Symposium on Catalysis, Ottawa (19-21 Aug. 1979).
111. Storch, H.H., Golumbic, N. and Anderson, R.B., "The Fischer-Tropsch and Related Syntheses", John Wiley and Sons, New York, 1951.
112. Stull, D.R., Westrum, E.F. and Sinke, G.C., "The Chemical Thermodynamics of Organic Compounds", John Wiley and Sons, New York, 1969.
113. Sundgren, J.E., Nath, P., Nilsson, H.T.G. and Söder, S., J. Vac. Sci. Technol., 16 (5), 1542 (1979).
114. Tajbl, D.G., Ind. Eng. Chem., Process Des. Develop., 8, 364 (1969).
115. Taylor, E.H. and Taylor, H.S., J. Amer. Chem. Soc., 61, 503 (1939).
116. Temkin, M.I. and Pyzhev, V.M., Acta Physicochim., 12, 327 (1940).
117. Tétényi, P., Guczi, L. and Sárkány, A., Acta Chim. Acad. Sci. Hung., 97 (2), 221 (1978).
118. Tsjeng, P.K. and Anderson, R.B., Can. J. Chem. Eng., 54, 101 (1976).
119. Weast, R.B., ed., "Handbook of Chemistry and Physics", The Chemical Rubber Co., Cleveland, 1968.
120. Weitkamp, A.W., Seelig, H.S., Bowman, N.J. and Cady, W.E., Ind. Eng. Chem., 45 (2), 343 (1953).
121. Weitkamp, A.W. and Frye, C.G., Ind. Eng. Chem., 45 (2), 363 (1953).

122. Wonnacott, T.H. and Wonnacott, R.J., "Introductory Statistics", John Wiley and Sons, New York, 1977.
123. Yates, D.J.C. and Sinfelt, J.H., J. Catal., 14, 182 (1969).

7

APPENDIX A

Characterization of Fe Catalysts by Mössbauer Spectroscopy

Iron catalysts were characterized by Mössbauer spectroscopy, MS, in the laboratory of Prof. T. Birchall in the Department of Chemistry. Dr. G. Dénès operated the MS equipment and interpreted the data. The present appendix is partly based on a paper submitted to the Can. J. Chem. Eng. (83).

The Mössbauer effect is the recoilless emission of  $\gamma$ -rays by a nucleus at the excited state and their resonant reabsorption by a similar nucleus at the ground state. Resonant reabsorption is possible only if both source and absorber are embedded in a solid material. In that case, the emitting and absorbing nuclei, tightly held in the solid, cannot recoil upon emission or absorption of  $\gamma$  photons.

The energy of the nuclear levels of an isotope varies slightly from one compound to another due to changes in the atomic environment and the magnetic properties of the material. Therefore,  $\alpha$ -Fe,  $\text{Fe}_3\text{C}$  and  $\text{Fe}_5\text{C}_2$  can be differentiated by MS.

For  $^{57}\text{Fe}$  Mössbauer spectroscopy, the source containing  $^{57}\text{Fe}$  at the excited state, produced by decay of  $^{57}\text{Co}$ , emits  $\gamma$ -rays with an energy of 14.41 keV. Oscillation of the source, in a constant acceleration mode, modulates the beam energy by Doppler effect to obtain resonant absorption that is otherwise destroyed by differences in electric or magnetic environments between source and absorber.



The samples, finely ground powders, usually contain no more than 20 mg Fe/cm<sup>2</sup> in order to avoid line broadening and saturation effect. MS is not limited to highly crystalline solids but can be used for amorphous materials, in contrast with X-ray diffraction. After transmission through a sample, the  $\gamma$ -radiation is detected and preamplified by a Kr-CO<sub>2</sub> (2200 mm Hg) proportional counter and the signal is accumulated in a multi-channel analyzer synchronized with the source drive. The intensity of the transmitted  $\gamma$ -rays is plotted in a Mössbauer spectrum as a function of their energy. The spectra were calibrated using a standard sample of iron foil, and they were recorded at room temperature.

The number of absorption peaks in a Mössbauer spectrum, as well as their position and intensity are characteristics of the electron density around the Fe nucleus, and the presence of electric and/or magnetic fields acting at the nucleus. Computer programs, GMFP and GMFP5 (31, 93) were used for fitting the Mössbauer spectra and obtaining the hyperfine parameters (isomer shift,  $\delta$ , quadrupole splitting,  $\Delta$ , linewidth,  $\Gamma$ , effective magnetic field,  $H_{\text{eff}}$ ) which are useful for the identification of the Fe compounds. When more than one hyperfine site (<sup>57</sup>Fe nucleus in a particular environment) are present, the relative contribution of each site to the total absorption spectrum is also fitted.

Mössbauer spectroscopy can give a rough estimate of the composition of solid mixtures by comparing the peak areas in the absorption spectra. However its accuracy is limited by the difference

(usually unknown) in the value of the recoil-free fraction of the components of the mixture. In that case, the absorption of  $\gamma$ -rays per Fe nucleus varies in intensity from one Fe compound to another, thus modifying the peak areas in the Mössbauer spectra.

Figures A1-A5 present Mössbauer spectra of some of the catalysts, which contain  $\alpha$ -Fe,  $\text{Fe}_3\text{C}$ ,  $\text{Fe}_5\text{C}_2$  or mixtures of Fe and  $\text{Fe}_3\text{C}$ .

Table A1 gives the hyperfine parameters obtained from the profile fitting of these spectra. Values of parameters from the literature are also reported in this Table. Fitting of the Mössbauer spectra by a non-linear regression program to obtain the hyperfine parameters is discussed in a paper submitted to the Can. J. Chem. Eng. (84).

A review on the application of MS to heterogeneous catalysis is presented by Dumesic and Topsoe (37) and by Hobson (51).

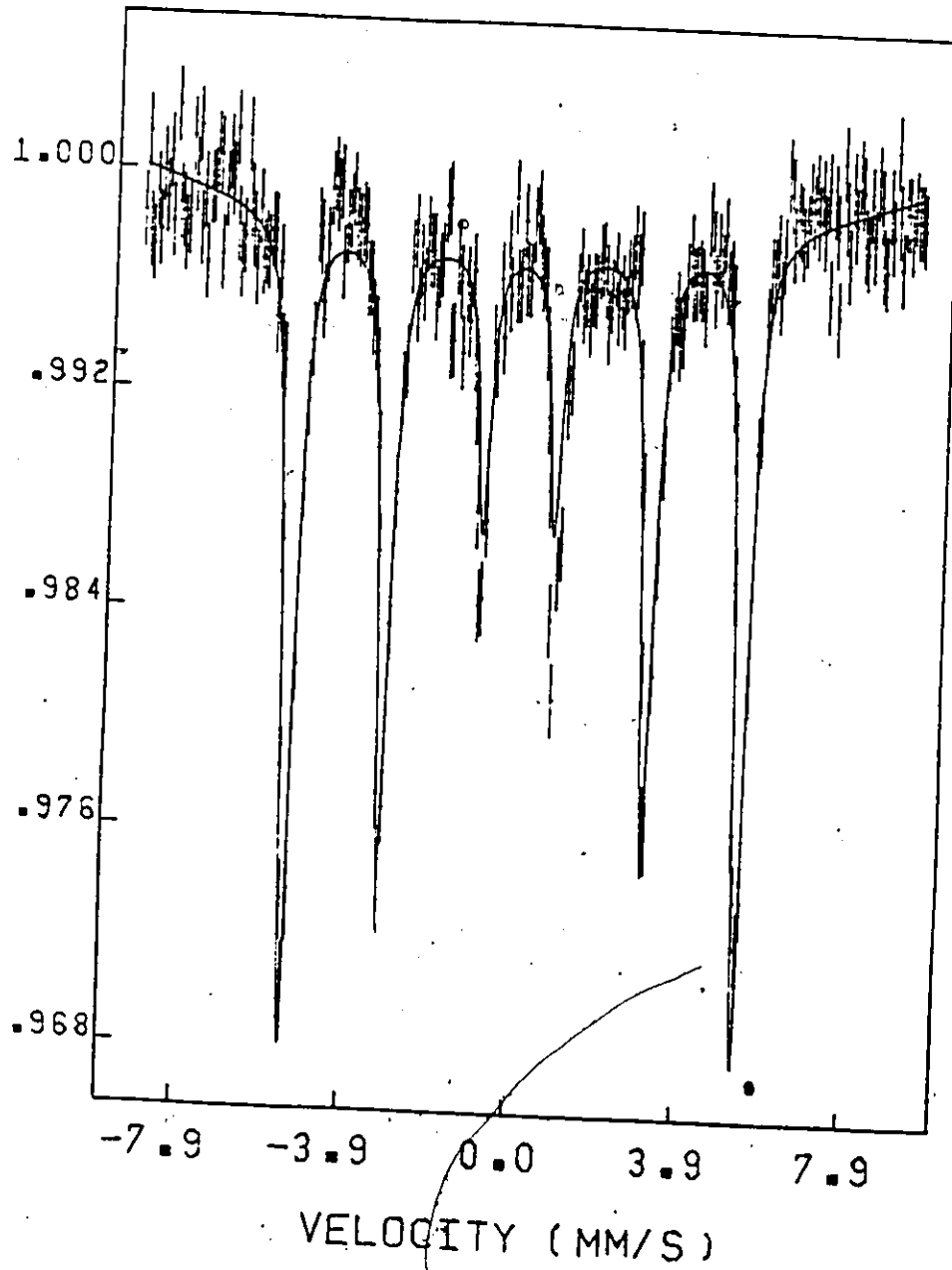


Figure A1: Mössbauer spectrum of used catalyst in test 5.1:  
only  $\alpha$ -Fe is found.

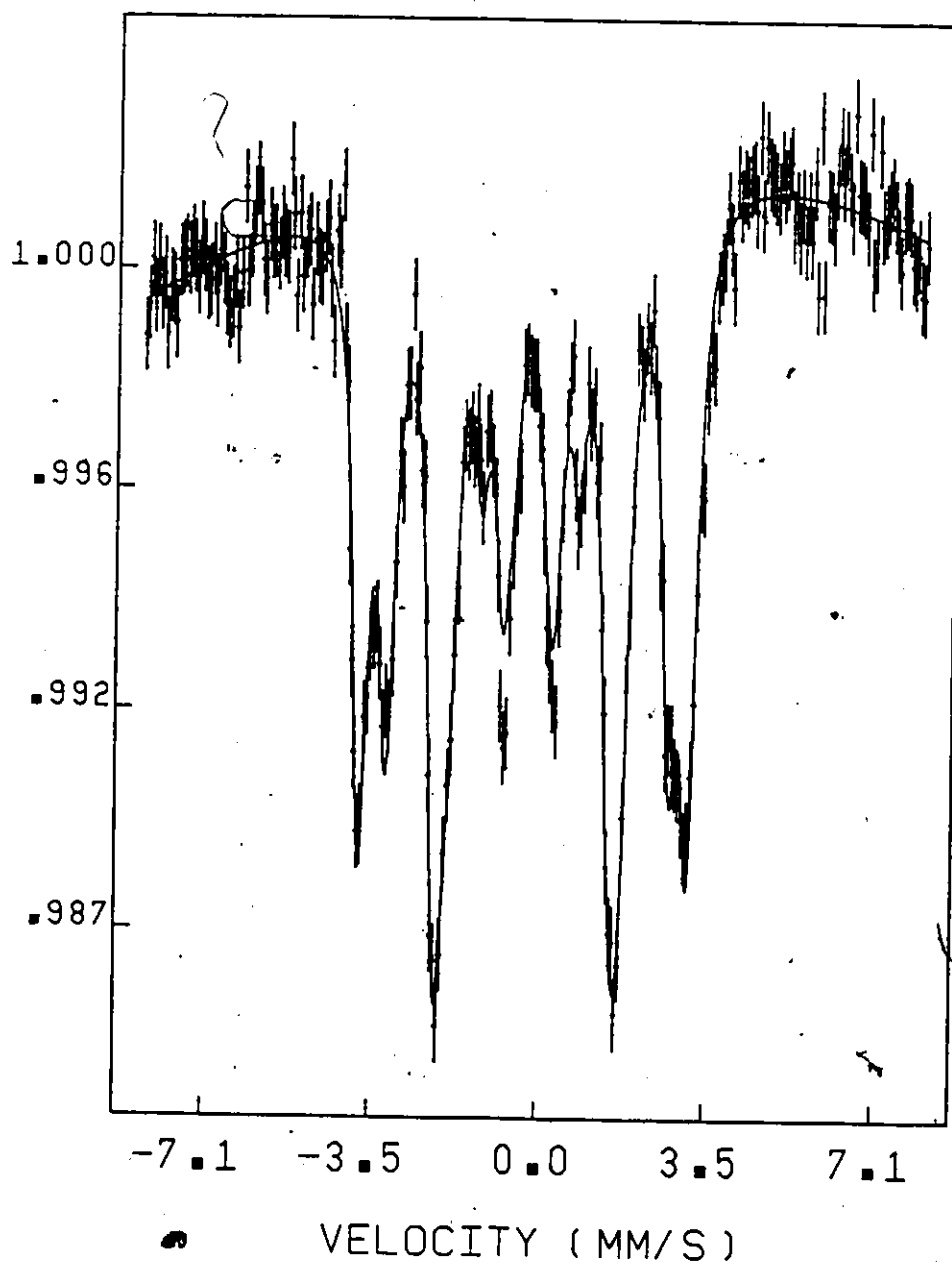


Figure A2: Mössbauer spectrum of fresh pre-carbided catalyst:  $\text{Fe}_5\text{C}_2$ .

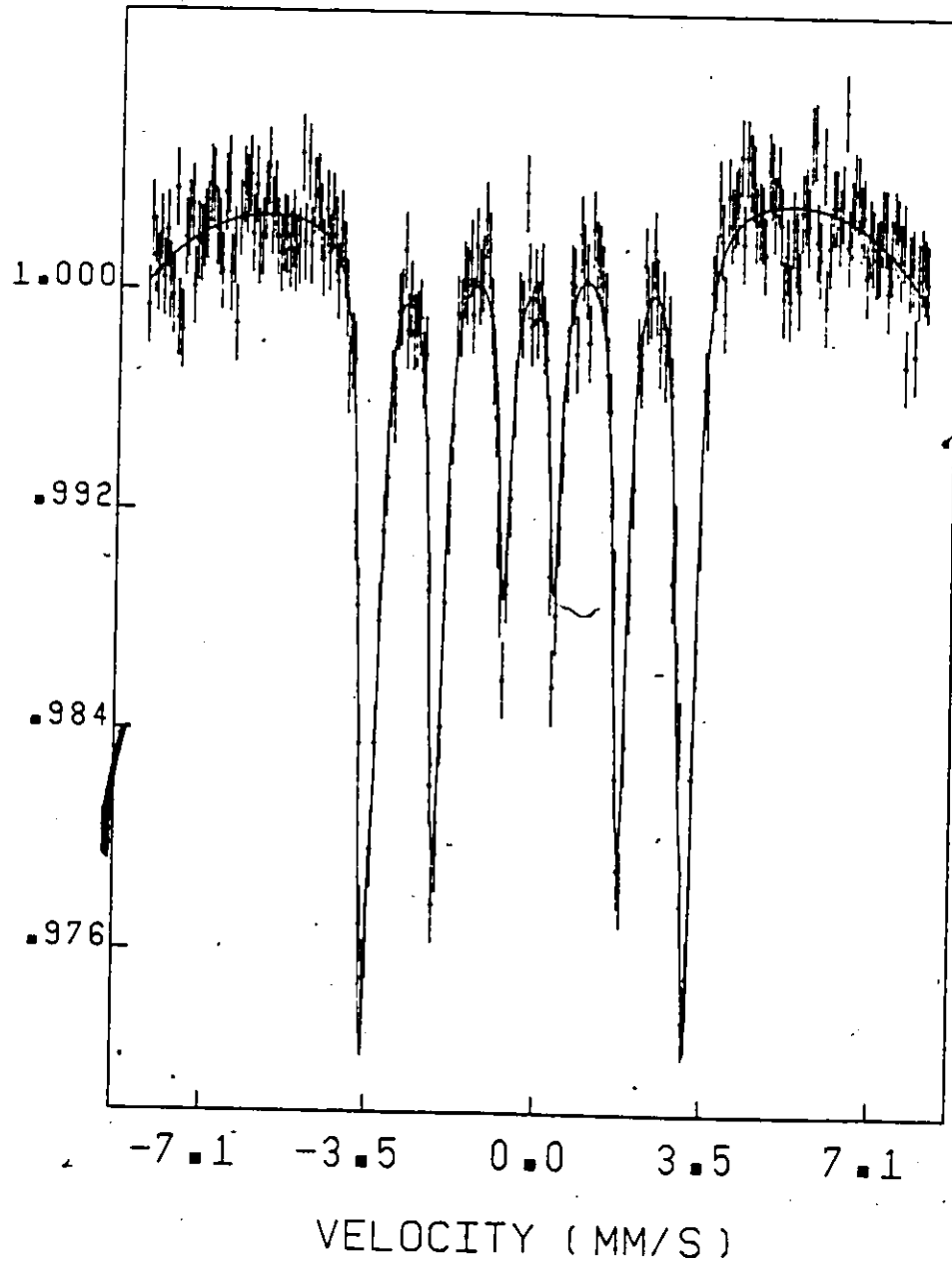


Figure A3: Mössbauer spectrum of used Fe catalyst after  $\text{1-C}_5\text{H}_{12}$  hydrogenolysis at  $355^\circ\text{C}$  and 0.8 FR (test 5.4):  $\text{Fe}_3\text{C}$ .

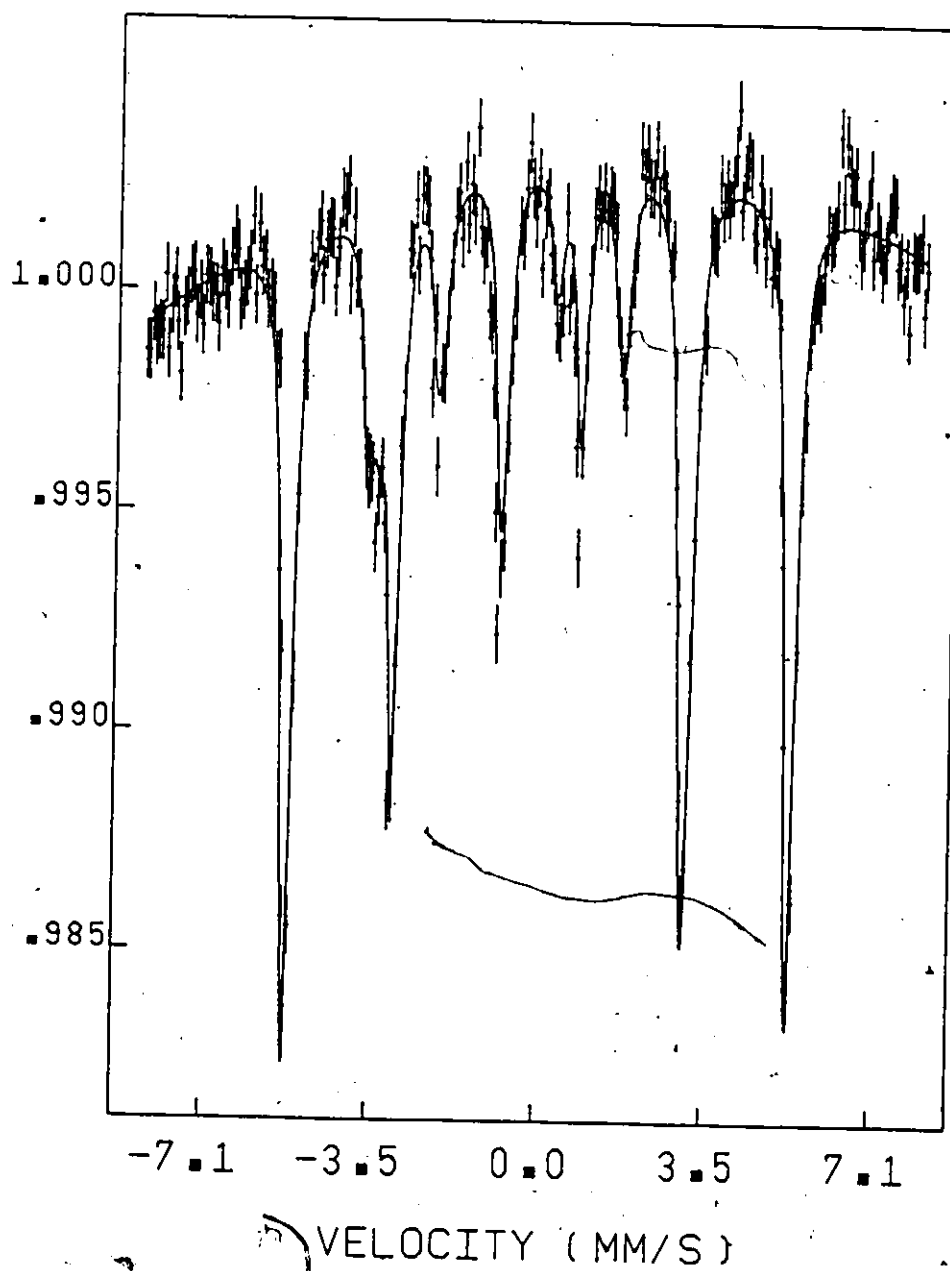


Figure A4: Mössbauer spectrum of used pre-carbided catalyst after hydrogenolysis at 325°C and 2.8 FR (test 5.2): the catalyst contains 66 weight %  $\alpha$ -Fe and 33%  $\text{Fe}_3\text{C}$ .

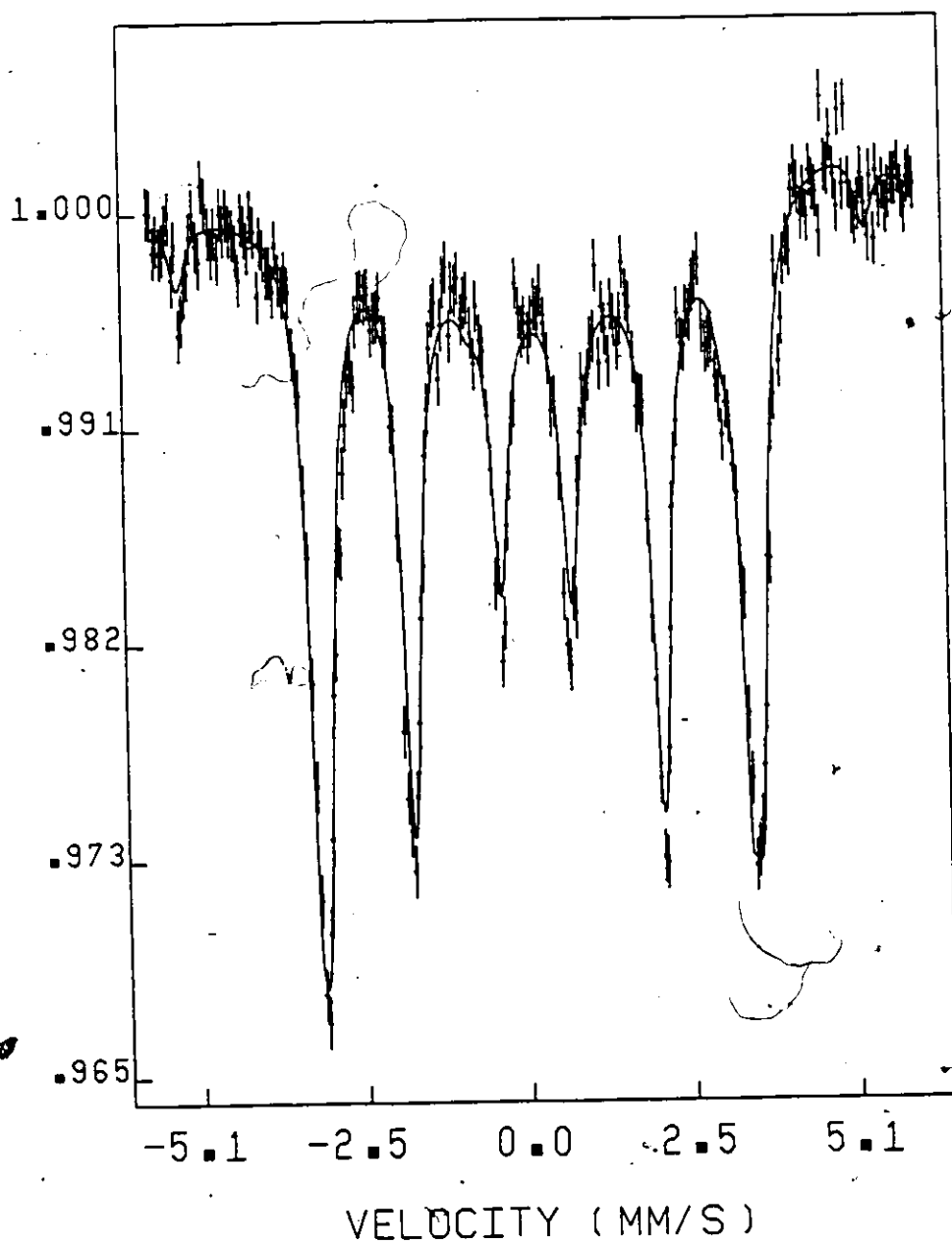


Figure A5: Mössbauer spectrum of used iron catalyst after hydrogenolysis of hexadecane at 325°C and 9.1 FR: the catalyst contains 93 weight % Fe<sub>3</sub>C and 7% α-Fe.

TABLE A1  
<sup>57</sup>Fe Mössbauer Data of the Catalysts at Room Temperature (82)

Compound <sup>a</sup>	Origin	$\delta_{(a-Fe)}$	$\epsilon$	$\Gamma$	$H_{eff}(kOe)$	Contr(S) <sup>b</sup>	$\chi^2/d. of f.°$					
Fe	(43)	0	0	-	330	100	-					
Fe	Fig. A1	.003(3)	.0000(0)	.22(1)	330.1(3)	100	1.52					
Fe		.005(1)	.000(6)	.207(4)	329.5(1)	100	1.85					
Fe <sub>3</sub> C	(65)	I	.18(1)	.010(5)	.206(2)	33.3 <sup>d</sup>	-					
								II	.18(1)	.010(5)	.208(2)	66.6 <sup>d</sup>
Fe <sub>3</sub> C	Fig. A3	I	.218(9)	.02(18)	.31(1)	27(3)	1.34					
								II	.218(3)	.05(6)	$\Gamma_1$	211.3(4)
Fe <sub>3</sub> C	Fig. A4	I	.218	.02	.28(2)	11(1)	2.07					
								II	.218	.06	$\Gamma_1$	211.3
Fe		.003(2)	.18(9)	.285(7)	330.2(2)	69(1)	-					
Fe <sub>3</sub> C	Fig. A5	I	.161(3)	.05(10)	0.30(1)	46(3)	93					
								II	.175(3)	.13(4)	$\Gamma_1$	212.5(5)
Fe		0 <sup>e</sup>	0 <sup>e</sup>	$\Gamma_1$	330 <sup>e</sup>	7.3(9)	2.21					
Fe <sub>5</sub> C <sub>2</sub>	(65)	I	.23(2)	.04(2)	-	40 <sup>d</sup>	-					
								II	.20(2)	.17(2)	-	195(2)
Fe <sub>5</sub> C <sub>2</sub>	Fig. A2	I	.268(5)	.036(6)	.21(2)	43(1)	1.61					
								II	.216(6)	.18(2)	.23(3)	35(1)
								III	.23(1)	.030(5)	.19(4)	113(1)

a) I, II, III stand for sites number 1, 2, 3 in phases having more than one Fe site.  
 b) CONTR(S) = contribution of the site to the total resonant absorption of the spectrum.  
 c)  $\chi^2/d$  of  $f = \chi^2$ -squared / number of degrees of freedom.  
 d) Theoretical values from the crystal structure.  
 e) Fixed.



## APPENDIX B

### Surface Characterization by Auger Electron Spectroscopy

The surface of solids can be characterized by Auger Electron Spectroscopy, AES. This highly sensitive technique probes atomic layers which are less than 20 Å from the surface. During some of our tests, samples of iron foil were placed in the differential reactor and were analyzed in the Department of Chemistry, courtesy of Prof. P.T. Dawson.

This characterization technique is based on the "Auger process" where the energy from electron deexcitation in a solid is transferred to secondary electrons which escape from the solid into the vacuum. Since the energy of an Auger electron is characteristic of its parent atom, the identification of chemical elements present on or near a surface becomes possible.

The samples to be analyzed are placed in a vacuum chamber where they are bombarded with an electron gun leading to the escape of Auger electrons of which only those with low energy, between 100 and 1000 eV, are detected by an electron energy analyzer. Higher energy electrons are eliminated because they could originate from atomic layers deeper than 20 Å. The analyzer signal, which represents the total energy distribution function,  $N(E)$ , is differentiated to accentuate the Auger peaks. The plots of  $dN(E)/dE$  as a function of  $E$  are called Auger spectra. The peaks in a spectrum indicate the Auger electron energies which are unique to each of the parent atoms. AES can also discriminate

between the following types of surface C, by the pattern of their Auger peaks: carbidic C and layers of graphitic or elemental C (48,107,113).

Layers of atoms can be removed from the surface by bombarding the sample with an ion beam, usually ionized argon. The concentration profile of a given element is obtained by successive sputtering and AES characterization.

Reviews on Auger electron spectroscopy, have been written by Joshi et al. (53), Chang (22) and Grant (42).

## APPENDIX C

### Combined Gas Chromatography-Mass Spectrometry

The  $C_8^+$  hydrocarbons produced in hydrogenolysis of normal hexadecane, were analyzed by combined gas chromatography-mass spectrometry, GC-MS, in the Department of Chemistry, courtesy of Prof. M. Quilliam.

Separation of the  $C_8^+$  hydrocarbons was done, by temperature-programmed gas chromatography, with a 50-meter capillary column coated with DB-5, a silicone rubber similar in properties to SE-52 (silicone chain with 5% phenyl and 95% methyl groups) and SE-54 (1% vinyl, 5% phenyl and 94% methyl). All of the effluent gases from the gas chromatograph were sent to a mass spectrometer, where the hydrocarbon molecules were first ionized and partly fragmented by an electron beam. After being separated from the other particles, the positive ions were accelerated and deflected by magnets, acquiring a circular course with a degree of curvature function of their mass and their charge. The impact of these ions on a detector was recorded by a computer and the ratio of mass to charge,  $m/e$ , was calculated for all the ions. The mass distribution data, for each chromatographic peak, were presented in a mass spectrum, as a histogram.

In each mass spectrum, the molecular ion gives information on the molecular weight of the unknown hydrocarbon, and the selected fragment

ions, on the structure of the molecule (branching, ...). Retention time, retention index (defined in Table 6.1) and homologous series are also valuable information. The identity of a compound is usually confirmed by matching its mass spectrum with those reported in the literature (50) and its retention time with that of an injected standard. More information on the technique of GC-MS and the interpretation of mass spectra can be found in McFadden (80) and in McLafferty (81).

Typical mass spectra are presented in Figures A6-A12 for normal and branched alkanes, A13-A16 for alkenes, A17-A31 for alkylbenzenes and A32 for naphthalene. The peak numbers refer to the gas chromatogram in Figure 6.3.

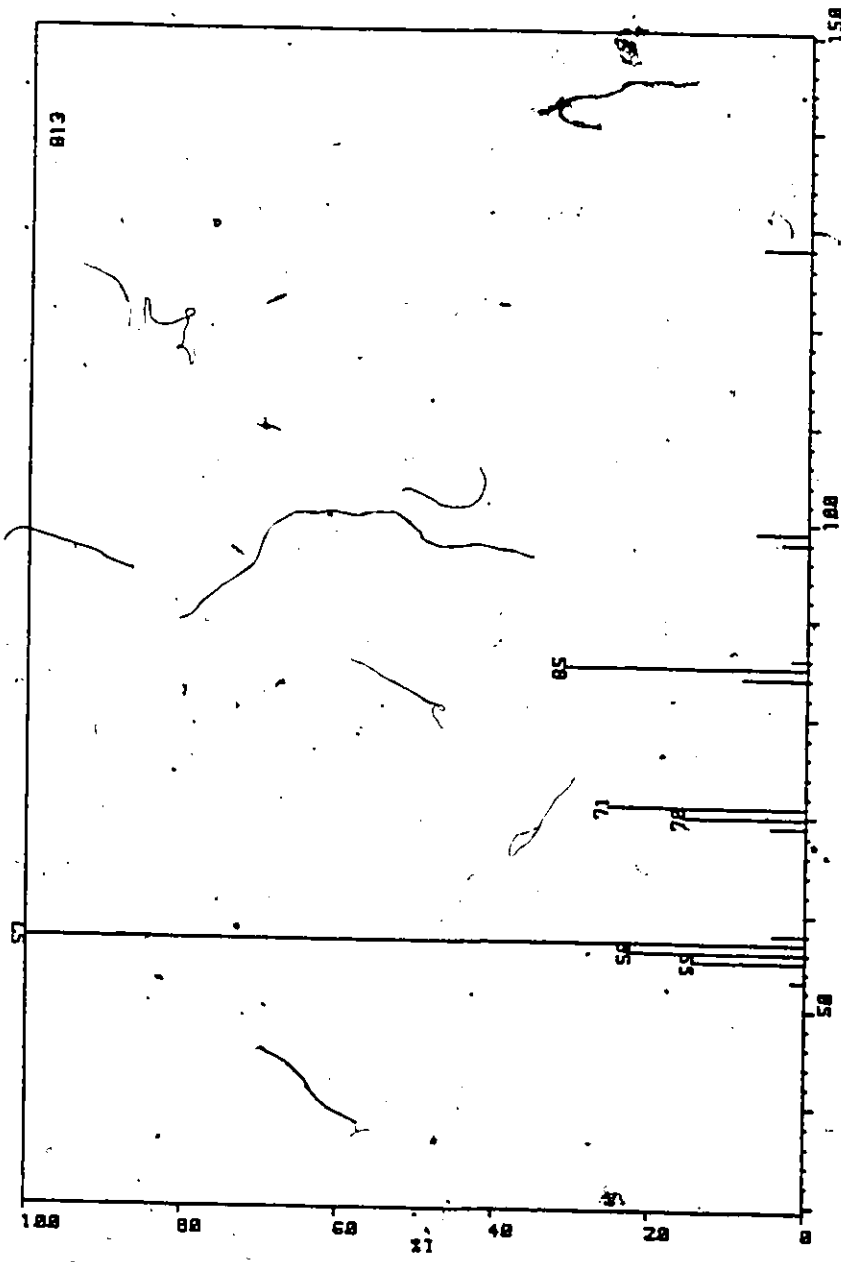


Figure A6:- Mass spectrum (% relative intensity vs m/e) of n-nonane (peak 15).

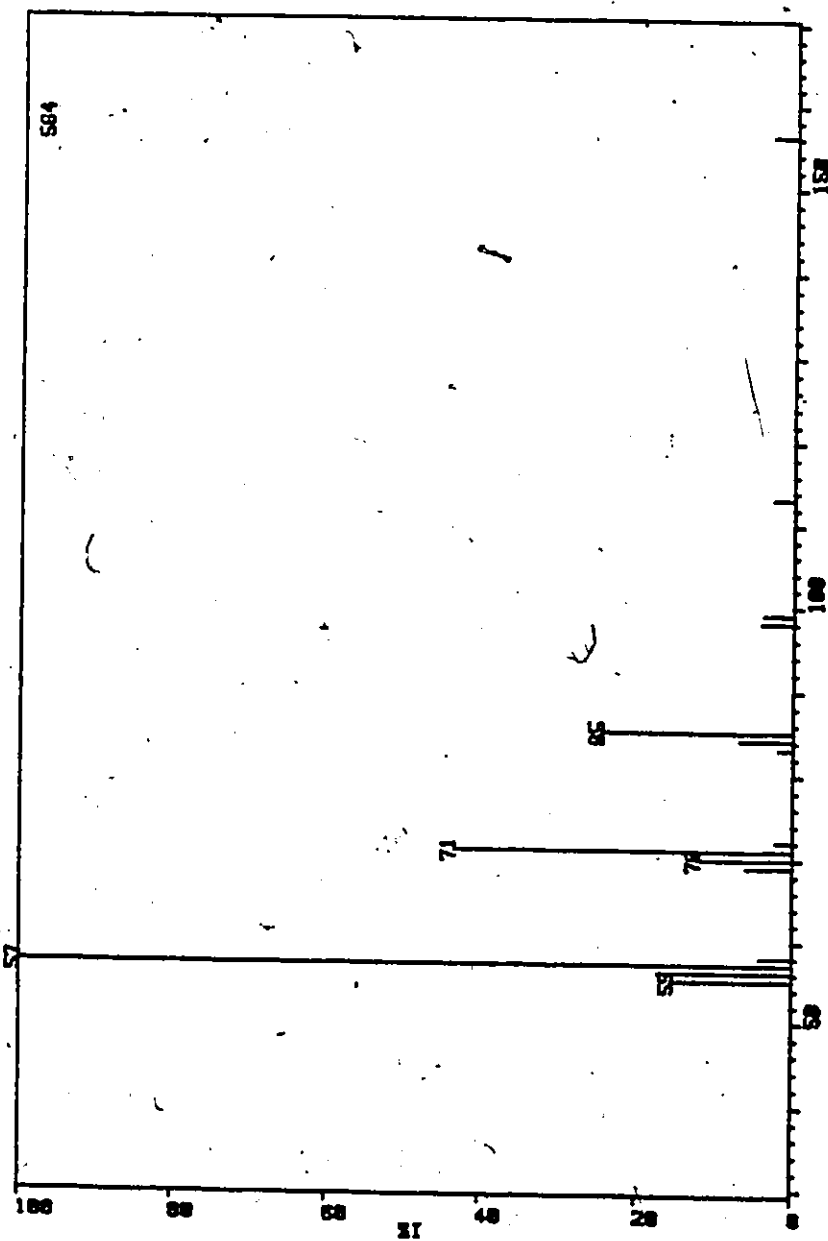


Figure A7: Mass spectrum (% relative intensity vs m/e) of n-undecane (peak 42).

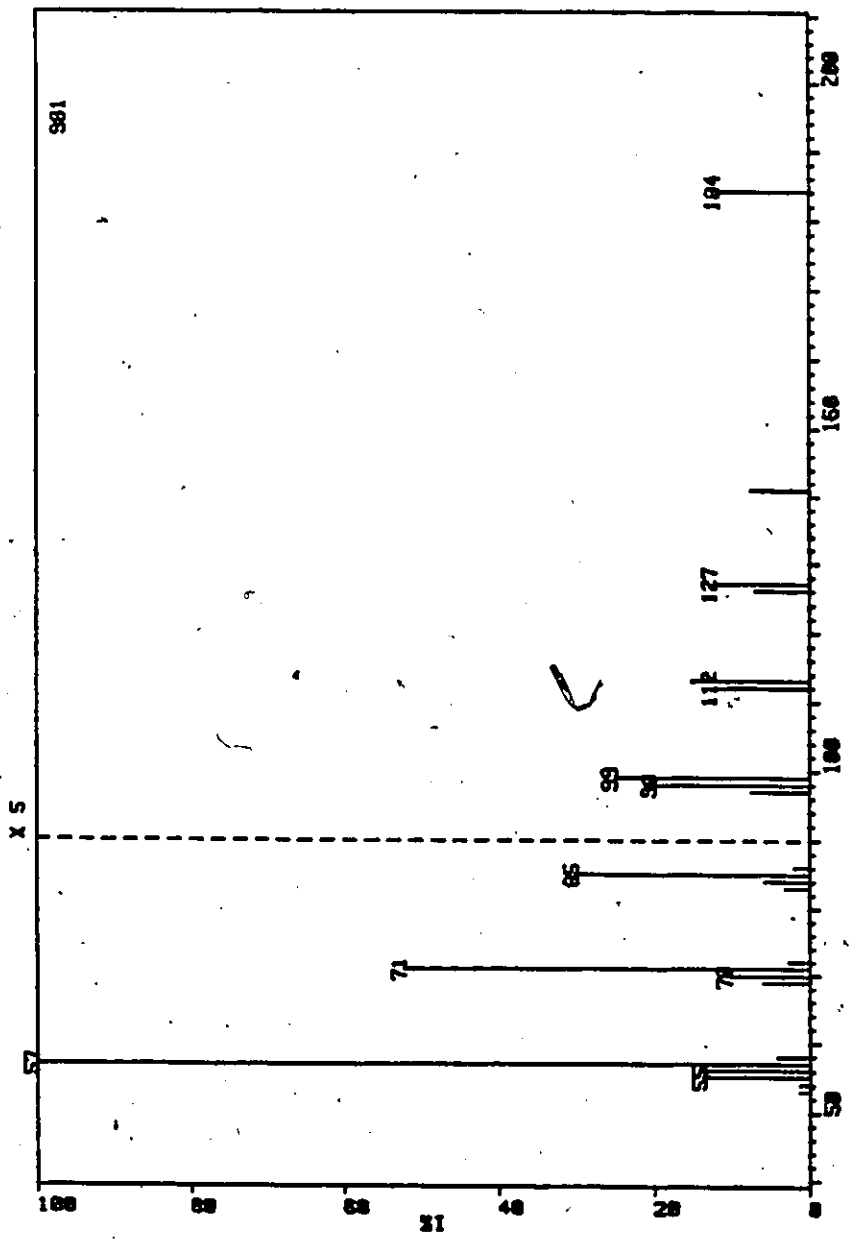


Figure A8: Mass spectrum (% relative intensity vs m/e) of n-tridecane (peak 65).

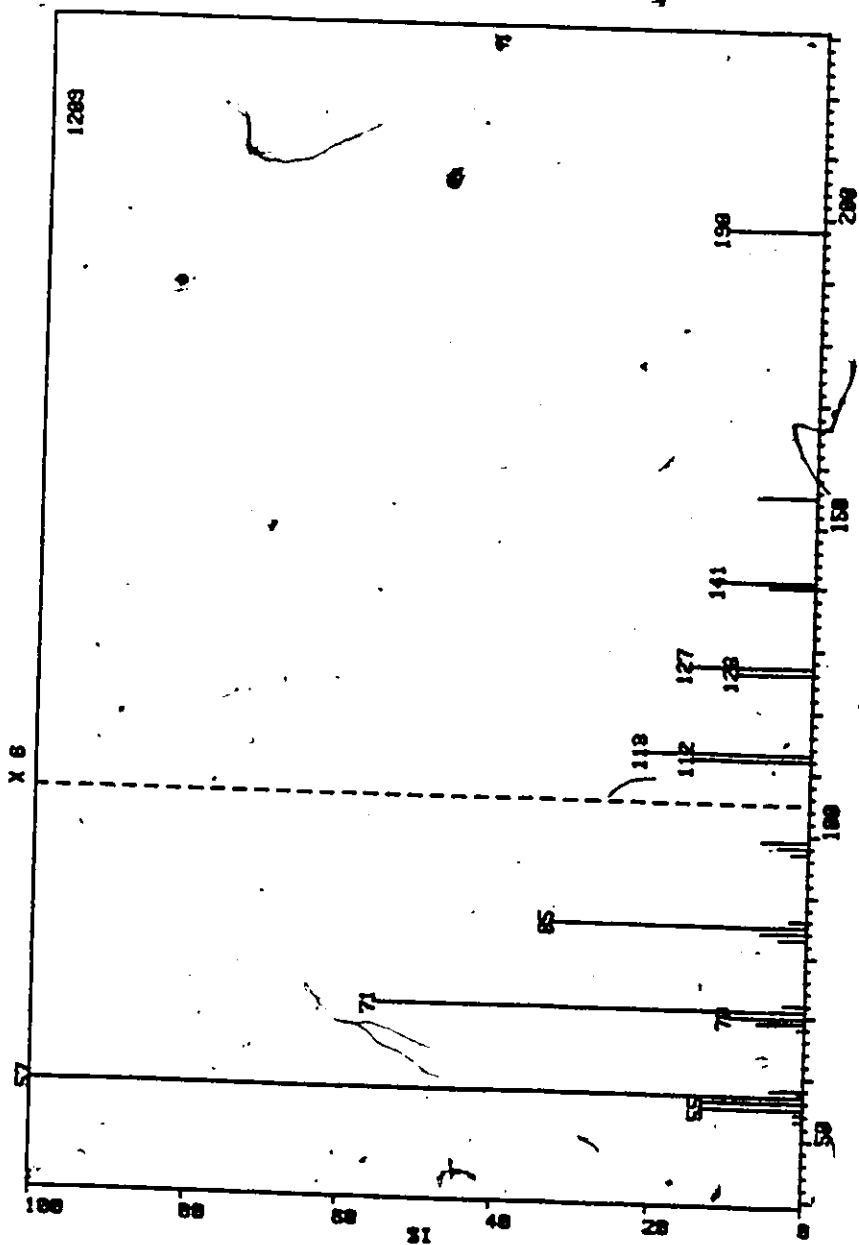


Figure A9: Mass spectrum (% relative intensity vs m/e) of n-tetradecane (peak 75).



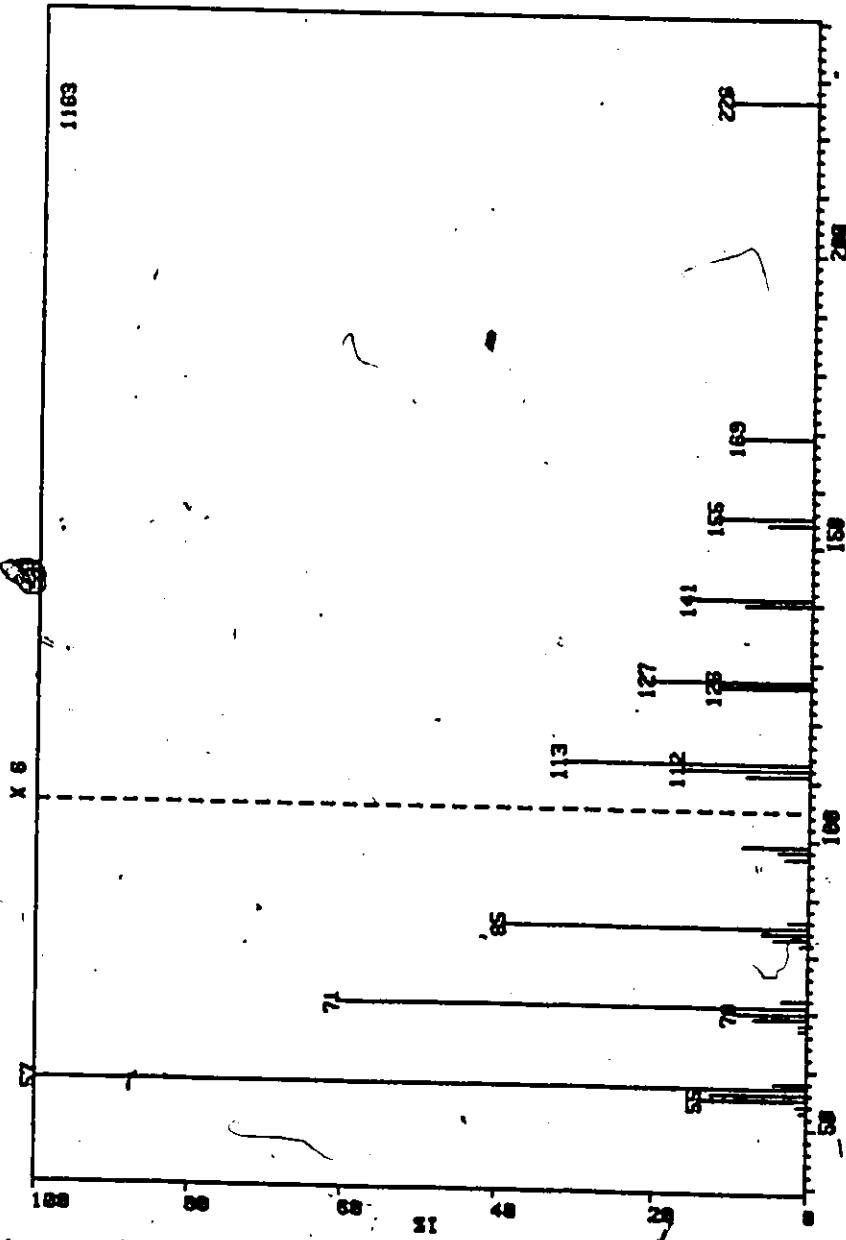


Figure A10: Mass spectrum (% relative intensity vs m/e) of n-hexadecane (peak 86).

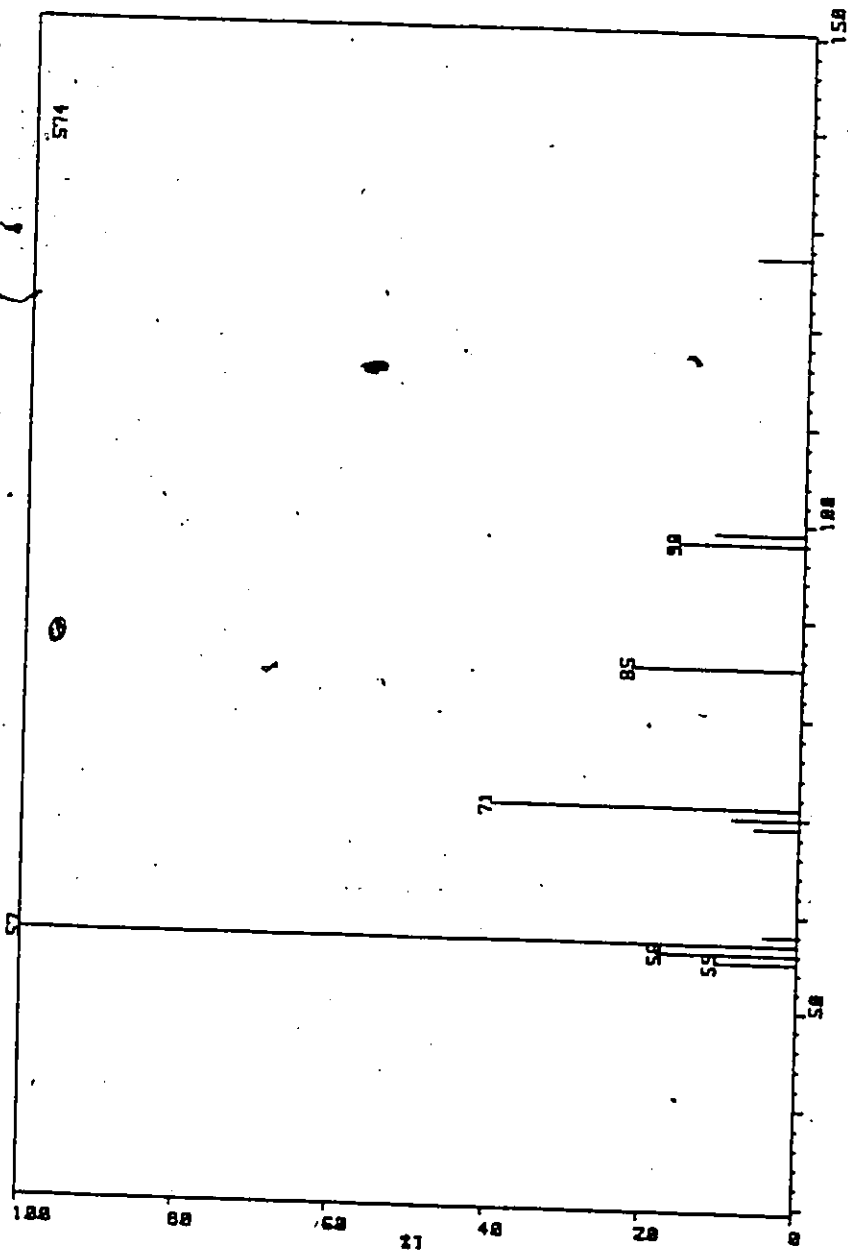


Figure A11: Mass spectrum (% relative intensity vs m/e) of branched decane (peak 22).

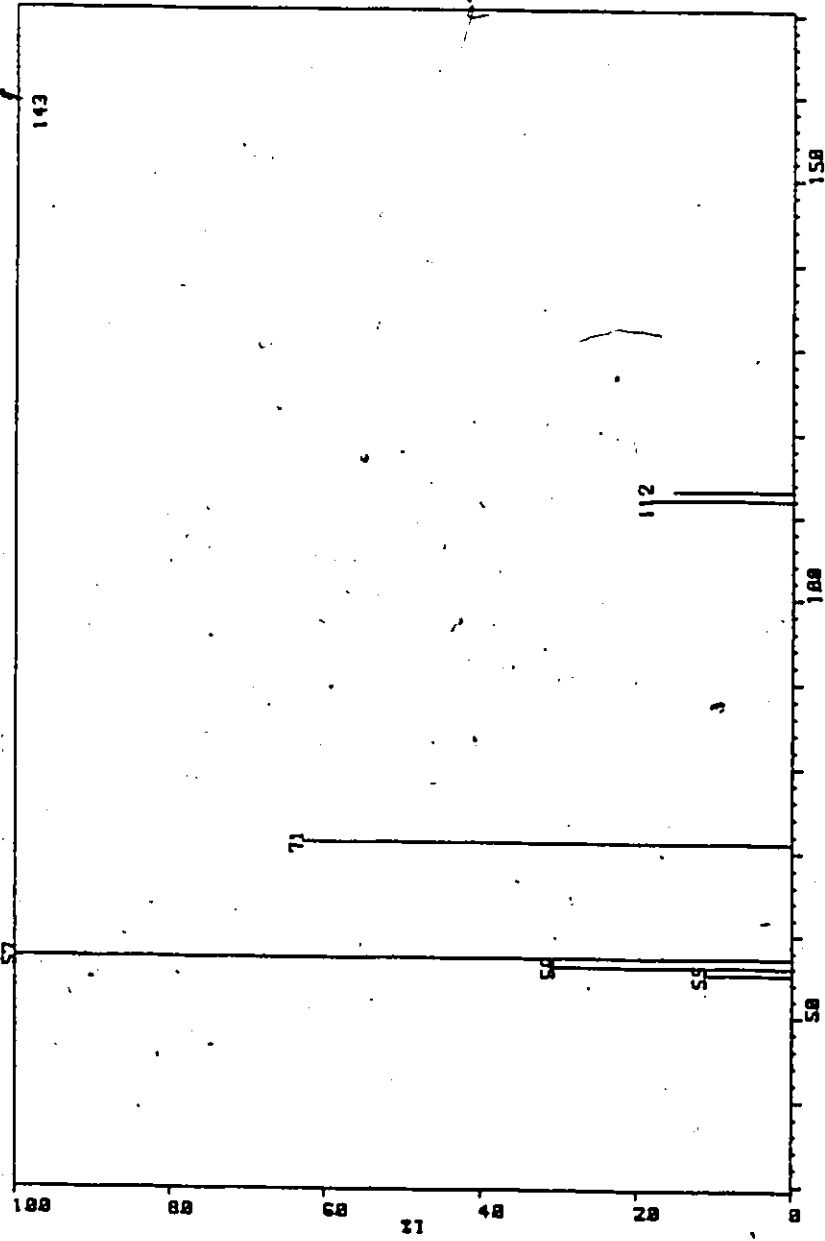


Figure A12: Mass spectrum (% relative intensity vs m/e) of branched decane (peak 23).

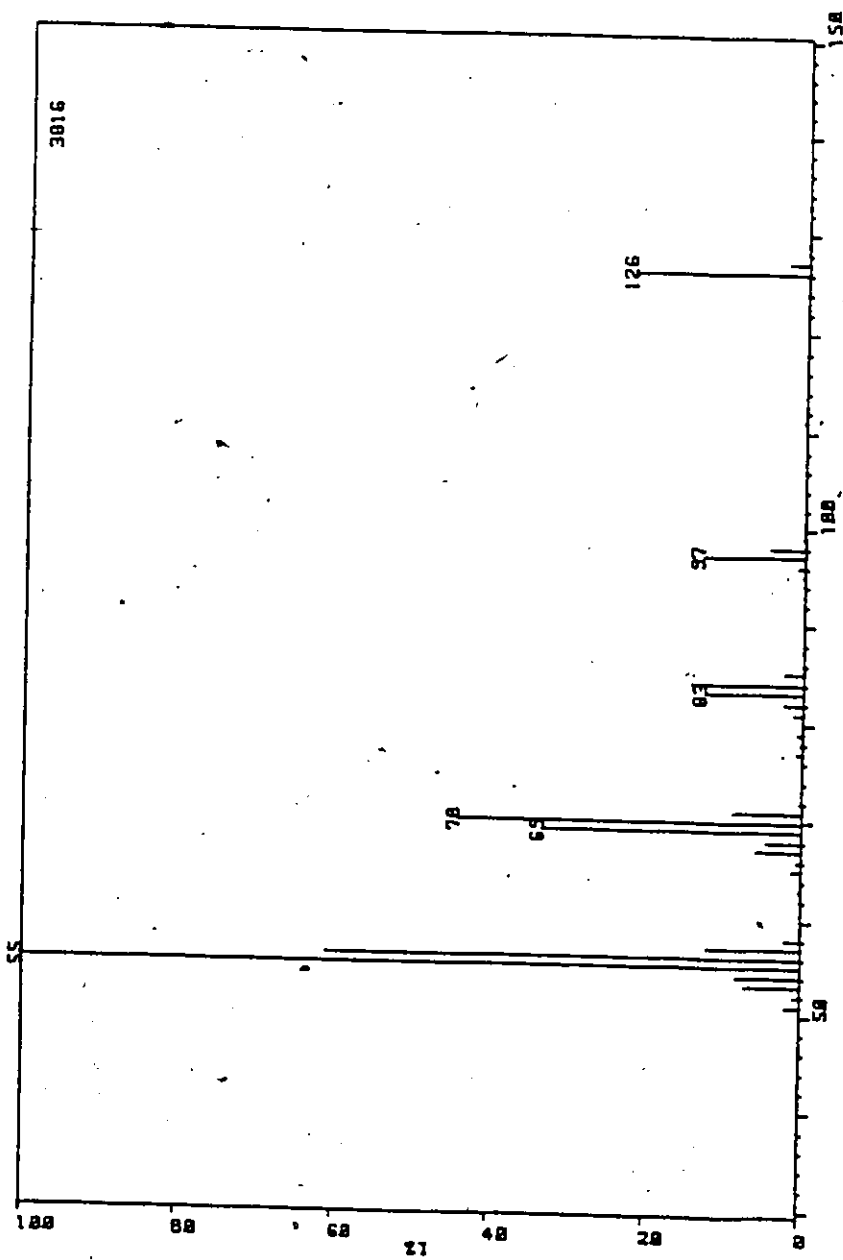


Figure A13: Mass spectrum (% relative intensity vs m/e) of nonene (peak 16).

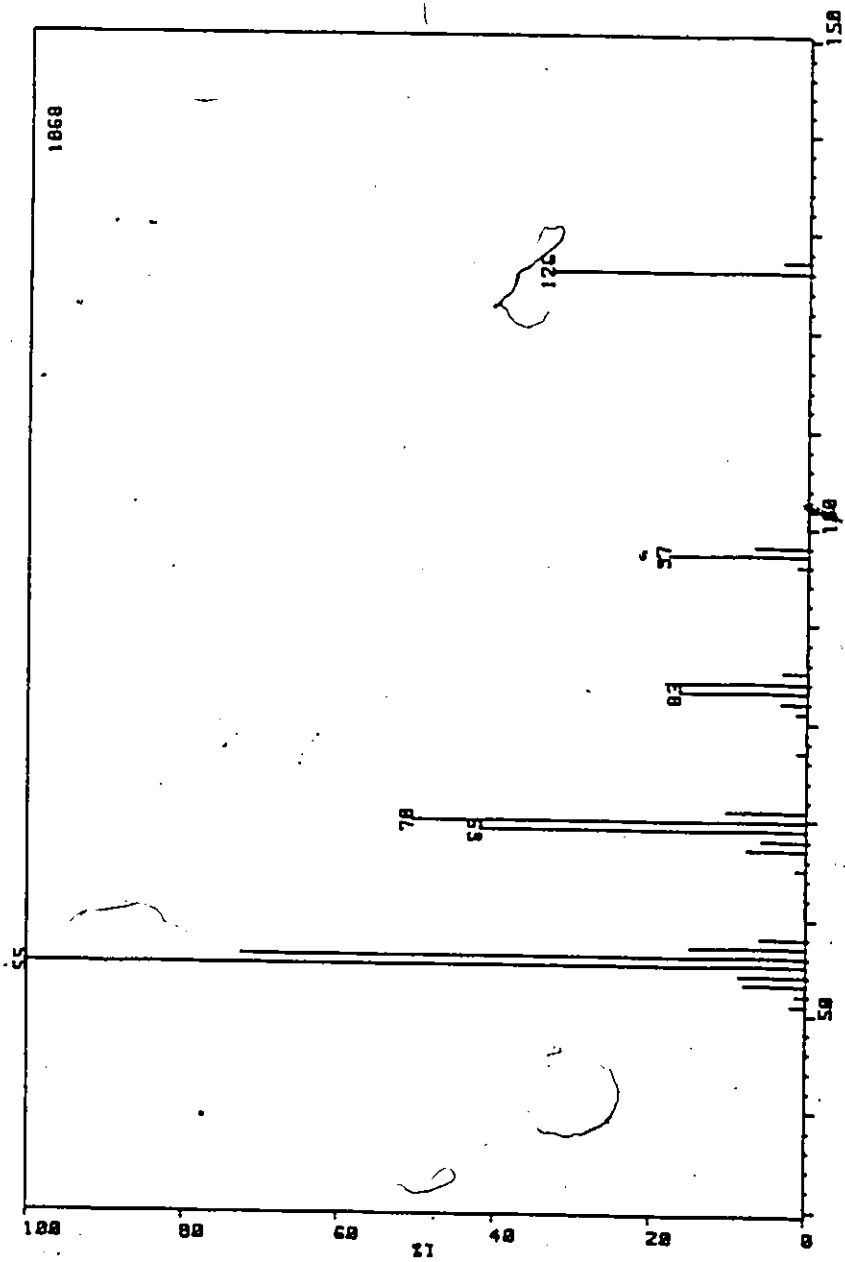


Figure A14: Mass spectrum (% relative intensity vs m/e) of nonene (peak 17).



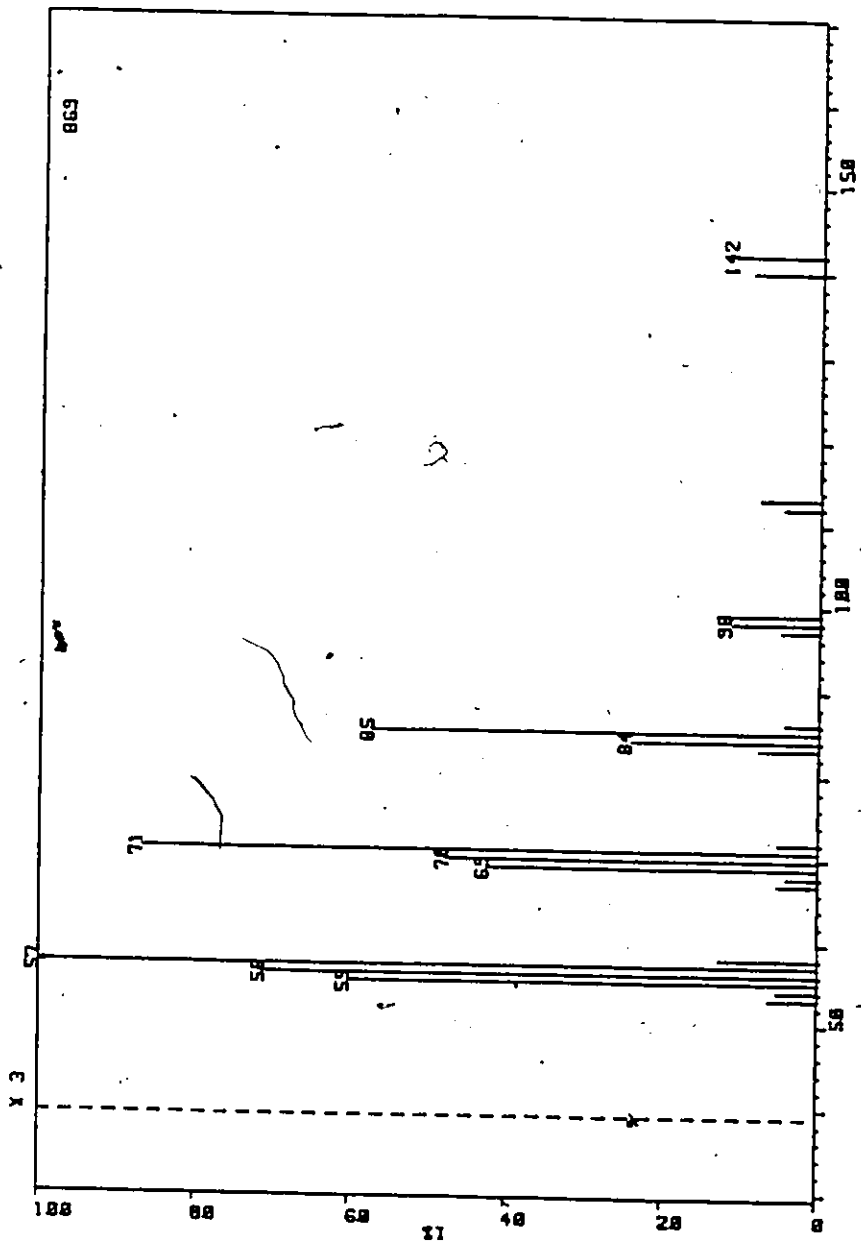


Figure A16: Mass spectrum (% relative intensity vs m/e) of decene (peak 28).

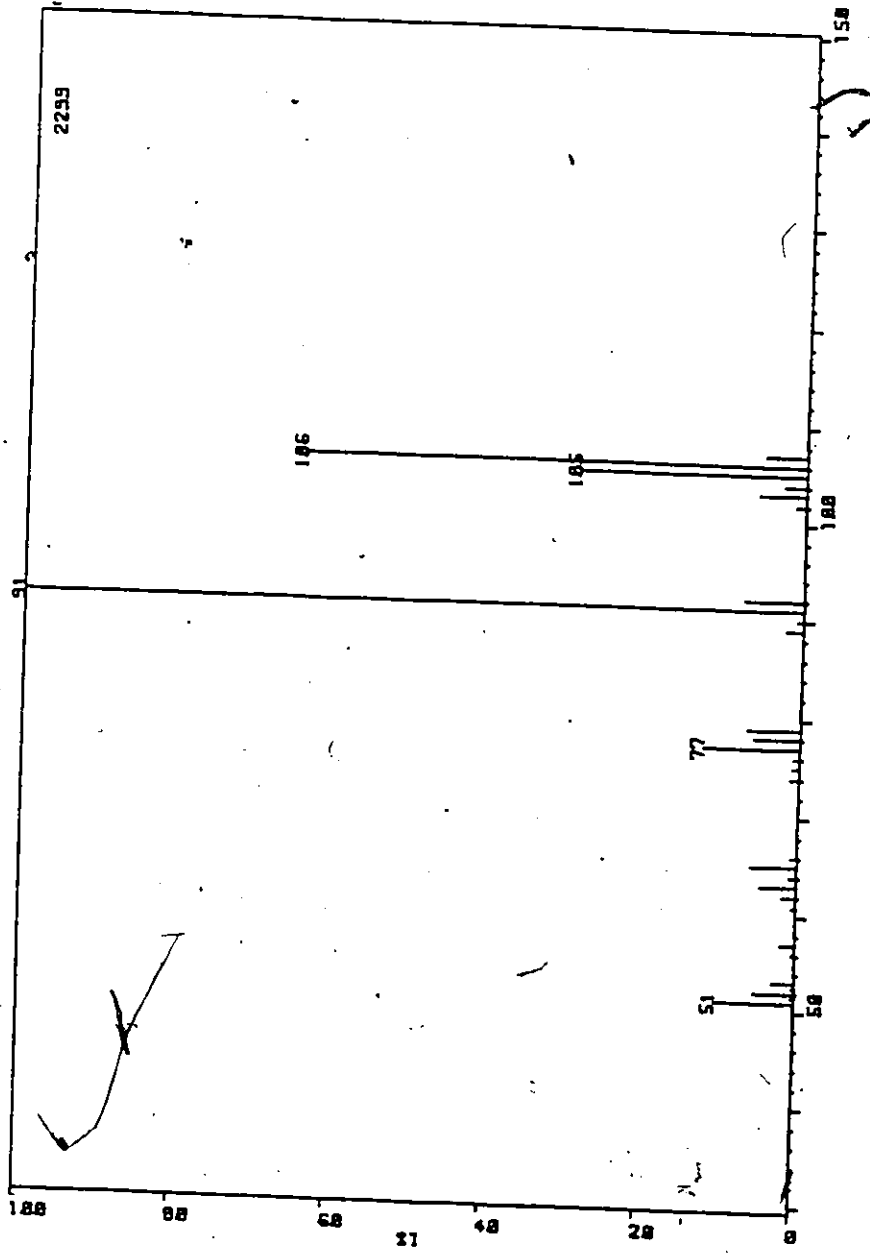


Figure A17: Mass spectrum (% relative intensity vs m/e) of m, p-xylene (peak 10).



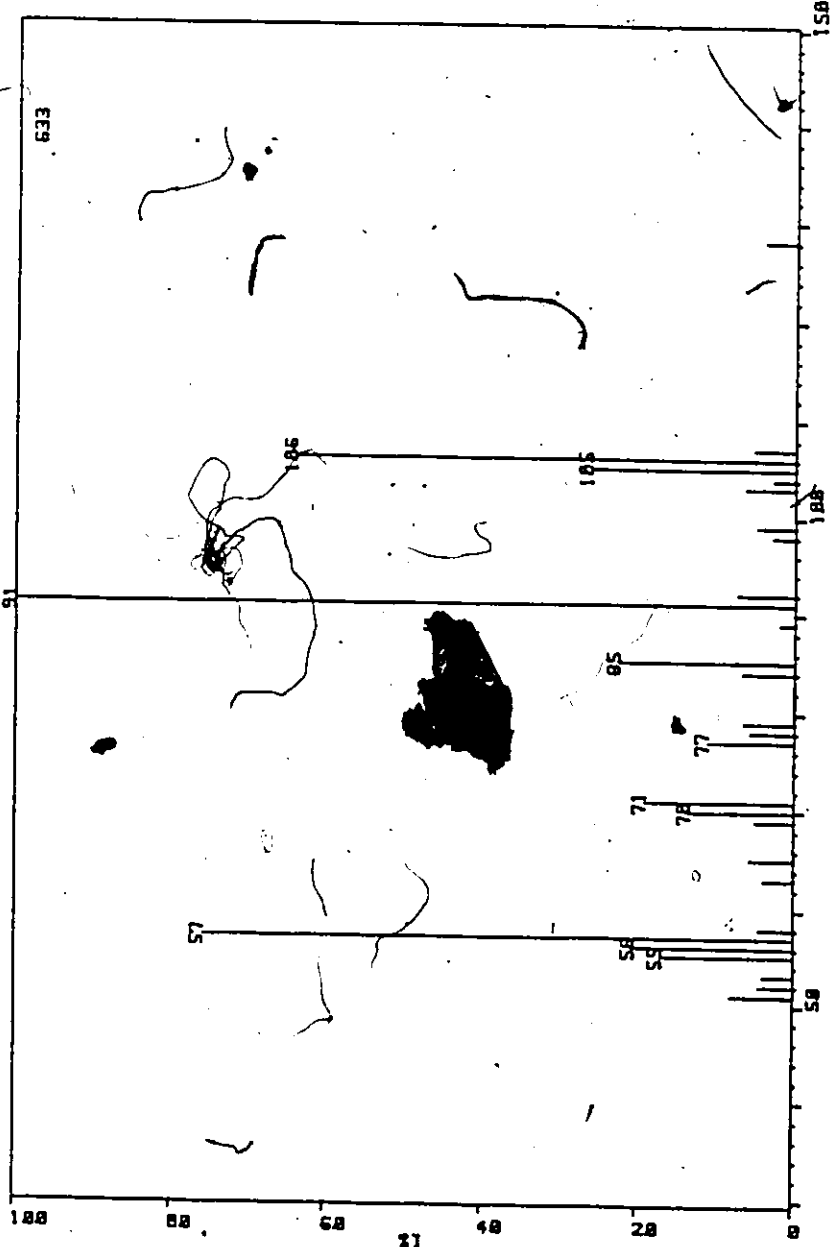


Figure A18: Mass spectrum (% relative intensity vs m/e) of o-xylene (peak 13).

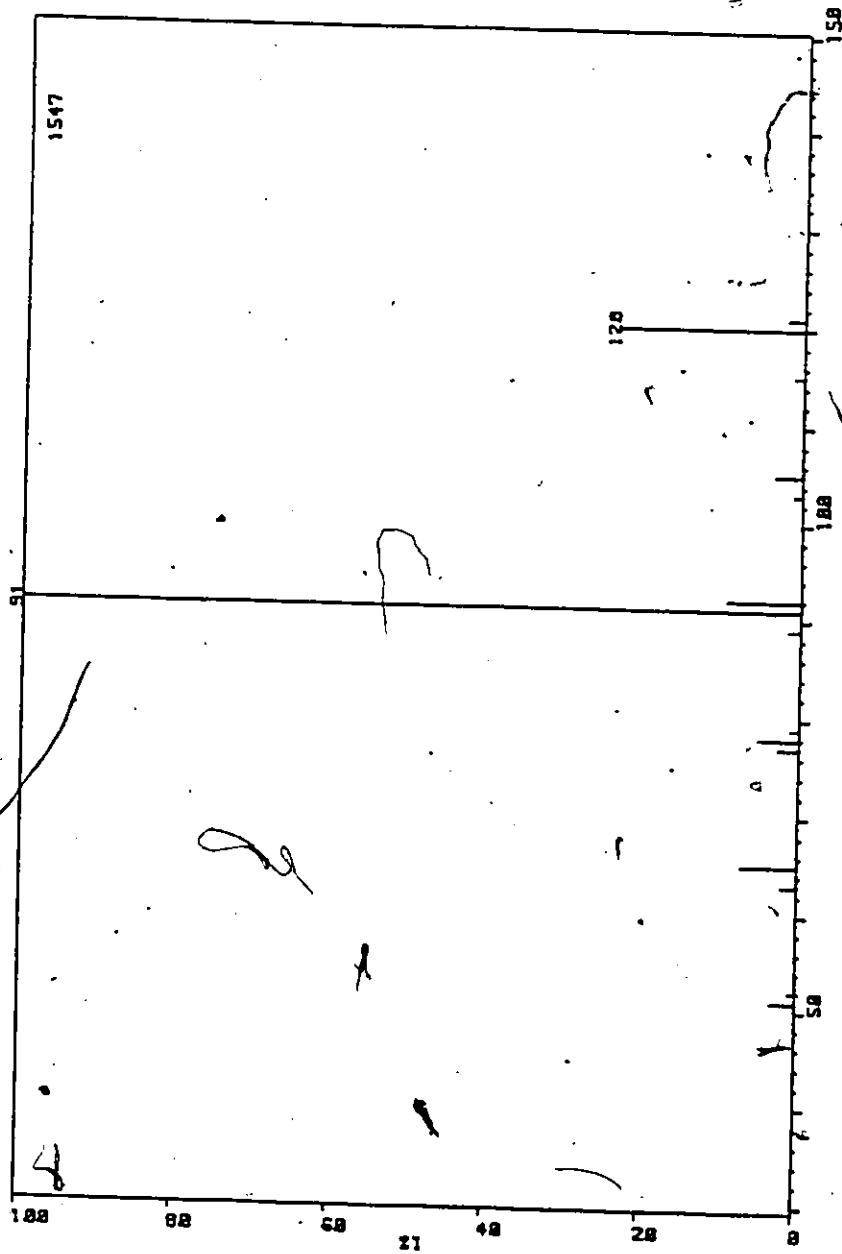


Figure A19: Mass spectrum (% relative intensity vs m/e) of n-propylbenzene (peak 19).

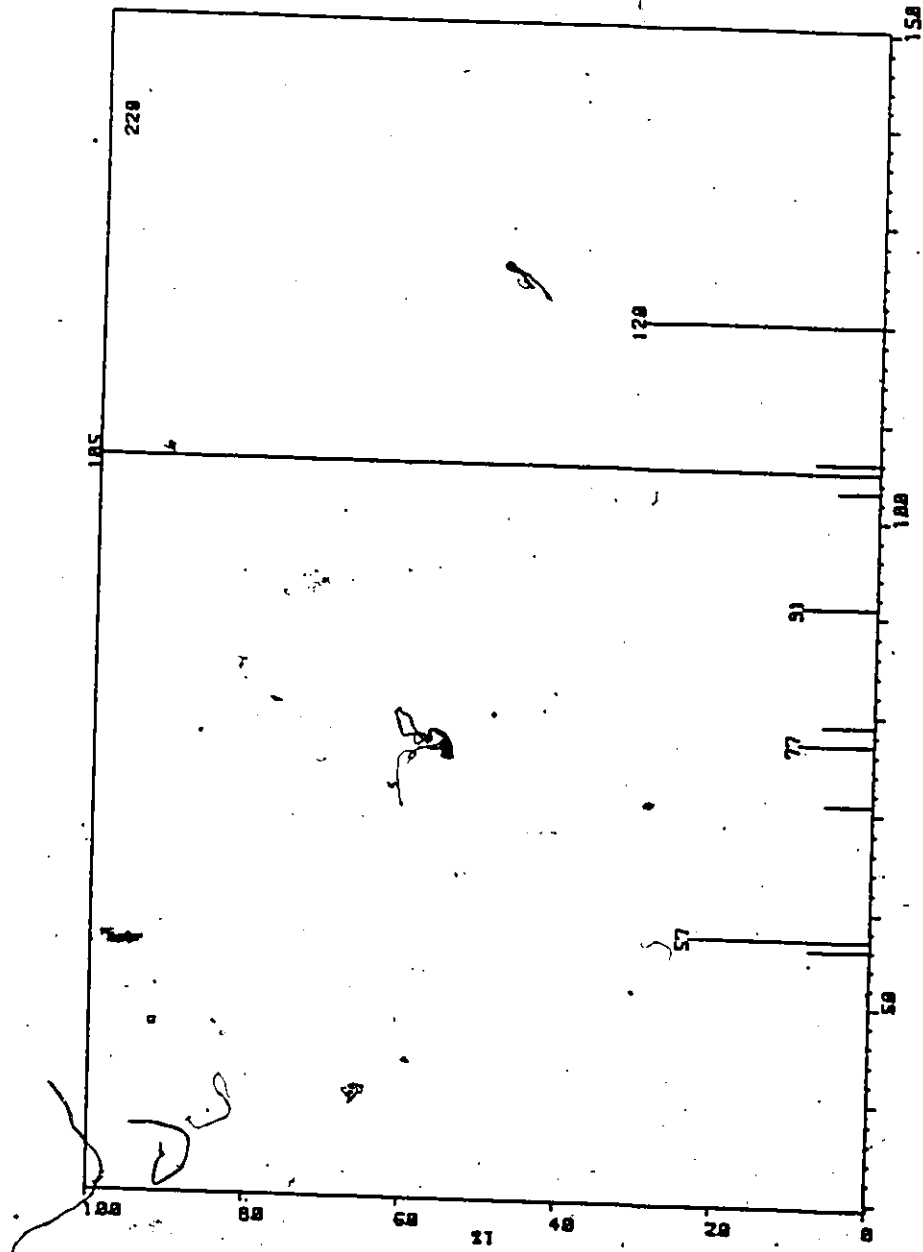


Figure A20: Mass spectrum (% relative intensity vs m/e) of C<sub>3</sub>-alkylbenzene (Peak 20).

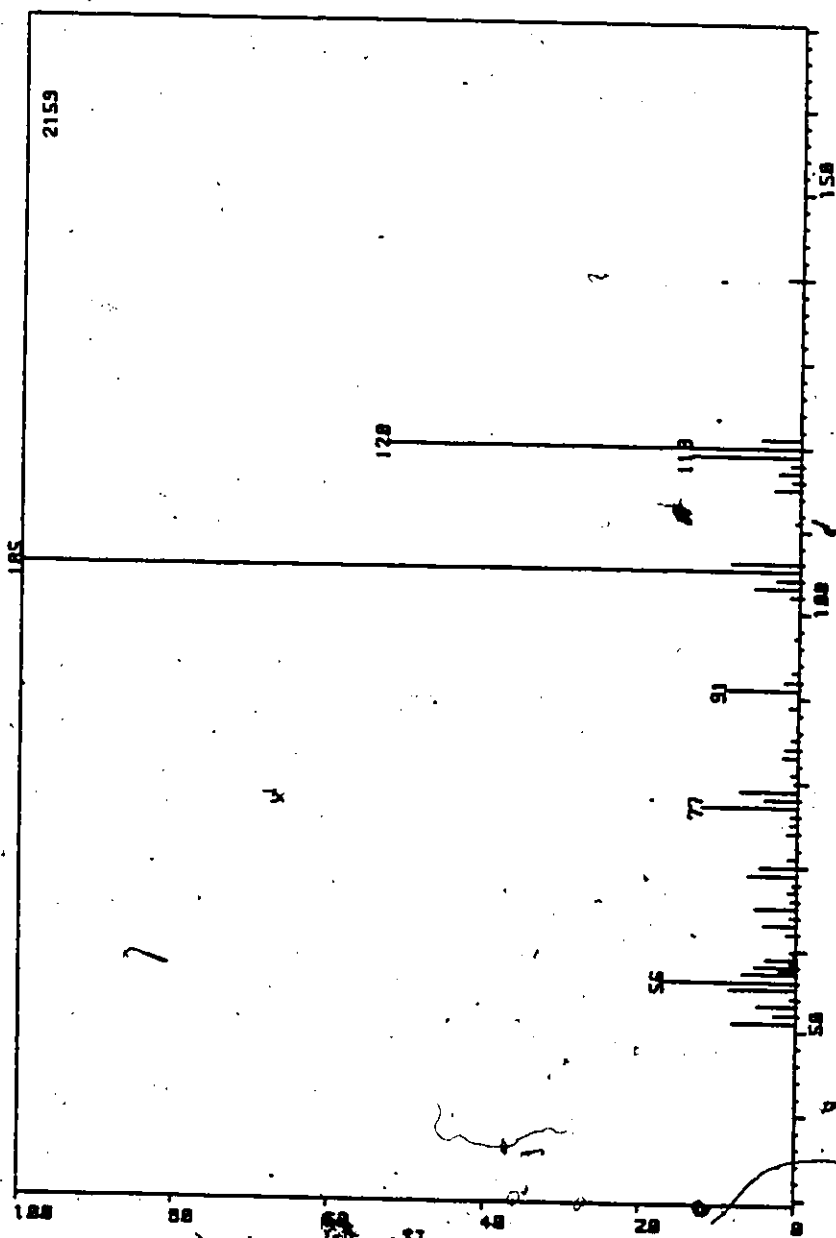


Figure A21: Mass spectrum (% relative intensity vs m/e) of C<sub>3</sub>-alkylbenzene (peak 26).

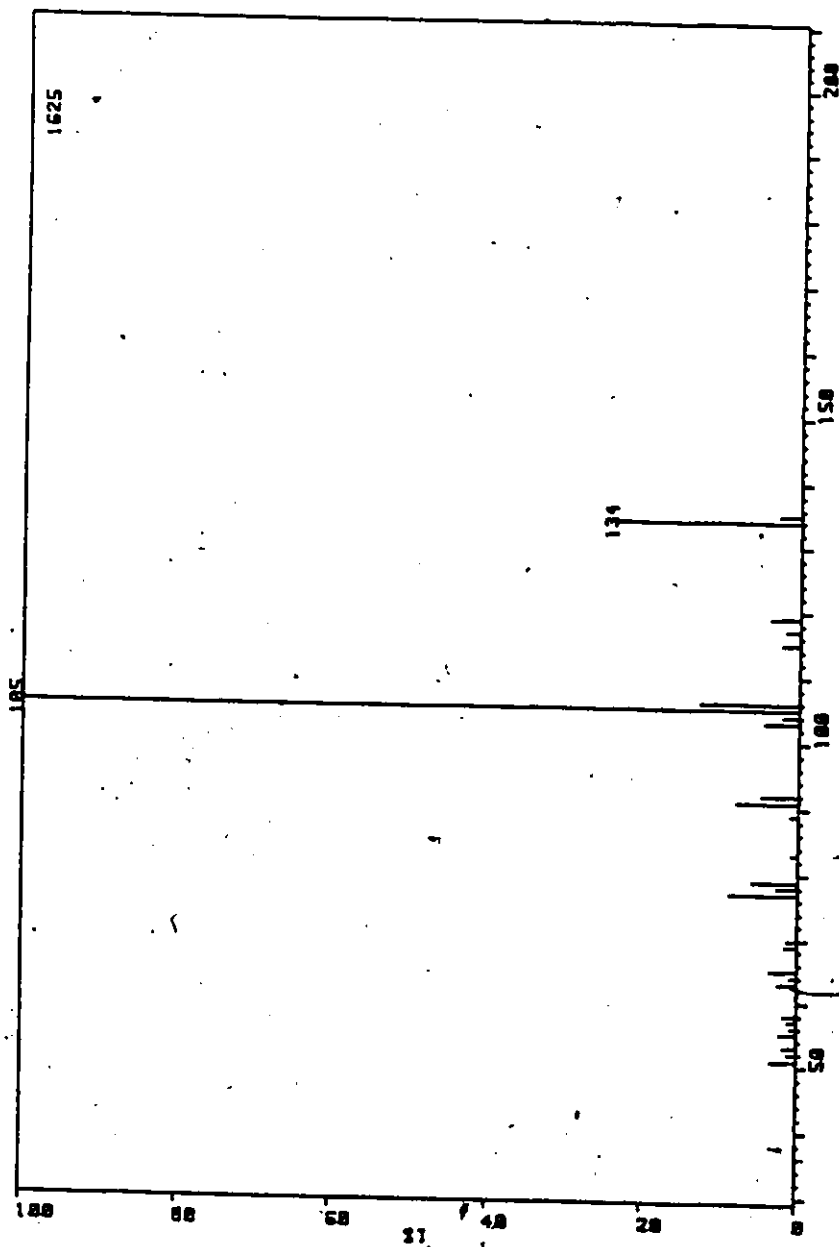


Figure A22: Mass spectrum (% relative intensity vs m/e) of C<sub>4</sub>-alkylbenzene (peak 33).

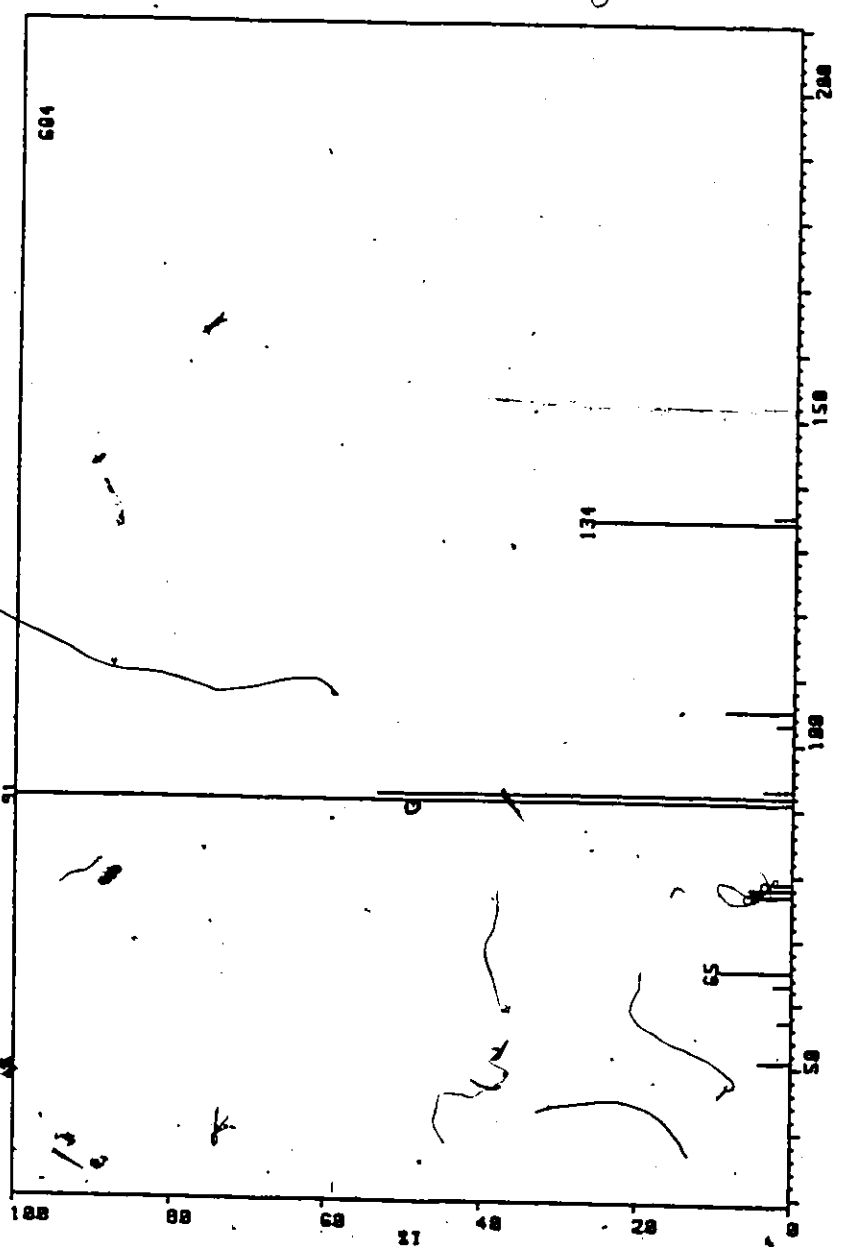


Figure A23: Mass spectrum (% relative intensity vs m/e) of n-propylbenzene (peak 34).

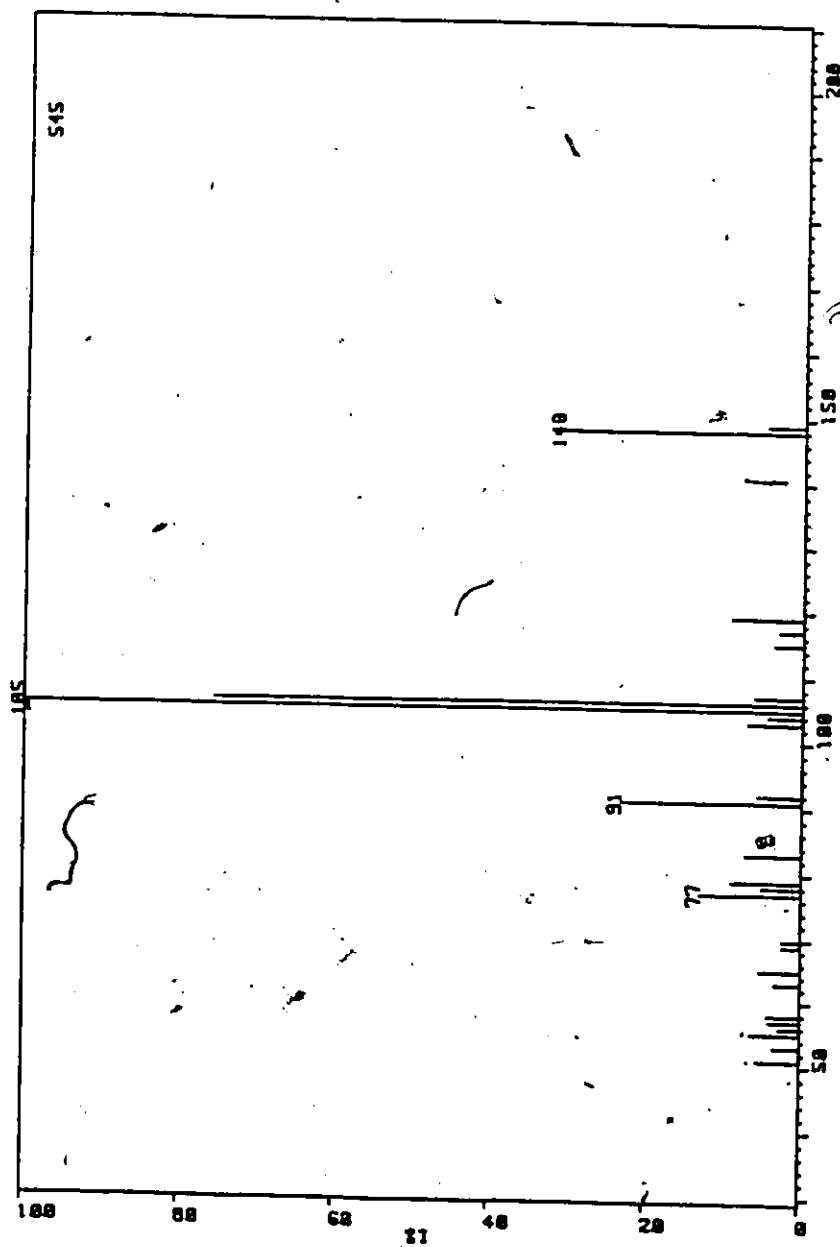


Figure A24: Mass spectrum (% relative intensity vs m/e) of C<sub>5</sub>-alkylbenzene (peak 45).

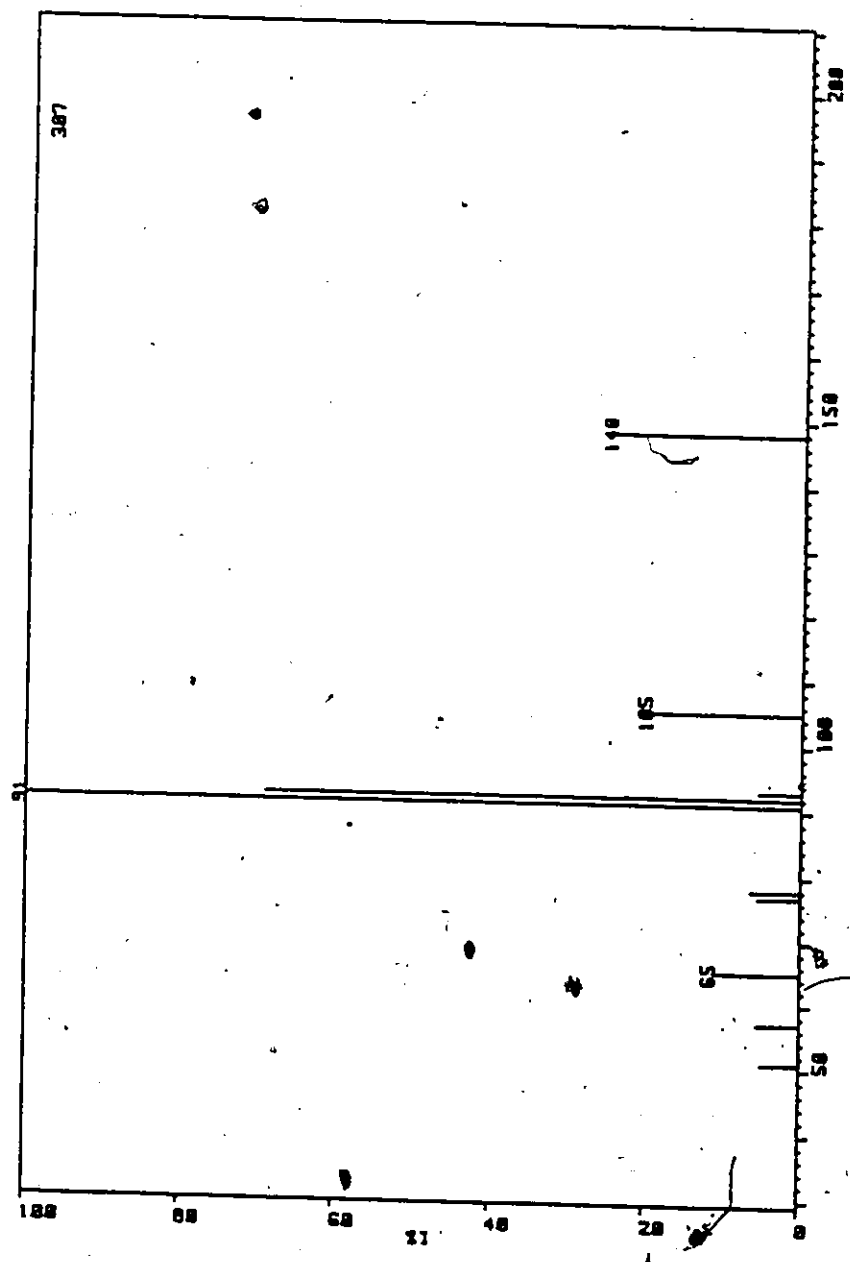


Figure A25: Mass spectrum (% relative intensity vs m/e) of C<sub>5</sub>-alkylbenzene (park 46).



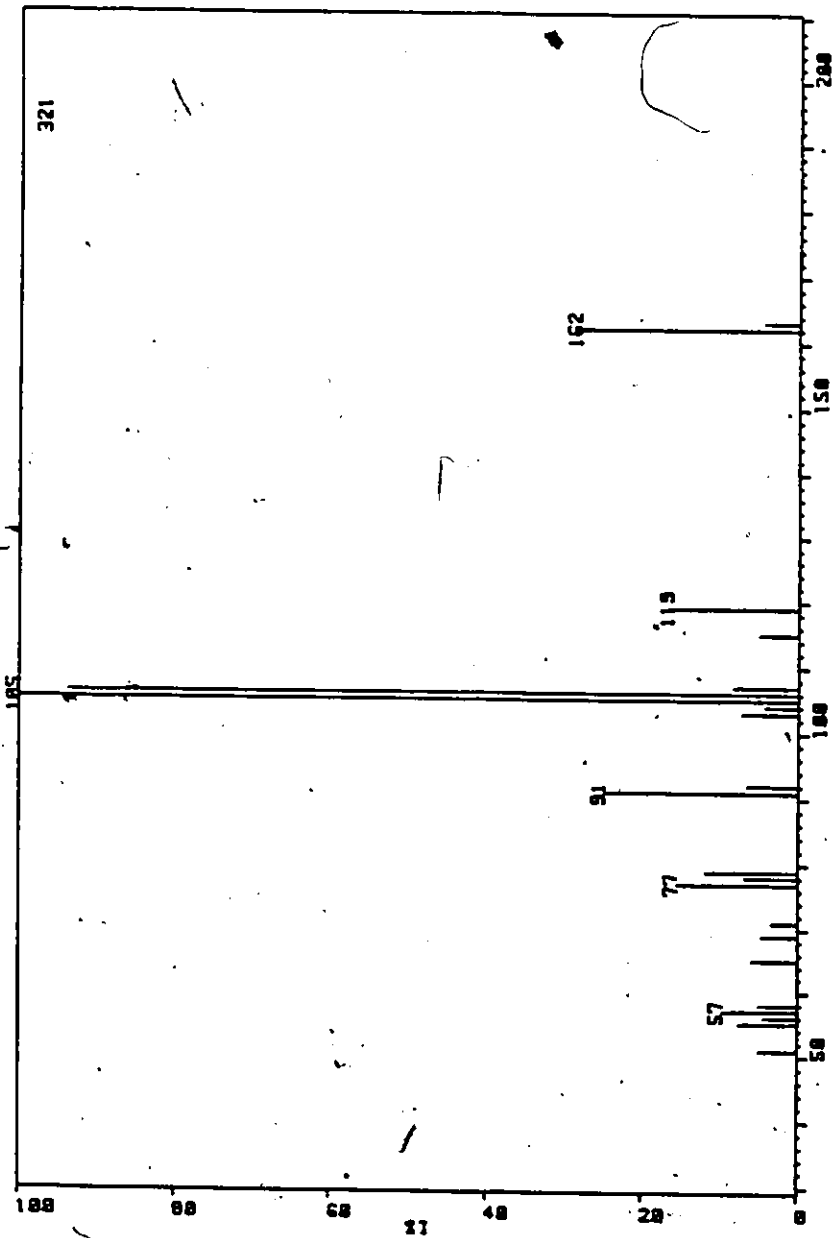


Figure A26: Mass spectrum (% relative intensity vs m/e) of C<sub>6</sub>-alkylbenzene (peak 57).

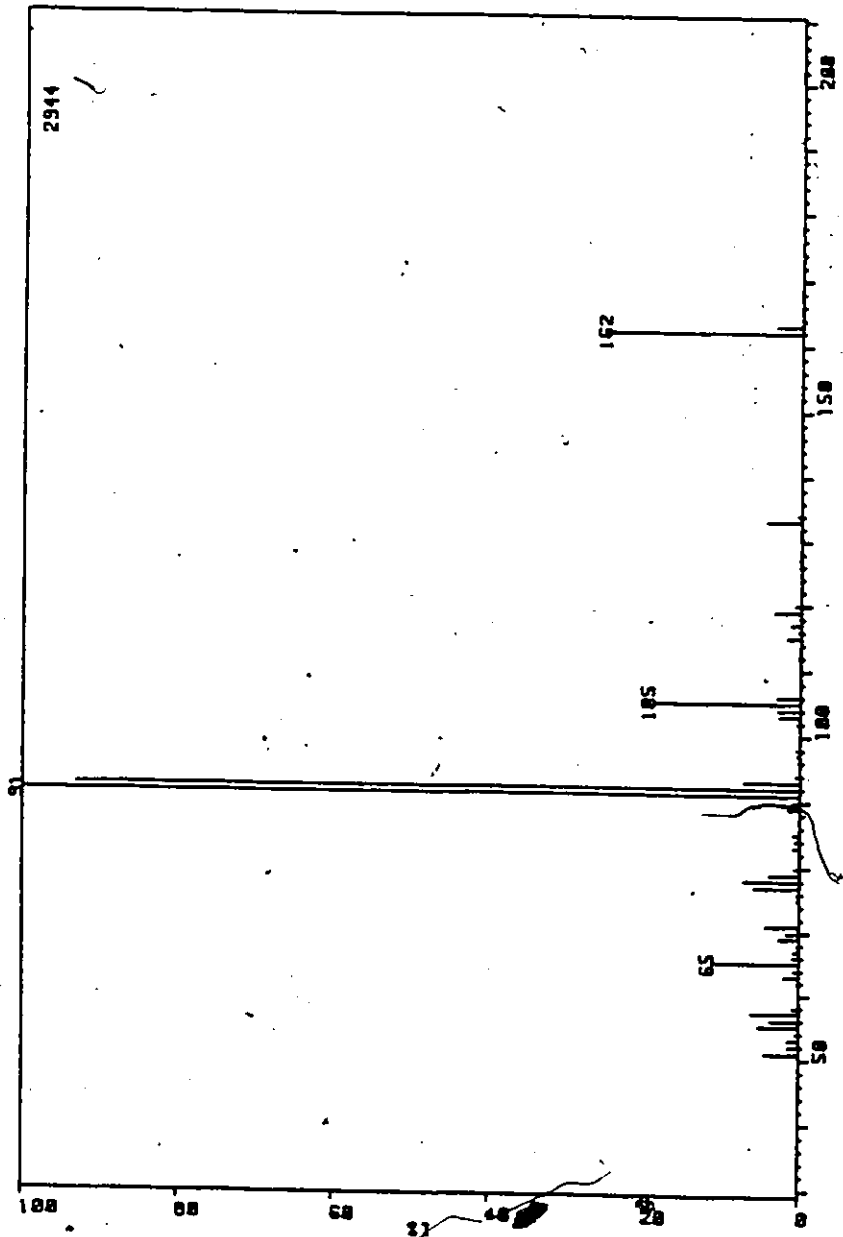


Figure A27: Mass spectrum (% relative intensity vs m/e) of n-hexylbenzene (peak 58).

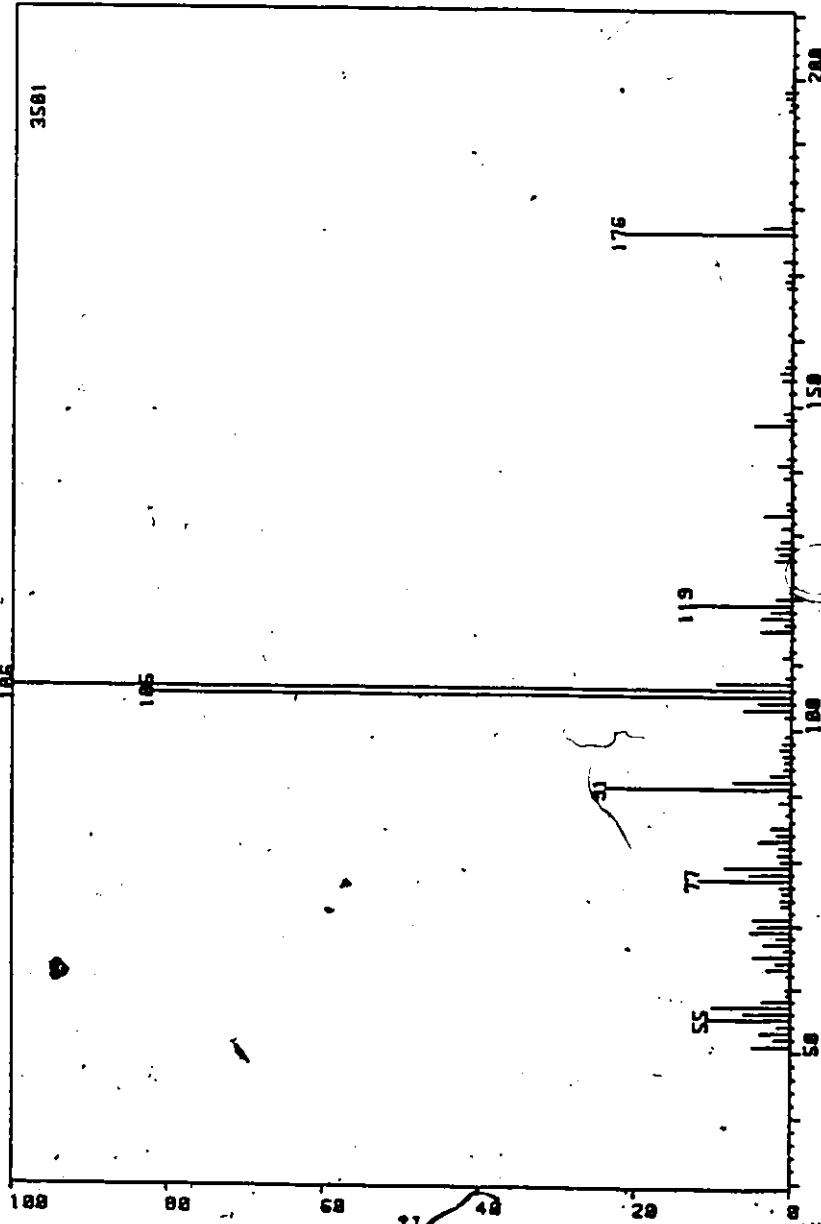


Figure A28: Mass spectrum (% relative intensity vs m/e) of C<sub>7</sub>-alkylbenzene (peak 68).

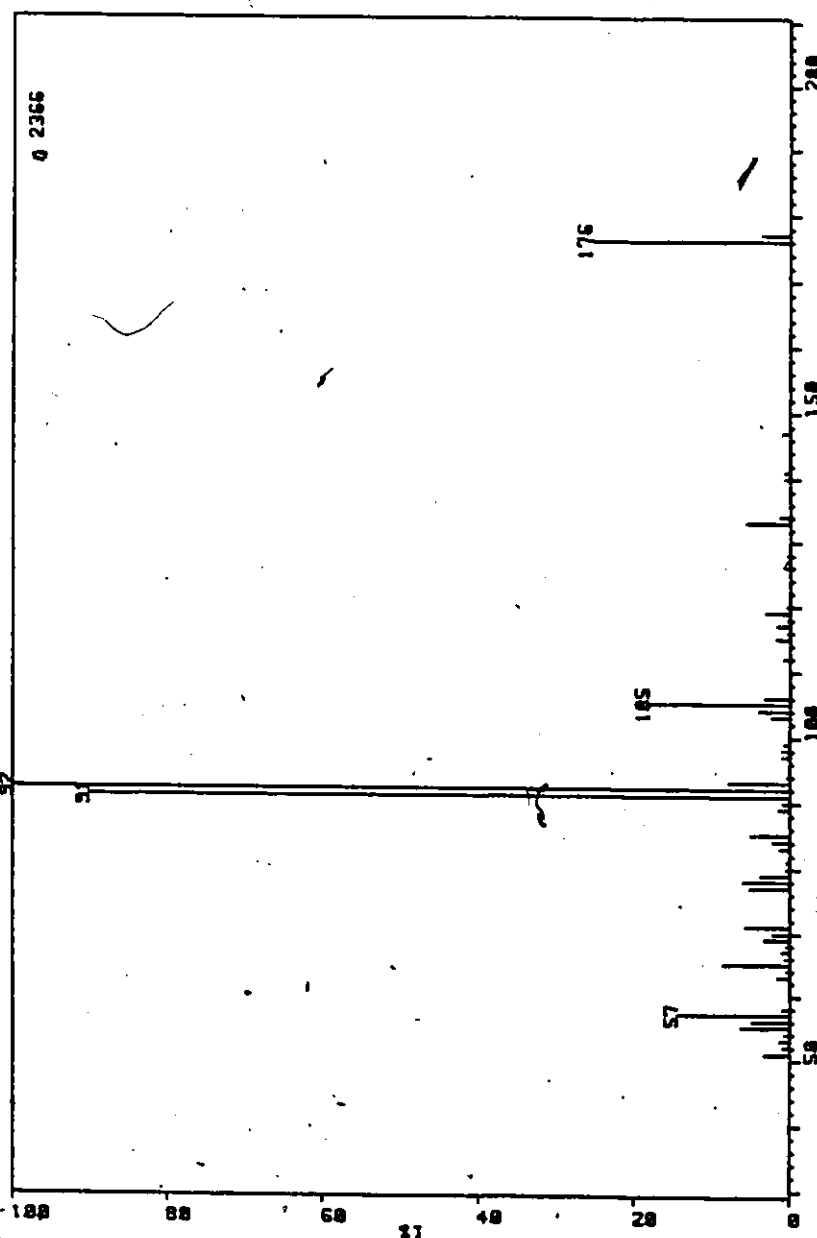


Figure A29: Mass spectrum (% relative intensity vs m/e) of C<sub>7</sub>-alkylbenzene (peak 69).

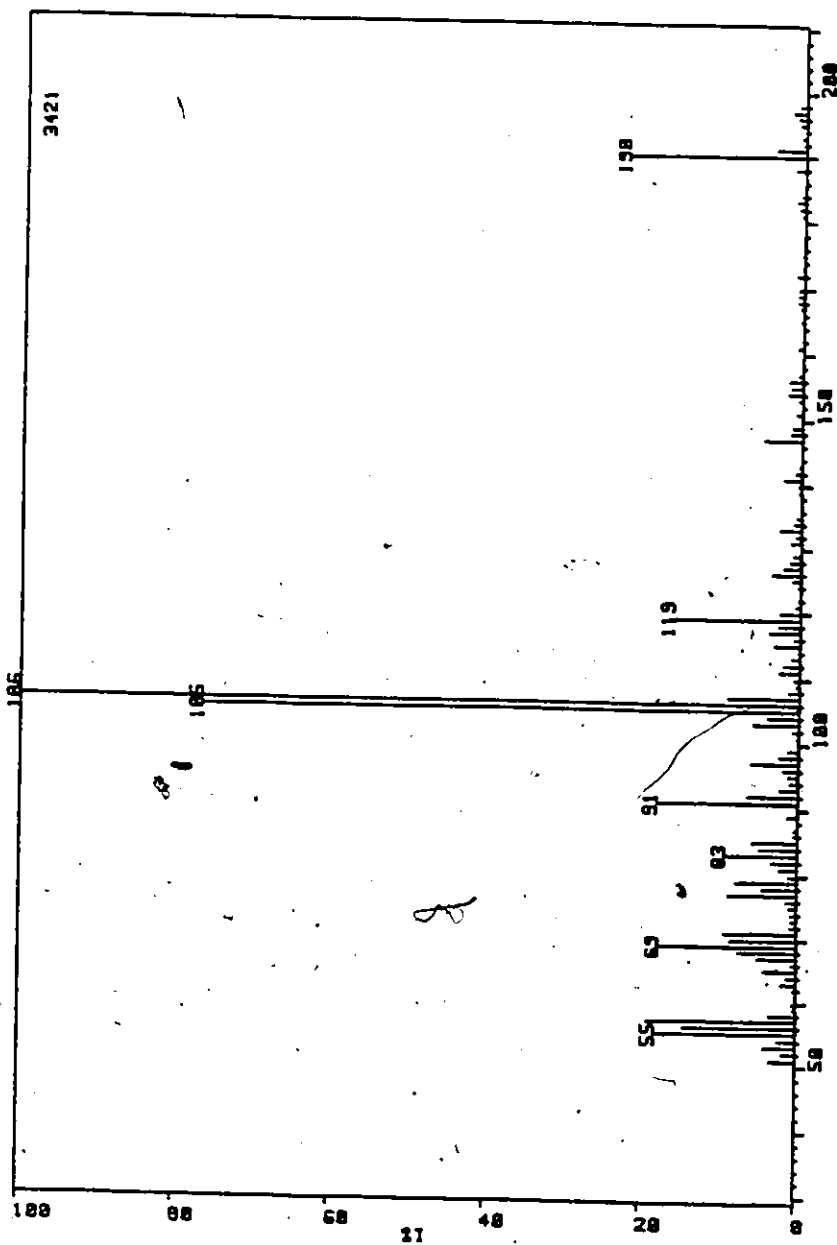


Figure A30: Mass spectrum (% relative intensity vs  $m/e$ ) of  $C_8$ -alkylbenzene (peak 78).

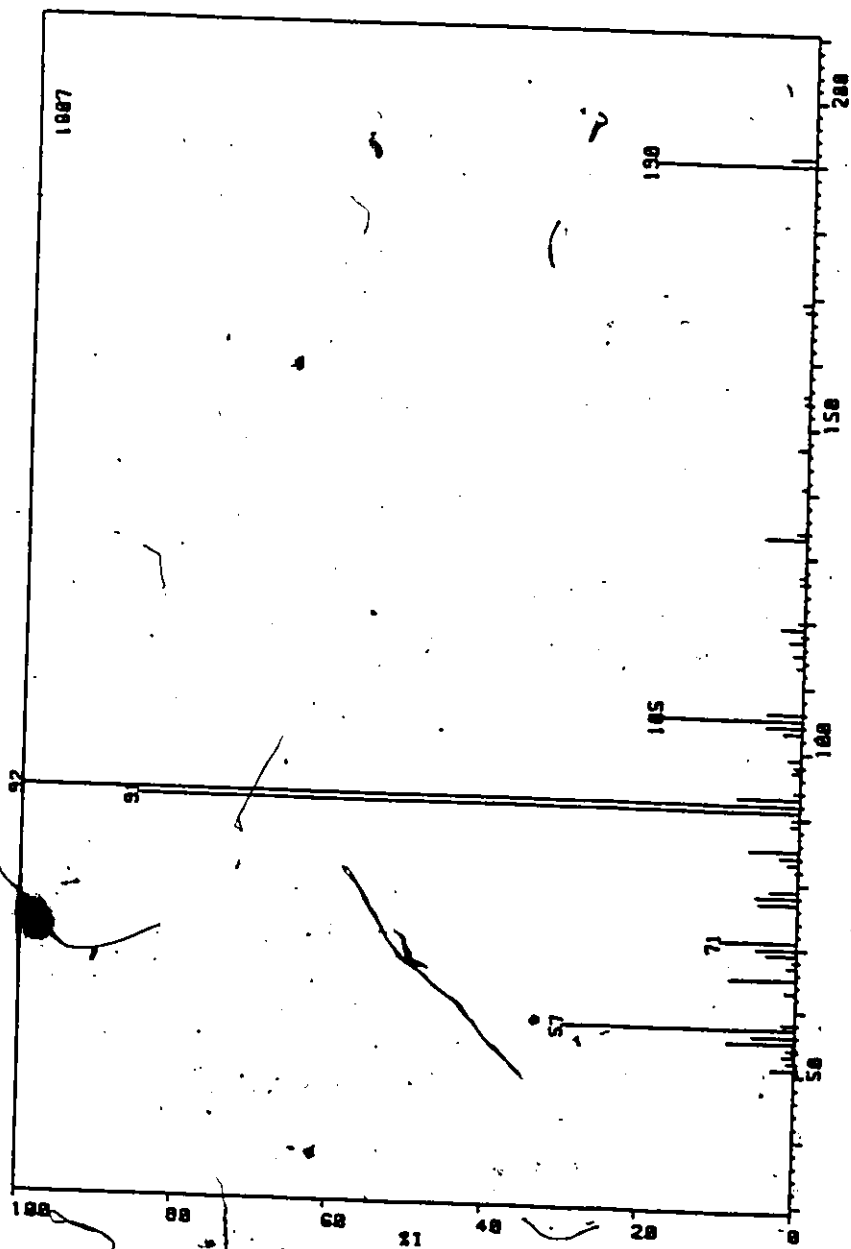


Figure A31: Mass spectrum (% relative intensity vs m/e) of C<sub>8</sub>-alkylbenzene (peak 79).

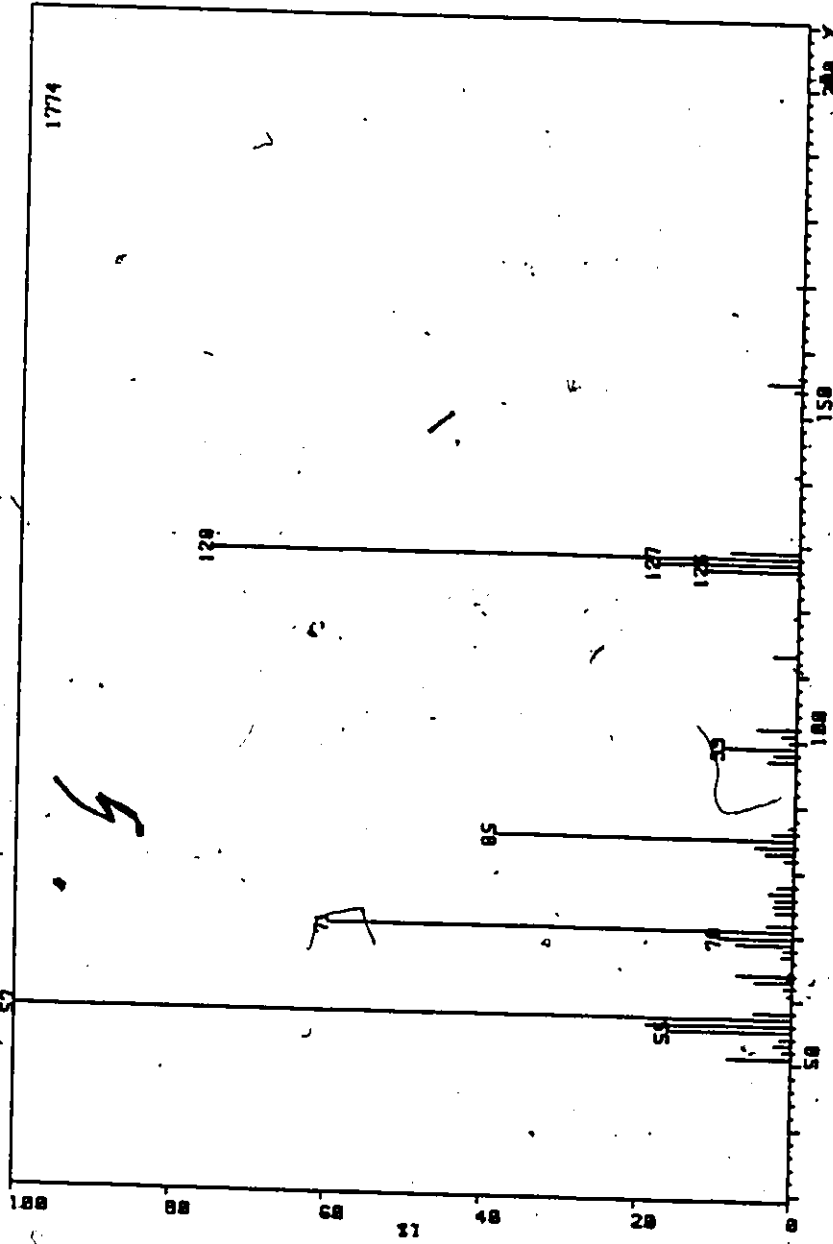


Figure A32: Mass spectrum (% relative intensity vs m/e) of Naphthalene and branched dodecane (peaks 48, 49).

## APPENDIX D

### Calculation Procedures and Experimental Data

The product composition was obtained by gas chromatographic analysis of the outlet gases. Peak areas from the chromatograms were converted to mole fractions using calibration curves. A carbon balance was done over the catalyst bed to obtain the values of selectivity, conversion and rate from the mole fraction data. It was assumed, for these calculations, that no significant amounts of carbon were deposited on the catalyst. Furthermore, the total number of moles was constant before and after the reactor since hydrogenolysis reactions are equimolar. The selectivity for product I was calculated with the following equation

$$S_I = \frac{n_R y_I}{\sum_{j=1}^P (n_j y_j)} \quad (D.1)$$

where  $n_R$  is the number of C atoms in molecules of hydrocarbon reactant,  $y_I$ , the mole fraction of product I and P, the number of products. The denominator is the summation of the mole fraction of each product,  $y_j$  multiplied by its carbon number,  $n_j$ . The conversion of the hydrocarbon reactant is defined as



$$X = \frac{\sum_{j=1}^P n_j y_j}{\sum_{j=1}^M n_j y_j}$$

(D.2)

where the denominator is a summation involving all the hydrocarbons in the outlet gases including the reactant. The rate of reaction, in  $\mu$ mole of reactant consumed /g sec, is calculated from

$$\text{RATE} = \frac{F}{W} \sum_{j=1}^P \frac{n_j y_j}{n_R}$$

(D.3)

where  $F$  is the flow rate of outlet gases and  $W$ , the weight of catalyst in the reactor.

The values of the parameters in the power rate expressions and in the selectivity equations were obtained by non-linear regression of the data from equations D.1, D.2 and D.3. The computer program that was used, UNHAUS, is based on Marquardt's method (36) which is a combination of the steepest descent method and the linearization method. The standard deviations between calculated and experimental values are given by the following equation:

$$\text{St. Dev. (\%)} = \frac{(\text{RSS} / \text{DF})^{1/2}}{\text{ACV}} \times 100$$

(D.4)

where RSS is the residual sum of squares, DF, the number of degrees of freedom and ACV, the average calculated value ( $T_{22}$ ).

TABLE A2  
 Hydrogenolysis of Isopentane at 325°C  
 and Various H<sub>2</sub> Concentration in the Feed (Fig. 5.3).

SELECTIVITY <sup>a</sup>					CONV.	% H <sub>2</sub> <sup>b</sup>
CH <sub>4</sub>	C <sub>2</sub> H <sub>6</sub>	C <sub>3</sub> H <sub>8</sub>	C <sub>4</sub> H <sub>10</sub>	1-C <sub>4</sub> H <sub>10</sub>		
4.891	.014	.014	.003	.007	.085	85.7
4.890	.014	.016	.002	.007	.082	85.4
4.886	.014	.015	.003	.007	.097	85.9
4.910	.012	.013	.002	.005	.103	88.3
4.904	.013	.015	.001	.005	.075	86.7
4.886	.015	.015	.004	.007	.102	85.7
4.887	.014	.017	.003	.006	.078	86.9
4.833	.019	.022	.003	.013	.051	82.8
4.896	.013	.017	.003	.004	.109	86.6
4.892	.014	.018	.002	.005	.084	87.0
4.903	.014	.012	.002	.006	.104	84.6
4.881	.015	.021	.002	.006	.059	87.2
4.758	.027	.022	.004	.027	.070	67.4
4.741	.028	.025	.005	.027	.071	64.5
4.752	.035	.021	.005	.023	.056	70.1
4.681	.050	.021	.006	.033	.071	59.4
4.512	.067	.036	.001	.052	.050	51.4
4.666	.047	.026	.006	.035	.050	63.7

TABLE A2 (continued)

SELECTIVITY <sup>a</sup>					CONV.	% H <sub>2</sub> <sup>b</sup>
CH <sub>4</sub>	C <sub>2</sub> H <sub>6</sub>	C <sub>3</sub> H <sub>8</sub>	C <sub>4</sub> H <sub>10</sub>	i-C <sub>4</sub> H <sub>10</sub>		
4.440	.078	.043	.010	.059	.048	50.0
4.476	.077	.037	.010	.055	.041	49.5
4.215	.128	.063	.017	.068	.051	48.3
4.059	.165	.075	.022	.075	.054	43.8
3.999	.161	.084	.027	.080	.059	44.4
4.184	.156	.060	.019	.063	.063	49.1
4.860	.012	.025	.002	.008	.067	86.6
4.078	.146	.072	.025	.079	.064	39.3
3.936	.151	.093	.030	.091	.070	40.3
4.230	.123	.064	.014	.070	.082	50.3
3.933	.179	.082	.027	.089	.063	52.0
3.981	.175	.085	.026	.078	.068	43.9
4.113	.155	.073	.020	.069	.072	48.1
4.435	.072	.033	.010	.071	.055	46.6
4.411	.075	.042	.011	.067	.060	47.2
4.743	.041	.032	.004	.016	.033	81.2
4.725	.024	.046	.005	.017	.028	85.4
4.398	.158	.063	.006	.018	.014	85.6

a) moles per mole of i-C<sub>5</sub>H<sub>12</sub> consumed

b) mole % in the feed.

TABLE A3  
 Data for Power Rate Expression in Hydrogenolysis  
 of Isopentane at 325°C.

Pressure (kPa)		Rate( $\mu$ mole /g sec)
H <sub>2</sub>	1-C <sub>5</sub> H <sub>12</sub>	
111.4	18.6	.727
110.6	18.9	.722
111.2	18.3	.754
110.6	16.8	.834
110.9	16.7	1.108
111.6	16.7	1.028
117.2	9.91	.639
112.2	16.5	.853
88.6	42.8	1.410
85.0	46.9	1.698
90.7	38.8	1.329
76.4	52.3	1.562
56.2	70.3	1.223
64.2	66.6	1.038
113.0	17.5	.710
50.5	77.8	1.209
53.6	79.5	1.125
67.1	66.3	1.229
56.9	77.7	1.085
58.9	75.2	1.116
64.1	69.2	1.171
61.9	70.8	.817
62.6	70.1	.902

TABLE A4  
 Hydrogenolysis of Isopentane over Reduced Iron  
 at 325°C and 2.8 Feed Ratio (Test 5.1)

SELECTIVITY <sup>a</sup>					CONVERSION	RATE <sup>b</sup>
CH <sub>4</sub>	C <sub>2</sub> H <sub>6</sub>	C <sub>3</sub> H <sub>8</sub>	C <sub>4</sub> H <sub>10</sub>	1-C <sub>4</sub> H <sub>10</sub>		
4.448	0.045	0.026	0.031	0.066	0.063	0.162
4.465	0.049	0.031	0.026	0.060	0.071	0.154
4.435	0.060	0.025	0.035	0.062	0.051	0.169
4.352	0.047	0.029	0.035	0.081	0.030	0.077
4.402	0.054	0.031	0.019	0.080	0.065	0.081
4.440	0.045	0.029	0.017	0.079	0.080	0.071
4.380	0.049	0.034	0.014	0.09	0.064	0.055
4.393	0.050	0.029	0.014	0.091	0.107	0.035

a) Moles per mole 1-C<sub>5</sub>H<sub>12</sub> consumed.

b) In  $\mu$ mole 1-C<sub>5</sub>H<sub>12</sub>/g sec.

TABLE A5

Hydrogenolysis of Isopentane over  $\text{Fe}_5\text{C}_2$   
at 325°C and 2.8 Feed Ratio (Test 5.2)<sup>2</sup>

	SELECTIVITY <sup>a</sup>					CONVERSION	RATE <sup>b</sup>
	$\text{CH}_4$	$\text{C}_2\text{H}_6$	$\text{C}_3\text{H}_8$	$\text{C}_4\text{H}_{10}$	$1-\text{C}_4\text{H}_{10}$		
4.556	.055	.049	.024	.023	.0083	2.175	
3.806	.054	.123	.142	.038	.0064	2.882	
3.342	.039	.088	.309	.020	.0038	-	
3.403	.096	.032	.291	.036	.0022	-	
3.574	.058	.077	.220	.050	.0050	-	
3.841	.039	.015	.235	.025	.0040	-	
4.372	.062	.035	.060	.040	.020	1.499	
4.604	.064	.037	.018	.021	.017	2.902	
4.204	.124	.048	.069	.032	.018	-	
4.274	.137	.051	.042	.033	.028	-	
4.379	.089	.030	.071	.018	.024	2.631	
4.298	.062	.039	.090	.026	.021	2.241	
4.351	.072	.034	.075	.025	.013	2.126	
4.465	.073	.039	.044	.024	.012	2.888	
4.227	.068	.032	.108	.027	.021	2.312	
4.633	.063	.015	.024	.025	.038	1.780	
4.638	.058	.017	.021	.028	.040	1.085	
4.638	.058	.017	.021	.028	.040	-	
4.651	.060	.025	.017	.022	.044	2.005	
4.654	.056	.027	.014	.025	.064	1.553	
4.616	.050	.020	.040	.016	.034	1.643	
4.474	.048	.034	.059	.023	.031	1.732	

a) moles per mole  $1-\text{C}_5\text{H}_{12}$  consumed.

b) in  $\mu\text{mole } 1-\text{C}_5\text{H}_{12}/\text{g sec.}$

TABLE A6  
 Hydrogenolysis of Isopentane over Reduced Fe  
 at 355°C and 7.0 Feed Ratio (Test 5.3)

SELECTIVITY <sup>a</sup>					CONVERSION <sup>b</sup>	RATE <sup>c</sup>
CH <sub>4</sub>	C <sub>2</sub> H <sub>6</sub>	C <sub>3</sub> H <sub>8</sub>	C <sub>4</sub> H <sub>10</sub>	1-C <sub>4</sub> H <sub>10</sub>		
4.912	.013	.0054	.0036	.0078	.430	.463
4.921	.014	.0026	.0020	.0086	.592	.165
4.878	.014	.0067	.0055	.013	.285	.484
4.892	.017	.0062	.0037	.010	.353	.422
4.894	.015	.0070	.0033	.010	.400	.332
4.883	.018	.0073	.0033	.012	.395	.310
4.876	.017	.0080	.0040	.013	.230	.491
4.870	.018	.0084	.0030	.015	.366	.240
4.855	.020	.0094	.0031	.016	.374	.167
4.870	.018	.0089	.0036	.013	.210	.406
4.863	.020	.0081	.0026	.016	.455	.118
4.857	.017	.0086	.0086	.012	.226	.425
4.872	.019	.0076	.0034	.013	.046	.147
4.910	.013	.0056	.0032	.009	.209	.642
4.850	.022	.0093	.0049	.015	.138	.410
4.858	.020	.0069	.0097	.011	.179	.673
4.904	.015	.0056	.0052	.0073	.241	.878
4.917	.013	.0046	.0066	.0040	.252	.920

a) moles per mole 1-C<sub>5</sub>H<sub>12</sub> consumed.

b) with recycle.

c) in  $\mu$ mole 1-C<sub>5</sub>H<sub>12</sub>/g sec.

TABLE A7

Hydrogenolysis of Isopentane over Reduced Iron at 355°C  
and 0.8 Feed Ratio, 1% < Conversion < 10% (Test 5.4)

SELECTIVITY <sup>a</sup>					CONVERSION	RATE <sup>b</sup>
CH <sub>4</sub>	C <sub>2</sub> H <sub>6</sub>	C <sub>3</sub> H <sub>8</sub>	C <sub>4</sub> H <sub>10</sub>	i-C <sub>4</sub> H <sub>10</sub>		
4.069	.119	.053	.054	.080	.023	.283
3.969	.156	.068	.040	.088	.027	.214
3.623	.200	.120	.042	.112	.075	.127
4.007	.069	.045	.079	.102	.015	.094
3.994	.103	.066	.047	.103	.021	.103
4.083	.125	.071	.026	.088	.059	.108
3.899	.147	.075	.075	.074	.015	.213
3.866	.182	.086	.045	.083	.079	.143
3.739	.209	.105	.042	.091	.090	.121
3.674	.212	.112	.042	.100	.087	.124
3.984	.180	.087	.034	.065	.068	-
3.717	.143	.092	.101	.079	.011	.182
4.022	.165	.087	.032	.065	.037	.332

a) moles per mole i-C<sub>5</sub>H<sub>12</sub> consumed.

b) in μmole i-C<sub>5</sub>H<sub>12</sub>/g sec.



TABLE A8

Hydrogenolysis of Isopentane over Reduced Iron at 355°C  
and 0.8 Feed Ratio with a Conversion less than 1% (Test 5.4)

SELECTIVITY <sup>a</sup>					CONVERSION	RATE <sup>b</sup>
CH <sub>4</sub>	C <sub>2</sub> H <sub>6</sub>	C <sub>3</sub> H <sub>8</sub>	C <sub>4</sub> H <sub>10</sub>	i-C <sub>4</sub> H <sub>10</sub>		
3.359	.116	.139	.113	.135	.0069	.054
3.758	.134	.118	.068	.086	.0080	.162
3.124	.167	.191	.142	.101	.0061	.166
3.660	.139	.175	.046	.088	.0072	.195
3.578	.147	.176	.056	.094	.0066	.209
3.795	.147	.139	.047	.077	.0063	.194
3.625	.177	.169	.059	.069	.0074	.226
3.763	.140	.129	.052	.091	.0083	.276
3.630	.133	.166	.076	.076	.0042	.131
4.088	.127	.066	.046	.069	.0064	.228
3.655	.115	.135	.059	.119	.0043	.188
2.989	.123	.233	.171	.096	.0026	.109
3.336	.166	.187	.104	.090	.0028	.106

a) moles per mole i-C<sub>5</sub>H<sub>12</sub> consumed.

b) in  $\mu$ mole i-C<sub>5</sub>H<sub>12</sub>/g sec.

TABLE A9  
 Data for Power Rate Expression in Hydrogenolysis  
 of Propane at 325°C.

Pressure (kPa)		Rate( $\mu$ mole /g sec)
$H_2$	$i-C_5H_{12}$	
100.4	24.8	.118
108.3	18.2	.100
110.3	16.1	.094
183.7	7.5	.052
183.8	6.8	.058
184.3	6.8	.061
199.0	6.6	.047
109.5	18.8	.107
123.2	6.2	.063
118.5	10.2	.095
118.2	10.2	.096
89.3	41.1	.308
110.7	18.4	.101
144.8	11.7	.136
146.0	11.7	.143
99.8	29.4	.182
93.9	35.2	.300
88.7	40.5	.271
79.1	49.7	.328
66.9	42.8	.272
66.5	42.6	.273

TABLE A10

Experimental Data from Hydrogenolysis of Propane  
at 325°C and Various H<sub>2</sub> Concentration in the Feed.

SELECTIVITY <sup>a</sup>		CONVERSION	% H <sub>2</sub>
CH <sub>4</sub>	C <sub>2</sub> H <sub>6</sub>		
2.974	.013	.044	80.2
2.981	.0096	.042	85.6
2.984	.0082	.045	87.3
2.977	.012	.056	96.1
2.978	.011	.058	96.4
2.974	.013	.054	96.4
2.976	.012	.065	96.8
2.981	.0095	.046	85.3
2.976	.012	.040	95.2
2.981	.0097	.051	92.1
2.979	.010	.045	92.1
2.978	.011	.046	68.5
2.983	.0083	.052	85.8
2.974	.013	.047	92.5
2.976	.012	.045	92.6
2.979	.010	.043	77.3
2.981	.0095	.056	72.8
2.980	.010	.052	68.7
2.978	.011	.055	61.4
2.976	.012	.044	61.0
2.977	.012	.046	61.0

a) in moles per mole C<sub>3</sub>H<sub>8</sub> consumed.

TABLE A11

Hydrogenolysis of Propane over Reduced Iron at 330°C  
and 4.7 FR, with or without Water in the Feed (Fig. 7.1)

	SELECTIVITY <sup>a</sup>		CONVERSION	RATE <sup>b</sup>
	CH <sub>4</sub>	C <sub>2</sub> H <sub>6</sub>		
With H <sub>2</sub> O:	2.548	.226	.0007	.003
	1.906	.547	.0004	.001
	2.732	.134	.0010	.003
	2.714	.143	.0012	.002
	2.855	.073	.0033	.003
	2.924	.038	.0187	.011
	2.896	.052	.0051	.005
	2.951	.024	.0235	.022
	2.945	.028	.0228	.022
	2.955	.023	.0258	.016
	2.947	.027	.0186	.014
	2.883	.059	.0035	.010
	2.947	.026	.0156	.010
	2.921	.040	.0040	.009
	2.944	.028	.0172	.017
Without H <sub>2</sub> O:	2.993	.003	.162	.416
	2.996	.002	.320	.662
	2.996	.002	.228	1.161
	2.995	.002	.184	1.339
	2.991	.005	.135	.500
	2.970	.015	.016	.034
	2.963	.019	.012	.026
	2.937	.032	.005	.012
	2.826	.087	.002	.004
	2.989	.006	.113	.292
	2.971	.014	.025	.130
	2.979	.011	.037	.177
	2.980	.010	.041	.182
	2.980	.010	.101	.056
	2.978	.011	.101	.058

a) moles per mole C<sub>3</sub>H<sub>8</sub> consumed.

b) in  $\mu$ mole C<sub>3</sub>H<sub>8</sub>/g sec.

TABLE A12  
Hydrogenolysis of Propane over Reduced Iron Catalyst  
at 327°C and 4.8 FR.

SELECTIVITY <sup>a</sup>		CONVERSION	RATE <sup>b</sup>
CH <sub>4</sub>	C <sub>2</sub> H <sub>6</sub>		
2.971	.014	.025	.130
2.979	.011	.037	.177
2.980	.010	.041	.182
2.977	.012	.037	.096

a) moles per mole C<sub>3</sub>H<sub>8</sub> consumed.

b) in  $\mu$ mole C<sub>3</sub>H<sub>8</sub>/g sec.

TABLE A13

Hydrogenolysis of Isobutane over Platinum on  
Catalyst at 425°C and 3.0 Feed Ratio (Fig. 4.7)

SELECTIVITY <sup>a</sup>				CONVERSION <sup>b</sup>	RATE <sup>c</sup>
CH <sub>4</sub>	C <sub>2</sub> H <sub>6</sub>	C <sub>3</sub> H <sub>8</sub>	nC <sub>4</sub> H <sub>10</sub>		
1.112	.342	.603	.099	.550	.206
.754	.099	.647	.277	.155	.420
.829	.156	.661	.219	.283	.366
1.001	.271	.645	.131	.472	.258
1.323	.471	.504	.055	.709	.160
1.343	.483	.496	.051	.718	.148
.728	.093	.641	.291	.160	.448
.865	.185	.655	.200	.338	.320
.882	.196	.659	.187	.349	.288
.902	.210	.659	.175	.377	.264
1.213	.418	.549	.077	.652	.180
.910	.179	.686	.169	.331	.342
.920	.179	.694	.160	.327	.337
.738	.079	.645	.292	.140	.387
.750	.083	.650	.283	.139	.376
.735	.083	.640	.295	.140	.388
1.196	.400	.566	.077	.626	.157
2.366	.583	.149	.006	.944	.052
1.336	.476	.487	.063	.689	.098
1.236	.423	.537	.077	.623	.105
1.598	.560	.381	.035	.777	.074
1.710	.602	.358	.003	.802	.071
.762	.100	.650	.272	.165	.362
.889	.189	.665	.184	.326	.292
.857	.164	.671	.201	.280	.292

a) Moles per mole i-C<sub>4</sub>H<sub>10</sub> consumed.

b) With recycle.

c) In  $\mu$ mole i-C<sub>4</sub>H<sub>10</sub>/g sec.